UC Berkeley
UC Berkeley Electronic Theses and Dissertations

Title
On the Inherently Nonlinear Dynamics of Unilateral Contact in Elastic Structures

Permalink
https://escholarship.org/uc/item/5b03c61b

Author
Goldberg, Nathaniel Niklas

Publication Date
2022

Peer reviewed|Thesis/dissertation

eScholarship.org Powered by the California Digital Library
University of California

On the Inherently Nonlinear Dynamics of Unilateral Contact in Elastic Structures

by

Nathaniel Niklas Goldberg

A dissertation submitted in partial satisfaction of the

requirements for the degree of

Doctor of Philosophy

in

Engineering – Mechanical Engineering

in the

Graduate Division

of the

University of California, Berkeley

Committee in charge:

Professor Oliver M. O'Reilly, Chair
Professor David J. Steigmann
Professor Jon Wilkening

Summer 2022

On the Inherently Nonlinear Dynamics of Unilateral Contact in Elastic Structures

Copyright 2022
by
Nathaniel Niklas Goldberg

Abstract

On the Inherently Nonlinear Dynamics of Unilateral Contact in Elastic Structures

by

Nathaniel Niklas Goldberg

Doctor of Philosophy in Engineering – Mechanical Engineering

University of California, Berkeley

Professor Oliver M. O'Reilly, Chair

Engineering and everyday experience alike provide countless examples of deformable objects coming into contact with effectively rigid objects, from a belt stretched between pulleys in an automobile engine to a ball bouncing on a blacktop. But despite the ubiquity of such systems, we have little in the way of a fundamental understanding of the dynamics they can be expected to display. The main obstacle to deeper understanding is mathematical: the unilateral constraint of contact creates free boundaries, and free-boundary-value problems are inherently nonlinear, even if the underlying differential equations are themselves linear. This dissertation explores the dynamics of contact in several prototypical problems inspired by engineering applications such as indentation testing, offshore oil exploration and production, and microelectromechanical systems (MEMS) design.

The first major thrust of the present work is the linear vibration analysis of a beam contacting a flat surface due to combined gravity and adhesion. In analyzing this problem we develop a technique for appropriately linearizing the conditions at a free boundary. We then extend the technique to study the nonlinear vibrations of the gravity-only problem using a second-order perturbation analysis, which shows that contact generates a rich array of nonlinear resonances. The results show good agreement with numerical solutions from a special finite element method that precisely tracks the free boundary. We conclude by using the gap function formalism common in computational contact mechanics to demonstrate that the same pattern of resonances can be expected to arise in a more general class of problems.

Having studied a problem involving a one-dimensional continuum, we shift attention to one with a two-dimensional continuum: an electrostatically actuated plate contacting a charged, dielectric-coated substrate. We use a variational method to derive one model in which the dielectric thickness is finite, and the other in which the thickness is small. The latter corresponds to a common type of surface adhesion. We formulate the linear stability equations for both models and characterize their equilibria in the case of a circular actuator before adopting an approximation from dynamic fracture mechanics to study the dynamics

of the thin-dielectric model, which display some unique mathematical properties, including finite-time blow-up. Finally, we discuss application of the model to the problem of vibration-assisted stiction repair.

This work incorporates many analytical and computational tools, from configurational mechanics, to perturbation theory, to arbitrary Lagrangian-Eulerian finite element methods, and represents a first step toward the development of rules-of-thumb for the design of vibration-critical mechanical systems with contact constraints.

To my parents

Contents

List of Figures

List of Tables

Acknowledgments

This dissertation is the culmination of five years of graduate school, four years of undergraduate studies, four years of high school, three years of middle school, five years of elementary school, a year of kindergarten, and a year of pre-school. So many people have been essential to this twenty-three-year-long journey that it would be impossible to acknowledge all of them in the limited space here. That said, I would like to extend my heartfelt gratitude to all those who have supported me along the way, regardless of whether they are specifically named below.

Foremost among those deserving of acknowledgment are my late parents, who endured tremendous hardship to provide the best upbringing possible for their only child. Hardly a day passes in which I am not reminded of their sacrifices. Their strength, wit, and charm undoubtedly live on in the hearts of the many whose lives they touched.

I have been fortunate to complete this dissertation under the tutelage of several exceptional faculty members in the Department of Mechanical Engineering at Berkeley. Professor O'Reilly has been integral to every aspect of my graduate studies. It is difficult to imagine another adviser having the patience to entertain my countless outlandish research ideas and strong opinions about typesetting. No less deserving of appreciation are the other professors in the Mechanics group. Professor Steigmann has been an invaluable source of advice on all manner of topics from the technical to the professional. Wide swaths of this dissertation would not exist were it not for the numerical expertise of Professor Papadopoulos, whom I must also acknowledge for his instruction in two of the most valuable courses I took in graduate school, MECENG 185 and MECENG 280B. Professor Casey, who called me on a fortuitous day in early 2017 to inform me I had been admitted to Berkeley, should be commended for guiding me with a steady hand through my first experience as a Graduate Student Instructor. Finally, I must thank Professor Zohdi for the pivotal role he played in securing my two fellowships, and for our many entertaining discussions.

It has been my distinct pleasure to get to know so many talented graduate students—current and former—during my time at Berkeley. Our debates about mechanics, nights of playing cards and pool, trips to Costco, and spontaneous conversations on every topic under the sun have been highlights of my time in Etcheverry Hall. I am especially appreciative of all my labmates in the Dynamics Laboratory, who stoically endured years of my percussive typing and penchant for rambling.

The research presented in this dissertation was conducted with the support of the United States Department of Defense through the National Defense Science and Engineering Graduate Fellowship, and the support of the University of California, Berkeley through the Berkeley Fellowship for Graduate Study. I am sincerely grateful for the backing these programs and for the taxpayers and donors who sustain them.

Chapter 1

Introduction

Contact is fundamental. It is the only way that purely mechanical bodies can interact with one another. Figure 1.1 shows just a few examples: a flat tire on a road, a cork being pulled from the neck of a bottle, and human blood cells bumping into each other. In all contact-mechanical systems, from the mundane to the extraordinary, the inanimate to the living, the microscopic to the macroscopic, the essential feature is that of impenetrability of the bodies. In other words, the two (or more) bodies in contact cannot pass through each other. Mathematically speaking, this requires the enforcement of a unilateral constraint on the displacements of the bodies. In general, for three-dimensional bodies, contact occurs along one or more surfaces, with the boundary of such a surface (a curve that is variously called the contact interface, contact boundary, or contact line) being unknown a priori in the typical problem where one must determine the displacement fields given the loads. Since there is a boundary in the mathematical domain that must be determined as part of the solution of the governing boundary-value problem, we are actually dealing with a *free-boundary* problem.[1]

Free-boundary problems are inherently nonlinear, and this fact has important consequences for the mechanics of contact. For one, it means that contact can induce strongly nonlinear behavior in even the simplest models of deformable bodies, such as linearly elastic, Euler-Bernoulli beams. Another consequence is that much of our intuition about the mechanics of deformable bodies is not applicable when contact is present. Take, for example, the following heuristic that can be found either explicitly or implicitly in numerous structural mechanics textbooks:

> Consider, then, a general structure loaded by an arbitrary set of equilibrated loads, and suppose these to increase in proportion. The configuration of forces being given, let their magnitude be denoted by ρ. For ρ sufficiently small, the

[1] It is important to distinguish between free- and moving-boundary problems. In both, all or part of the boundary of the mathematical domain varies as a certain parameter is changed, often a temporal variable. In moving-boundary problems, the boundary moves in a prescribed fashion, while in free-boundary problems, the location of the boundary is unknown a priori and must be determined as a part of the solution of the problem.

Figure 1.1: Practical examples of contact between deformable bodies.

> entire structure is elastic, and the increase in a typical deformation Δ is proportional to the increase in ρ. [1]

This notion, treated as fundamental by some, can be egregiously violated in systems with contact, as we will demonstrate shortly.

If mechanicians' intuition for the statics of contact is often insufficient, their intuition for the dynamics of contact is even more often so. (One exception is that there exist several rules-of-thumb for so-called contact-impact systems, but our interest is in systems with continuous contact.) Having the ultimate goal of developing engineering intuition for the sort of nonlinear dynamics that can arise in contact-mechanical systems, this dissertation focuses on detailed mathematical analyses of some of the simplest possible problems. Some of the questions we seek to answer include the following:

- How do we consistently linearize contact-mechanical systems?
- How do we consistently apply perturbation methods to study contact-mechanical systems?
- Does the frequency response of contact-mechanical systems exhibit hardening behavior or softening behavior?
- What sort of nonlinear resonances can contact generate?
- How does adhesion affect the dynamics of contact?
- What constitutes a "good" numerical method for solving dynamic contact problems?

Whenever possible, sources of nonlinearity other than contact are neglected so that any observed effects can be ascribed directly to contact, rather than some other source, such as material nonlinearity. Furthermore, all problems in this dissertation concern structural systems (i.e., beams and plates). While the bulk of the contact mechanics literature focuses

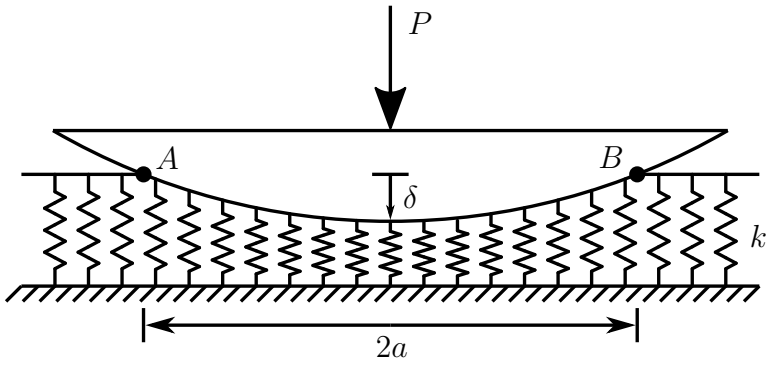

Figure 1.2: Cross-sectional schematic of a spherical indenter being pressed into an elastic foundation by a dead load.

on solids (i.e., three-dimensional bodies), our consideration of structural systems enables the use of mathematical tools that would be simply too cumbersome to apply to solids. We also consider only systems in which one of the two contacting bodies can be treated as rigid—a good approximation when the two differ greatly in stiffness.

The remainder of this chapter serves to familiarize the reader with several of the unique features that are encountered in contact problems by way of example. While many of the features we present are quite common, contact mechanics encompasses such a wide array of problems that there are certainly many exotic mechanical behaviors enabled by contact that we simply do not have the space to discuss here. Furthermore, there are also scenarios in which none of the features shown in the forthcoming sections are present.[2]

1.1 Contact is a Nonlinearity

Figure 1.2 is a cross-sectional view of a rigid, frictionless, spherical indenter of radius R being pressed into a foundation of stiffness per unit area k by a force P, resulting in a deflection δ from the location of incipient contact. The surface of contact is then the arc AB revolved about the axis of symmetry, while the contact interface (also known as the contact boundary) is the curve generated by revolving the points A and B about the axis of symmetry. Our task is to determine δ given P, R, and k. As is the case in contact problems in general, the location of the contact interface, defined by the quantity a, must also be determined as part of the solution.

[2]As an example, a sphere compressed between two parallel elastic foundations (the two-sided version of the system illustrated in Fig. 1.2) will exhibit entirely linear dynamics in the normal direction. This is part of reason we chose to focus on unilateral rather than bilateral contact in this dissertation.

A balance of vertical forces shows that

$$F = \int_0^a k\Big(\delta - R + \sqrt{R^2 - x^2}\Big) \cdot 2\pi r \, \mathrm{d}r \approx \int_0^a k\left(\delta - \frac{r^2}{2R}\right) \cdot 2\pi r \, \mathrm{d}r = \pi a^2 k\left(\delta - \frac{a^2}{4R}\right), \quad (1.1)$$

where we have employed the (often reasonable) approximation that $a/R \ll 1$. Notice that this equation involves the additional unknown a. Closure is provided by the geometric condition[3]

$$a = \sqrt{R^2 - (R - \delta)^2} \approx \sqrt{2\delta R}. \quad (1.2)$$

which leads to

$$F \approx \pi R k \delta^2. \quad (1.3)$$

The important result here is that $F \propto \delta^2$. The relation between force and displacement is therefore, to borrow terminology sometimes used in dynamics, *essentially nonlinear* [2]. A small but positive force F does not lead to a proportional displacement δ, and the engineering heuristic mentioned earlier is clearly violated. Care should be taken not to overgeneralize this result, however, because although the force-displacement relationship is not incrementally linear about $\delta = 0$, it *is* incrementally linear about any $\delta > 0$. One application of a closely related nonlinearity is in the study of wave propagation in pre-compressed chains of elastic spheres, which can support solitary waves [3].

1.2 Contact is Often Asymmetric

It should be obvious that the indenter-foundation model in Fig. 1.2 is fundamentally asymmetric. As the indenter is pushed into the foundation, it engages more and more of the springs, and hence the force response hardens. On the other hand, as the indenter is retracted from some $\delta > 0$, it engages fewer and fewer springs. This asymmetry is a geometric property that persists even in the most realistic models of contact that include friction, a deformable indenter, a properly modeled foundation, and so on. What's more, the asymmetry can have profound consequences for dynamics. To illustrate this, consider the system illustrated in Fig. 1.3, a crude model of an indenter attached to a testing machine with effective stiffness K and effective mass m. The machine is commanded under displacement-control to move downward by a distance Δ, which sets the equilibrium displacement δ_0 of the indenter relative to the undeformed state. Let us investigate the dynamics of the indenter about this equilibrium state.

Scaling lengths by R and letting $\alpha = \pi k R^2/K$, it can be shown that the static deflection induced by the initial compression of the testing machine is, adopting the approximation

[3]The need for geometric compatibility conditions to close the system of equations is typical of contact problems. They can be regarded as equations for the location of the contact interface, which here means the quantity a.

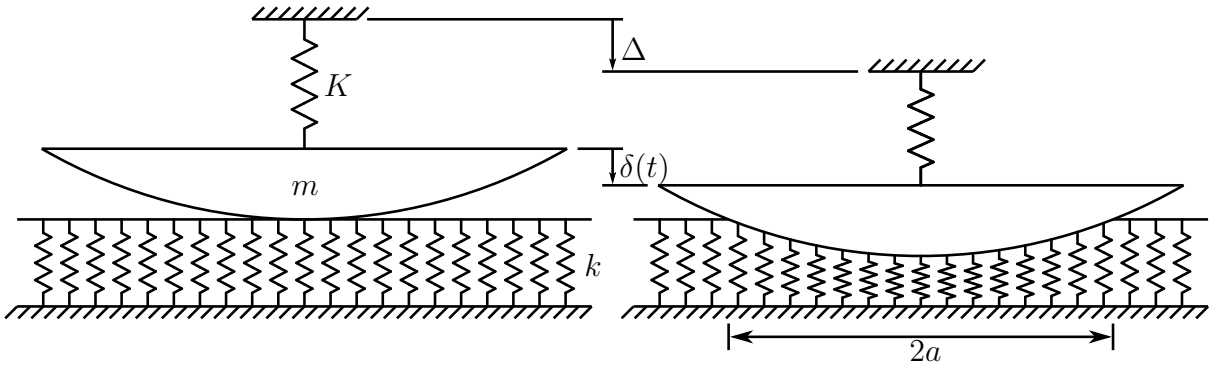

Figure 1.3: Cross-sectional schematic of a spherical indenter being pressed into an elastic foundation by a testing machine modeled by an effective spring.

from Section 1.1,

$$\delta_0 = \frac{\sqrt{1+4\alpha\Delta}-1}{2\alpha}. \tag{1.4}$$

With time scaled by $\sqrt{m/K}$, the equation of motion for the (dimensionless) absolute displacement δ of the indenter is

$$\ddot{\delta} + \delta + \alpha\delta^2 = \Delta. \tag{1.5}$$

Letting $x = \delta - \delta_0$ be the deviation of the indenter's position away from equilibrium, the equation of motion can be rewritten

$$\ddot{x} + \sqrt{1+4\alpha\Delta}\, x + \alpha x^2 = 0. \tag{1.6}$$

When the machine is very stiff relative to the foundation, $\alpha \ll 1$, and Eq. (1.6) is well-approximated by

$$\ddot{x} + x + \alpha x^2 = 0. \tag{1.7}$$

Equation (1.7) is the prototypical asymmetrical system in nonlinear vibration theory, sometimes called a quadratic Duffing equation, though this terminology is controversial. Since $\alpha > 0$, the nonlinearity is of hardening type, as is to be expected from the basic fact that increasingly large displacements cause the indenter to engage increasingly many springs in the foundation. As is the case for any nonlinear oscillator with an even nonlinearity, solutions of Eq. (1.7) will exhibit a dynamic offset so that the mean position about which oscillations take place is not $x = 0$. The quadratic nonlinearity also gives rise to a 2:1 superharmonic resonance, an occurrence we will encounter again in a more sophisticated system in Chapter 3. Adding forcing to this system can cause chaos in certain parameter regimes. Readers interested in the analysis of Eq. (1.7) should consult Nayfeh and Mook [4].

The system in Fig. 1.3 bears resemblance to an experimental apparatus constructed by Shui et al. [5] to demonstrate the use of small-amplitude, high-frequency vibrations to

increase the pull-off force of an indenter from an adhesive substrate. The authors observed experimentally that $a(t) - a_0$ exhibited both a dynamic offset and asymmetric oscillations about that offset. These effects were ascribed to asymmetry in the behavior of the adhesive during crack closure ($\dot{a} > 0$) and crack opening ($\dot{a} < 0$), but as our crude model shows, the same behaviors can theoretically occur in an indenter-foundation system with no adhesion at all.

1.3 Adhesive Contact Problems Can Have Multiple Solutions

The addition of adhesion can cause contact problems to have multiple solutions. Let us investigate the effect of adhesion on a variation of the system from Section 1.1. Here we will model the adhesion with the work-of-adhesion approach. This is a good model when adhesive bonds are broken over very small distances.

Let w_{ad} denote the work of adhesion, the energy required to break a unit area of adhesive bonds. Then, under the usual approximation $a/R \ll 1$, the total potential energy is

$$U = \int_0^a \frac{1}{2} k \left(\delta - \frac{r^2}{2R} \right)^2 \cdot 2\pi r \, \mathrm{d}r - F\delta - w_{\text{ad}} \pi a^2. \tag{1.8}$$

The previous relation of geometric compatibility, Eq. (1.2), no longer holds since the foundation is in tension in an annular region $b < r < a$. At $r = b$, material points of the indenter coincide with the original location of the foundation, while at $r = a$, the adhesive fibers are at their maximum extension $\sqrt{2w_{\text{ad}}/k}$. Geometry then dictates the following:

$$\delta = \frac{a^2}{2R} - \sqrt{\frac{2w_{\text{ad}}}{k}}, \tag{1.9}$$

which can then be used to express Eq. (1.8) as a function of a alone. Defining

$$a_c = \left(\frac{8R^2 w_{\text{ad}}}{k} \right)^{1/4}, \quad \delta_c = \sqrt{\frac{2w_{\text{ad}}}{k}}, \quad \text{and} \quad F_c = 2\pi R w_{\text{ad}}, \tag{1.10}$$

it can be shown that the condition $\mathrm{d}U/\mathrm{d}a = 0$ gives

$$\frac{F}{F_c} = \left(\frac{a}{a_c} \right)^4 - 2 \left(\frac{a}{a_c} \right)^2 \quad \Leftrightarrow \quad \frac{a}{a_c} = \sqrt{1 \pm \sqrt{1 + F/F_c}}. \tag{1.11}$$

Regarding Eq. (1.11) as a quadratic in $(a/a_c)^2$, we see that while just one solution exists when the indenter is under a compressive load ($F/F_c > 0$), there can be zero ($F/F_c < -1$), one ($F/F_c = -1$), or two solutions ($-1 < F/F_c < 0$) when the indenter is under tension. In the two-solution regime, the solution corresponding to the smaller value of a is unstable and

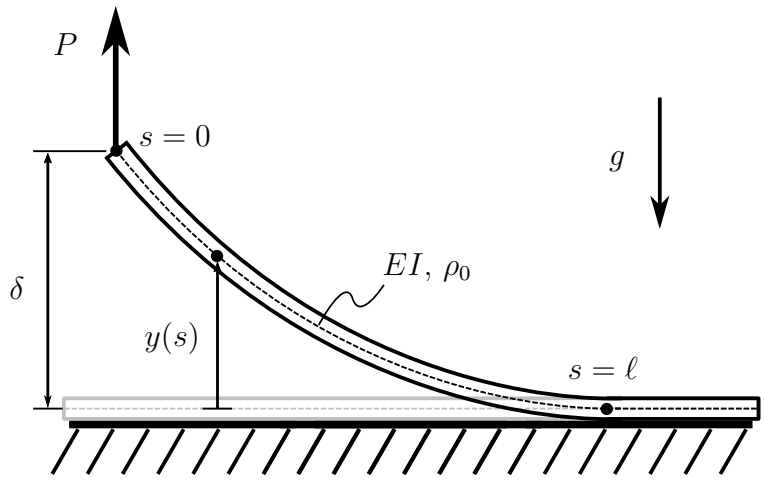

Figure 1.4: Heavy elastica being lifted from a rigid surface by a dead load.

therefore can only be realized experimentally under displacement-control. F_c is the pull-off force.

The appearance of a regime of multiple solutions is typical of models incorporating JKR adhesion. Chapter 4 explores such a problem in detail and also discusses a model of electrostatic adhesion that gives rise to *three* static solutions in certain parameter regimes, two stable and one unstable.

1.4 Contact Problems Can Be Approximately Linear

The lesson of Section 1.1 was that contact problems are inherently nonlinear, and that the nonlinearity is often *essential*, meaning that the force-displacement relationship cannot be linearized about the initial state. Here we showcase a system in which the relevant force-displacement relationship is essentially nonlinear, but becomes asymptotically linear for very large forces/displacements. The system is the heavy elastica: an unshearable, inextensible, semi-infinite elastic rod that is lifted by its end from a frictionless, rigid surface against the force of gravity. The presentation here is by no means novel [6].

Referring to the notation introduced in Fig. 1.4, elastica theory (cf. O'Reilly [7]) readily leads to the boundary-value problem

$$\begin{cases} EI\theta'' + (\rho_0 g s - P)\cos\theta = 0 & \text{for} \quad 0 < s < \ell \\ y' = \sin\theta & \text{for} \quad 0 < s < \ell \\ EI\theta' = 0 & \text{at} \quad s = 0 \\ \theta = 0, \quad EI\theta' = 0, \quad y = 0 & \text{at} \quad s = \ell \end{cases} . \tag{1.12}$$

Although the unknowns in the differential equations are only $\theta(s)$ and $y(s)$, a solution of Eq. (1.12) must also include ℓ, which specifies the location of the contact interface (a free

boundary). The condition $EI\theta'(\ell) = 0$ can be regarded an equation for ℓ, just as Eq. (1.2) served as an equation for a in the indenter problem. After solving Eq. (1.12), one can recover the tip displacement $\delta = y(0)$. Scaling lengths by $(EI/\rho_0 g)^{1/3}$ and forces by $(EI)^{1/3}(\rho_0 g)^{2/3}$, Eq. (1.12) can be written in the following dimensionless form:

$$\begin{cases} \theta'' + (s - P)\cos\theta = 0 & \text{for} \quad 0 < s < \ell \\ y' = \sin\theta & \text{for} \quad 0 < s < \ell \\ \theta' = 0 & \text{at} \quad s = 0 \\ \theta = 0, \quad \theta' = 0, \quad y = 0 & \text{at} \quad s = \ell \end{cases}. \tag{1.13}$$

A detailed treatment of Eq. (1.13) using perturbation theory can be found in the literature [6]. Here we instead focus on approximate solutions developed in an ad hoc fashion.

Consider first an approximation where θ is small, which is equivalent to using Euler-Bernoulli beam theory rather than elastica theory. The solution of the linearized problem is then as follows:

$$\begin{aligned} \theta(s) &\approx \frac{P}{2}\left(s^2 - \ell^2\right) - \frac{1}{6}\left(s^3 - \ell^3\right), \quad \ell \approx 2P, \\ y(s) &\approx \frac{P}{2}\left(\frac{1}{3}s^2 - \ell^2 s + \frac{2}{3}\ell^3\right) - \frac{1}{6}\left(\frac{1}{4}s^4 - \ell^3 s + \frac{3}{4}\ell^4\right). \end{aligned} \tag{1.14}$$

Simply evaluating $y(0)$, we find

$$\delta \approx \frac{2}{3}P^4, \tag{1.15}$$

which clearly shows $P \propto \delta^{1/4}$ when the problem is geometrically linearized. Once again the presence of a free boundary induces a nonlinear force-displacement relationship in an otherwise linear problem. It is interesting to note the one-quarter power on the displacement in this example, which is quite distinct from the power of two found for the indenter in Section 1.1.

Tackling the approximate solution for very large P is straightforward. Intuitively speaking, when the load is very large, the deformed rod will consist of an extremely long "outer" region where it essentially vertical and a very small boundary layer near $s = \ell$ where the it bends rapidly in order to ensure that $\theta = 0$, $\theta' = 0$, and $y = 0$ at $s = \ell$. Thus, for s outside of the boundary layer, we have an approximate solution as follows:

$$\theta(s) \approx -\frac{\pi}{2}, \quad y(s) \approx \ell - s, \quad \ell \approx P. \tag{1.16}$$

Again evaluating $y(0)$, it follows that

$$\delta \approx P. \tag{1.17}$$

Shockingly, despite being nonlinear at small displacements, the force-displacement relationship is asymptotically linear at large displacements! Solving Eq. (1.13) MATLAB's `bvp4c` and plotting the resulting force-displacement curve in Fig. 1.5, we see that the approximate analytical results from Eqs. (1.15) and (1.17) correctly reflect the limiting behavior of solutions.

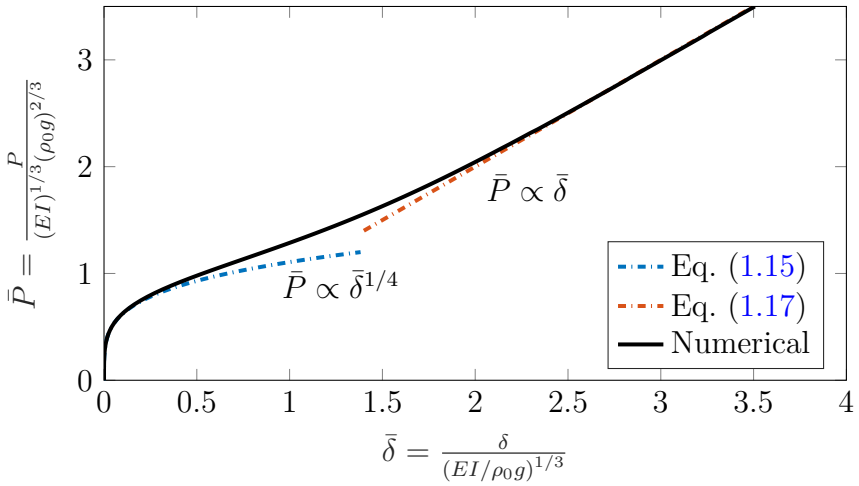

Figure 1.5: Dimensionless force versus displacement for the heavy elastica.

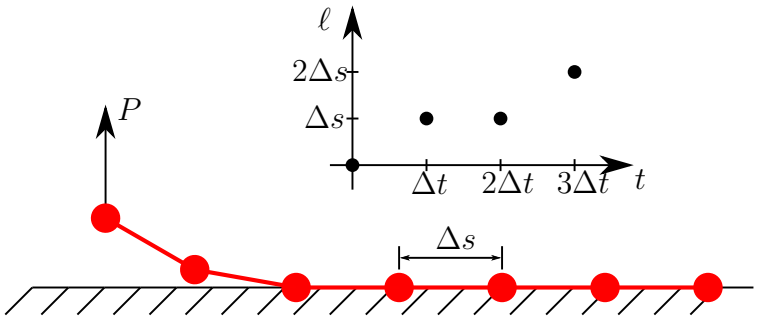

Figure 1.6: Problem with standard method for dynamic contact in finite element codes. The red dots are the nodes of a finite element mesh and the red segments the elements.

1.5 Contact Poses Computational Difficulties

Free-boundary problems require special numerical methods compared to their fixed-boundary counterparts, and contact problems are no exception. It should come as no surprise that the development of finite element methods for solid and structural mechanics that incorporate contact is a major area of ongoing research [8]. Standard algorithms implemented in most commercial finite element software, while sufficient for many practical applications where the bulk motion of the body is the most important feature to capture, have major shortcomings in applications where small-scale vibrations induced by repeated contact-impacts are the feature of interest and where long-run energy conservation is needed [9]. Since this is exactly the sort of problem that this dissertation concerns, we will require special numerical methods.

The shortcoming of the basic approach to contact in finite elements that is most deleterious for the type of problems that interest us is that the location of the contact interface

can only be resolved to within the typical element size. An illustration of what this means in the context of the dynamic version of the problem discussed in the preceding section is shown in Fig. 1.6. In this hypothetical scenario, the rod begins at $t = 0$ entirely in contact with the substrate. The load P is then applied instantaneously. After the first time step, the free length of the rod advances by one element, yielding $\ell(\Delta t) = \Delta s$. The rod continues to move upward during the next time step, but not enough to cause the next node to overcome the force of gravity, and thus $\ell(2\Delta t) = \Delta s$. After the third time step, the obstinate node releases and we find $\ell(3\Delta t) = 2\Delta s$.

The entirely fictional result for $\ell(t)$ is certainly not very accurate. After realizing this, our first instinct may be to reduce the time step and try again, but a moment of thought reveals that this would have absolutely no effect whatsoever on the resolution of ℓ, which can only take on the values $n\Delta s$, where n is a non-negative integer. We must refine the spatial mesh in order to increase the resolution. While halving the mesh size certainly yields a more computationally expensive calculation than halving the time step, the former may at first seem not to yield a prohibitively expensive problem. However, since the motion of the contact interface has an absolutely critical impact on the overall dynamics of the rod (see Chapter 3), the fact that ℓ is limited to certain quantized values means that, in essence, the rod "sees" a step-function input at each time step, a broadband excitation that can give rise to spurious frequency content in the resulting solution. This means that we must resolve the mesh as finely as possible (preferably to machine precision) if we wish to accurately capture the small-scale vibrations of the rod rather. The resulting computations would certainly be of prohibitive expense.

There exist several numerical techniques that can be used to overcome the problem described above. Finite element practitioners will be familiar with mortar-based contact, but those in the dynamics community tend to eschew it and similar approaches in favor of methods that explicitly follow the contact interface—what some might refer to as front-tracking methods. One such method that plays a prominent role in Chapters 2 to 4 involves mapping the unknown, variable domain at any given time/load step to some known, fixed domain. The idea is perhaps best illustrated by revisiting the problem from Section 1.4. Introducing a new coordinate $z = s/\ell$ maps the spatial domain from $0 < s < \ell$ to $0 < z < 1$. The mapped version of the original boundary-value problem, Eq. (1.13), no longer has a free boundary. Rather, ℓ is introduced into the equation of motion itself and can be treated simply as an unknown parameter. Any number of standard techniques, such as finite elements, can then be used to obtain a numerical solution. The downside of performing this variable transformation is that it greatly complicates the expression for the acceleration operator. Several other techniques for explicitly tracking the contact interface are discussed briefly in Chapter 3.

1.6 Outline

The remaining four chapters of this dissertation concern three case studies in contact dynamics. The spirit of each is to study the most basic representation of a structural-dynamic contact problem, neglecting as many nonlinearities as possible in order to isolate the effects of contact. The models we develop are not meant to be quantitatively accurate depictions of any real-life system, but rather qualitatively correct ones that help uncover some of the basic features one might expect to see in practice. Our approach is entirely analytical and computational, synthesizing techniques and terminology from several distantly related disciplines, from configurational mechanics to nonlinear vibrations.

Chapter 2, which is based on previously published work [10], concerns the *linear* vibration analysis of a rod problem inspired by two structural systems that experience contact at drastically different scales: microelectromechanical cantilevers (micron-scale) and flexible risers (kilometer-scale). The crux of the problem is how to perform a consistent linearization of the boundary conditions at the contact interface, and to determine the conditions under which the contact interface can be regarded as fixed during small superposed motions. We show that, when JKR adhesion is present, the naive approach to linearizing the boundary results is incorrect. Our procedure shows that this type of adhesion, at linear order, acts as a rotational spring at the boundary whose stiffness is set by the strength of adhesion. We also present extensive numerical results that show subtle connections between the existence of static solutions, their stability, and the nature of superposed linear vibrations.

In Chapter 3, also based on previously published work [11], we explore the *nonlinear* vibrations of the system studied in Chapter 2 using two techniques that are shown to have good agreement for typical parameter values: a finite element method and a perturbation method. The finite element method could be called an arbitrary Lagrangian-Eulerian method, and is used to track the moving contact interface accurately. After observing unusual features in the frequency response of the system as determined by the finite element method, we use the analytical perturbation method to show that these features are actually nonlinear resonances induced by the motion of the contact interface. We then go on to demonstrate that the same resonances can be expected to persist in a much broader class of problems in which a planar, elastic rod contacts a frictionless, smooth obstacle in the plane. This analysis is formulated using the gap function, a notion frequently employed in computational contact mechanics.

Having devoted considerable attention to one-dimensional structures deforming in the plane, we shift focus in Chapter 4, which is based on yet another published work [12], to a problem of a two-dimensional structure (a plate) deforming in space. The application is to electrostatically actuated microelectromechanical systems (MEMS), in particular the issue of "touchdown," where electrostatic forces cause an actuator (or sensor, or other device) to come into contact with the substrate on top of which it is built. After formulating the theory for non-axisymmetric deformations, we present detailed results for an axisymmetric actuator undergoing axisymmetric deformations. While some of the terminology may be unfamiliar to a typical mechanician, this chapter is meant to be accessible to those with no prior knowledge of MEMS, and serves as an exercise in theoretical mechanics that synthesizes a diverse array

of topics.

Finally, in the brief Chapter 5, we summarize the contributions of this dissertation and offer suggestions for further work in the exciting area of contact dynamics.

Chapter 2

On Contact Point Motion in the Vibration Analysis of Elastic Rods

2.1 Introduction

In studying the mechanics of elastic rods, one occasionally encounters problems in which the effective length of the rod is unknown a priori. Such problems are sometimes referred to as "variable-length" or "variable-arc-length" problems among rod mechanicians,[1] a simple example being the lifting of a heavy strip of paper from a table by an upward force applied to one end. Here the effective length is the length of the portion that is not in contact with the table. For a given upward force, this length (and hence the mathematical domain) is not immediately known and must instead be found as part of the solution. The formation of troublesome rucks in rugs and the nesting of rubber bands are other examples involving variable-length rods [16, 17].

Problems of the aforementioned type belong to the class of free boundary-value problems in mathematics. Because one cannot simply add functions defined on disparate domains, free boundary problems are inherently nonlinear and can produce nonlinear effects even if the underlying differential equations are linear. Furthermore, their solution requires the specification of more boundary conditions than their standard counterparts do. This is apparent in the case of the Euler-Bernoulli beam: a fixed-length beam needs four boundary conditions while a variable-length beam needs five.

It is a largely straightforward numerical computation to solve for the static configuration of a variable-length rod [18], and closed-form analytical solutions are typically available for the small-amplitude regime [6]. There is less understanding, however, on how to appropriately treat small-amplitude vibrations about a statically deformed configuration (both the

[1] The terms "variable-length" and "variable-arc-length" are sometimes used to refer to problems in which the rod's length varies as a prescribed function of time [13, 14], for example the ejection of paper from a photocopier [15]. However, we use these terms exclusively to refer to problems in which the length is variable *and also initially unknown*.

"small-on-small" and "small-on-large" analyses), even though this task is well-understood for rods of fixed length [19].

A more fundamental insight into the vibration of variable-length rods is certainly of interest from a theoretical point-of-view, but it is also relevant to several vibration-critical engineering applications. Submarine pipelines, flexible risers, and other marine structures that touch the seafloor are essentially variable-length rods [20, 21], as are micro-scale cantilever beams when they adhere electrostatically to the substrate of microelectromechanical systems (MEMS) [22]. Belt-driven transmissions at high speeds and/or with considerable slack can also be effectively modeled as variable-length (and axially translating) rods [23].

The principal difficulty in analyzing the vibrations of variable-length rods is readily illustrated in unilateral contact problems, such as the one illustrated in Fig. 2.1, in which the contact point moves left and right over the course of the vibratory motion. Some authors argue heuristically that the oscillations of this point are "small" in some sense relative to the overall amplitude of vibrations and proceed to treat the point as being fixed [24, 25]. Others apply variable transformations to map the free boundary to a fixed one [20, 22, 26], while others yet apply perturbation methods to the boundary conditions [21, 27, 28].

The goal of this chapter is to clarify the third approach, use it to explain when the first is applicable, and highlight why the second is an unnecessary complication if only linear vibrations are considered. We do all this in the context of the foregoing contact problem, but the technique we outline can be readily applied to a number of other situations involving variable-length rods, such as a roller support or sleeve constraint [29, 30]. Over the course of our analysis, which we present in considerable detail, we explain several counter-intuitive results from the literature. We conclude by providing a thorough numerical exploration of the parameter space for the problem depicted in Fig. 2.1.

2.2 Small-Amplitude Vibrations Superposed on Small-Amplitude Equilibria

We now study small-amplitude free vibrations about small-amplitude static equilibria of the system illustrated in Fig. 2.1, which was first introduced by Roy and Chatterjee [22] and is closely related to a system considered earlier by Demeio and Lenci [20]. In this section we treat the rod as an Euler-Bernoulli beam of linear density ρ_0 and flexural rigidity EI. It is clamped on its left end at a height a from a frictionless, adhesion-free horizontal substrate and is subjected to a downward gravitational force per unit length of magnitude $\rho_0 g$. The length $\ell = \ell(t)$ of the non-contacting segment of the beam is unknown a priori and must be determined as part of the solution. Under static conditions, the non-contacting length is denoted ℓ_0. The total length of the beam is L, which must be greater than $\ell(t)$ for physically meaningful solutions to exist.

As is usual with Euler-Bernoulli beams, it is permissible to exchange the arc-length coordinate s with the abscissa x, making $y = y(x,t)$ and $\ell = \ell(t)$ the sole dependent

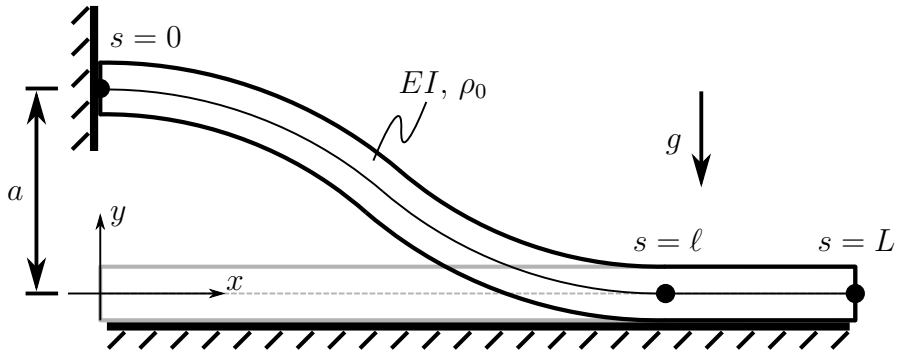

Figure 2.1: Schematic of the problem first considered by Roy and Chatterjee [22].

variables. The dynamics are governed by the familiar equation

$$\rho_0 \frac{\partial^2 y}{\partial t^2} + EI \frac{\partial^4 y}{\partial x^4} + \rho_0 g = 0, \quad 0 < x < \ell(t), \quad t > 0. \tag{2.1}$$

We now nondimensionalize Eq. (2.1). Scaling all lengths by a, scaling time t by $a^2\sqrt{\rho_0/EI}$, and defining $w = \rho_0 g a^3/EI$, we have

$$\frac{\partial^2 y}{\partial t^2} + \frac{\partial^4 y}{\partial x^4} + w = 0, \quad 0 < x < \ell(t), \quad t > 0. \tag{2.2}$$

We will work in dimensionless terms for the remainder of the chapter. Equation (2.2) is to be solved subject to the boundary conditions

$$y(0,t) = 1, \quad \frac{\partial y}{\partial x}(0,t) = 0, \tag{2.3}$$

and

$$y(\ell(t),t) = 0, \quad \frac{\partial y}{\partial x}(\ell(t),t) = 0, \quad \frac{\partial^2 y}{\partial x^2}(\ell(t),t) = 0. \tag{2.4}$$

Equation $(2.4)_3$ is a consequence of the lack of adhesion between the beam and the substrate.[2] Notice that five boundary conditions are required rather than the usual four because $\ell(t)$ is an additional unknown.

We briefly mention that the solution to the right of $x = \ell(t)$ is trivial and need not be given special consideration in the case of an Euler-Bernoulli beam, though this issue must be revisited in the nonlinear regime. Finally, we note that our interest is entirely in steady, oscillatory solutions so we do not specify initial conditions.

[2] If reversible adhesion were present, the right-hand side would be replaced by a constant $M_\ell > 0$ related to the adhesive energy between the beam and the substrate [31, 32].

Solution via Variable Transformation

The essence of the method used by Roy and Chatterjee [22] to analyze oscillatory solutions of Eqs. (2.2) to (2.4), first introduced by Demeio and Lenci [20] in a slightly different context, is to perform a change-of-variable that maps $x \in (0, \ell(t))$ to a fixed interval, namely $z = x/\ell(t) \in (0, 1)$. Such a transformation changes the free boundary-value problem into a standard boundary-value problem with the additional unknown $\ell(t)$ pushed into the differential equation itself. It also induces the interesting concept of an "extended" mode shape of a vibrating system that contains different material points at different instants in time.

However, the transformation comes at the cost of increased algebraic complexity, as is evident in the resulting expression for the acceleration operator. Writing $y(x,t) = y(\ell(t)z, t) =: \tilde{y}(z,t)$, it can be shown that Eq. (2.2) becomes

$$\frac{\partial^2 \tilde{y}}{\partial t^2} + \left(\frac{2\dot{\ell}^2}{\ell} - \ddot{\ell} \right) \frac{z}{\ell} \frac{\partial \tilde{y}}{\partial z} - \frac{2\dot{\ell} z}{\ell} \frac{\partial^2 \tilde{y}}{\partial t \partial z} + \left(\frac{\dot{\ell} z}{\ell} \right)^2 \frac{\partial^2 \tilde{y}}{\partial z^2} + \frac{1}{\ell^4} \frac{\partial^4 \tilde{y}}{\partial z^4} + w = 0, \tag{2.5}$$

where $0 < z < 1$ and $t > 0$. The increased complexity apparent in Eq. (2.5) does not make analysis impossible, but it does obscure some critical facets of the problem. An extensive calculation shows that the natural frequencies ω of small free vibrations about a static solution of Eq. (2.5), subject to the appropriate boundary conditions in the z-domain derived from Eqs. (2.3) and (2.4), are governed by

$$\cos\left(\sqrt{\omega}\ell_0\right) \cosh\left(\sqrt{\omega}\ell_0\right) - 1 = 0. \tag{2.6}$$

After unraveling the nondimensionalization, it becomes evident that Eq. (2.6) is *exactly* the same as the characteristic equation for the natural frequencies of a fixed-fixed beam with length equal to the static non-contacting length ℓ_0. This unexpected correspondence, first recognized by Roy and Chatterjee [22], seems nothing less than miraculous from the perspective of the preceding procedure. In the sequel, we demonstrate that the same result follows transparently from an alternative approach that also elucidates the conditions under which similarly unexpected correspondences may exist.

Solution via Regular Perturbation Expansion

Rather than transform the domain to one of a fixed length, we now elect to work directly with the original statement of the problem in the x-domain, Eqs. (2.2) to (2.4). To begin, we expand $y(x,t)$ and $\ell(t)$ in regular perturbation series:

$$y(x,t) = y_0(x) + \epsilon y_1(x,t) + O(\epsilon^2), \quad \ell(t) = \ell_0 + \epsilon \ell_1(t) + O(\epsilon^2). \tag{2.7}$$

We will truncate these series to $O(\epsilon)$ in order to obtain the leading-order dynamics about the static equilibrium. Inserting Eq. $(2.7)_1$ into Eq. (2.2) and grouping powers of ϵ, we find

$$\frac{d^4 y_0}{dx^4} + w = 0, \quad \frac{\partial^2 y_1}{\partial t^2} + \frac{\partial^4 y_1}{\partial x^4} = 0. \tag{2.8}$$

Equation (2.3) then implies the following boundary conditions at $x = 0$:

$$y_0(0) = 1, \quad y_1(0,t) = 0, \quad \frac{dy_0}{dx}(0) = 0, \quad \frac{\partial y_1}{\partial x}(0,t) = 0. \tag{2.9}$$

It is slightly more complicated to determine the consequences of the perturbation expansion for Eq. (2.4), the boundary conditions at the free boundary $x = \ell(t)$. Starting with Eq. $(2.4)_3$ and neglecting terms quadratic or higher in ϵ,

$$\begin{aligned} 0 &= \frac{\partial^2 y}{\partial x^2}(\ell(t),t) \\ &= \frac{\partial^2 y}{\partial x^2}(\ell_0 + \epsilon\ell_1(t),t) \\ &= \frac{d^2 y_0}{dx^2}(\ell_0 + \epsilon\ell_1(t)) + \epsilon\frac{\partial^2 y_1}{\partial x^2}(\ell_0 + \epsilon\ell_1(t),t) \\ &= \frac{d^2 y_0}{dx^2}(\ell_0) + \epsilon\left[\frac{d^3 y_0}{dx^3}(\ell_0)\ell_1(t) + \frac{\partial^2 y_1}{\partial x^2}(\ell_0,t)\right], \end{aligned} \tag{2.10}$$

which immediately yields

$$\frac{d^2 y_0}{dx^2}(\ell_0) = 0, \quad \frac{d^3 y_0}{dx^3}(\ell_0)\ell_1(t) + \frac{\partial^2 y_1}{\partial x^2}(\ell_0,t) = 0. \tag{2.11}$$

Carefully applying the same procedure to Eq. $(2.4)_2$, we obtain

$$\frac{dy_0}{dx}(\ell_0) = 0, \quad \underbrace{\frac{d^2 y_0}{dx^2}(\ell_0)}_{=0 \text{ by Eq. } (2.11)_1}\ell_1(t) + \frac{\partial y_1}{\partial x}(\ell_0,t) = 0. \tag{2.12}$$

Finally, we obtain from Eq. $(2.4)_1$,

$$y_0(\ell_0) = 0, \quad \underbrace{\frac{dy_0}{dx}(\ell_0)}_{=0 \text{ by Eq. } (2.12)_1}\ell_1(t) + y_1(\ell_0,t) = 0. \tag{2.13}$$

To summarize, we have the following straightforward-to-solve free boundary-value problem for the static equilibrium:

$$\frac{d^4 y_0}{dx^4} + w = 0, \tag{2.14}$$

$$y_0(0) = 1, \tag{2.15}$$

$$\frac{dy_0}{dx}(0) = 0, \tag{2.16}$$

$$y_0(\ell_0) = 0, \tag{2.17}$$

$$\frac{dy_0}{dx}(\ell_0) = 0, \tag{2.18}$$

$$\frac{d^2 y_0}{dx^2}(\ell_0) = 0, \tag{2.19}$$

which has the solution

$$y_0(x) = \left(1 - \frac{x}{\ell_0}\right)^3 \left(1 + \frac{3x}{\ell_0}\right), \quad \ell_0 = \left(\frac{72}{w}\right)^{1/4}. \tag{2.20}$$

Additionally, $y_1(x,t)$ is governed by

$$\frac{\partial^2 y_1}{\partial t^2} + \frac{\partial^4 y_1}{\partial x^4} = 0, \tag{2.21}$$

$$y_1(0,t) = 0, \tag{2.22}$$

$$\frac{\partial y_1}{\partial x}(0,t) = 0, \tag{2.23}$$

$$y_1(\ell_0,t) = 0, \tag{2.24}$$

$$\frac{\partial y_1}{\partial x}(\ell_0,t) = 0. \tag{2.25}$$

Finally, $\ell_1(t)$ is determined from the sole remaining piece of information derived from the original boundary conditions, Eq. $(2.11)_2$.

Equations (2.21) *to* (2.25) *are precisely the equations governing the dynamics of a fixed-fixed beam of length* ℓ_0*!* This transparently shows the same result obtained in Section 2.2 by way of a clever but substantially more involved computation. In fact, our result is somewhat more general: it is not just the natural frequencies that are the same as those for a fixed-fixed beam of appropriate length, but rather the *entire first-order dynamics*. The present method also illustrates the interesting fact that *the dynamical effect of the motion of the contact point is negligible to first order and hence the concept of an "extended" mode shape as introduced in Section 2.2 is superfluous*. Lastly, it is interesting to observe that the neither the static solution, Eq. (2.20), nor the dynamics defined by Eqs. (2.21) to (2.25) depend on the specific weight w except through ℓ_0.

Solution to a Modified Problem

Roy and Chatterjee also consider an alternate problem without gravity but with an adhesive substrate [22]. They find that the equation for the natural frequencies in this case does *not* correspond to any well-known formula. Our method makes it easy to see why this is the case. We will consider the combined effect of gravity and adhesion, but the results readily degenerate to the adhesion-only case.

When adhesion is present, Eq. $(2.4)_3$ is replaced by

$$\frac{\partial^2 y}{\partial x^2}(\ell(t),t) = M_\ell, \tag{2.26}$$

where $M_\ell > 0$ is a specified constant related to the adhesion energy between the rod and the substrate [31, 32]. Equation $(2.11)_1$ is then replaced by

$$\frac{d^2 y_0}{dx^2}(\ell_0) = M_\ell, \tag{2.27}$$

whence Eq. $(2.12)_2$ becomes

$$M_\ell \ell_1(t) + \frac{\partial y_1}{\partial x}(\ell_0, t) = 0, \tag{2.28}$$

or, upon combination with Eq. $(2.11)_2$,

$$\underbrace{\frac{\partial^2 y_1}{\partial x^2}(\ell_0, t)}_{\text{bending moment}} = K \underbrace{\frac{\partial y_1}{\partial x}(\ell_0, t)}_{\text{rotation angle}}, \quad K = \frac{1}{M_\ell}\frac{d^3 y_0}{dx^3}(\ell_0). \tag{2.29}$$

Notice that Eq. (2.29) is equivalent to a rotational spring at the boundary $x = \ell_0$ with (dimensionless) stiffness K, which in general depends on the constant M_ℓ that characterizes adhesion as well as the static configuration $\{y_0(x), \ell_0\}$. Omitting some minor details, said configuration can be shown to be governed by Eqs. (2.14) to (2.18) and Eq. (2.27). The solution is

$$y_0(x) = (\ell_0 - x)^2 \left[\frac{1}{2}M_\ell + \frac{1}{6}\left(\frac{1}{3}w\ell_0 - \frac{2}{\ell_0}M_\ell\right)(\ell_0 - x) - \frac{1}{24}w(\ell_0 - x)^2\right], \tag{2.30}$$

where the non-contacting length ℓ_0 is such that is satisfies

$$w\ell_0^4 + 12M_\ell\ell_0^2 - 72 = 0. \tag{2.31}$$

Equation (2.31) is quadratic in ℓ_0^2 and hence physically meaningful solutions exist only if the discriminant is non-negative, which implies the simple constraint $M_\ell^2 + 2w \geq 0$. The system can therefore only access a certain region of the (w, M_ℓ)-plane.

Where solutions do exist, it is instructive to classify them into two types. We call a solution *gravity-dominant* if the vertical force between the beam and the substrate at $x = \ell_0$ is compressive. If said force is tensile, we call the solution *adhesion-dominant*. The boundary between these two regions in the (w, M_ℓ)-plane is characterized by zero vertical force at $x = \ell_0$. It can be shown using Eq. (2.30) and Eq. (2.31) that points on the boundary satisfy $2w = 3M_\ell^2$. Figure 2.2 is a graphical classification of the static equilibria in the parameter space.

The first-order dynamics[3] in the case of combined gravity and adhesion are governed by Eqs. (2.21) to (2.24) and Eq. (2.29), except with the rotational spring stiffness K given according to

$$K = \frac{1}{M_\ell}\frac{d^3 y_0}{dx^3}(\ell_0) = \frac{2}{\ell_0} - \frac{w\ell_0}{3M_\ell}. \tag{2.32}$$

Such a set of equations of course describe a beam fixed at $x = 0$ and restrained by a rotational spring at $x = \ell_0$. This specific combination of boundary conditions does not constitute a standard case and hence it is natural that Roy and Chatterjee [22] did not recognize the correspondence from the characteristic equation for the natural frequencies of free vibration.

[3]Notice that when $w = 0$ the dynamics depend on M_ℓ only through ℓ_0, just as the dynamics depend on w only through ℓ_0 when $M_\ell = 0$.

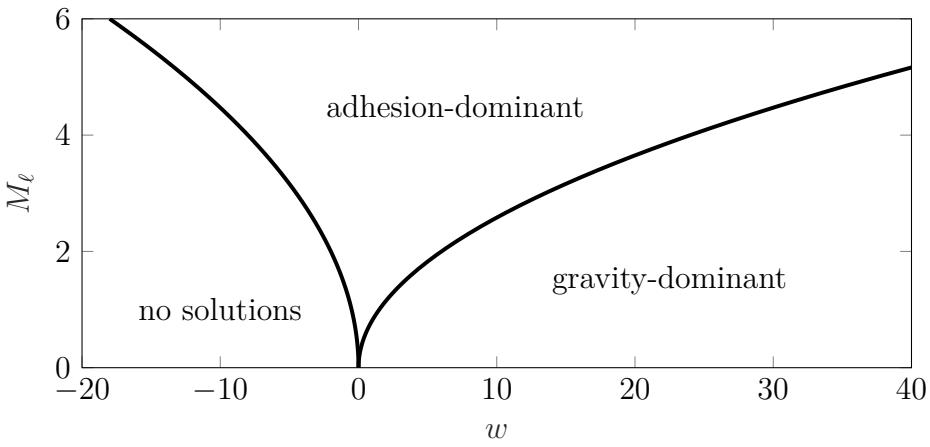

Figure 2.2: Classification of solutions to the static problem in terms of the parameters w and M_ℓ, according to the linear (Euler-Bernoulli) analysis.

It is a mostly elementary exercise to solve for the natural frequencies and we report the procedure in A.1; when $w = 0$ the results agree with Roy and Chatterjee's.[4]

2.3 Small-Amplitude Vibrations Superposed on Large-Amplitude Equilibria

Understanding now the general procedure by which one can analyze small-amplitude vibrations of variable-length Euler-Bernoulli beams about small-amplitude static configurations, it is not a particularly challenging task to pass through to the small-on-large regime for an inextensible, unshearable, planar elastica of variable length. In this section and the next we again specialize our results to the problem considered in the linear context in Section 2.2, including the effects of both gravity and adhesion, but the procedure by which one would solve a more general class of problems should be evident.

[4]Roy and Chatterjee [22] use a different nondimensionalization than we do. Their angular natural frequencies are numerically equivalent to our $\omega\ell_0^2$.

General Solution Procedure

Following notation similar to that used elsewhere [7, 19, 24], the dimensionless governing equations can be expressed in slightly modified form as

$$\frac{\partial F}{\partial s} = \frac{\partial^2 x}{\partial t^2}, \tag{2.33}$$

$$\frac{\partial G}{\partial s} = \frac{\partial^2 y}{\partial t^2} + w, \tag{2.34}$$

$$\frac{\partial m}{\partial s} = F\sin\theta - G\cos\theta, \tag{2.35}$$

$$\frac{\partial \theta}{\partial s} = m, \tag{2.36}$$

$$\frac{\partial x}{\partial s} = \cos\theta, \tag{2.37}$$

$$\frac{\partial y}{\partial s} = \sin\theta, \tag{2.38}$$

all of which hold for $0 < s < \ell(t)$ and $t > 0$. All lengths have been scaled by a, the forces F and G by EI/a^2, the bending moment m by EI/a, and time t by $a^2\sqrt{\rho_0/EI}$. As in Section 2.3, $w = \rho_0 g a^3/EI$.

Equations (2.33) and (2.34) are the horizontal and vertical components of the balance of linear momentum, respectively, while Eq. (2.35) is the balance of angular momentum, neglecting rotary inertia. Equation (2.36) is the moment-curvature constitutive law. Finally, Eqs. (2.37) and (2.38) are collectively the definition of the angle θ. Equations (2.33) to (2.38) require seven total boundary conditions rather than the usual six, as $\ell(t)$ is an additional unknown.

Our derivation follows a recipe only incrementally more complex than that employed in Section 2.2. It is as follows:

- Assume that each of the seven dependent variables—F, G, m, θ, x, y, and ℓ—can be written as a static term plus a small dynamic term, e.g., $m(s,t) = m_0(s) + \epsilon m_1(s,t)$, $\epsilon \ll 1$.

- Plug the aforementioned *Ansätze* into Eqs. (2.33) to (2.38) and expand terms in Taylor series as needed to isolate the coefficients of ϵ^0 and ϵ^1. The former yield the differential equations governing the static terms (e.g., $m_0(s)$), while the latter yield those governing the dynamic terms (e.g., $m_1(s,t)$), which will depend parametrically on the static solution.

- Plug the *Ansätze* into the boundary conditions and again expand in Taylor series as needed to isolate a hierarchy of boundary conditions, paying special attention to the conditions at $s = \ell(t)$. Seven boundary conditions for the static variables will result as well as seven for the dynamic variables. However, the latter can be combined in

such a way so as to produce just six conditions (the total number needed to specify the solution for the dynamic problem on the fixed interval $0 < s < \ell_0$), as well as an equation for $\ell_1(t)$ in terms of the static and dynamic solutions.

- Assume that each dynamic term (except for $\ell_1(t)$) is the product of a function of s and a sinusoid, e.g., $m_1(s,t) = \hat{m}_1(s)\cos(\omega t)$. The collection of the "hatted" functions constitutes the mode shape of the rod and ω is the natural frequency that must be determined as part of the solution.
- Obtain boundary conditions for the mode shapes from the boundary conditions for the dynamic variables.

This procedure is in fact quite general and can be applied to a range of problems.

Perturbation Expansion of Governing Equations

We now explicitly apply the small-on-large analysis procedure introduced in Section 2.3 to the familiar example illustrated in Fig. 2.1, and for which Eqs. (2.33) to (2.38) govern the solution. After linearization we find the following equations for the static configuration:

$$\frac{dF_0}{ds} = 0, \tag{2.39}$$

$$\frac{dG_0}{ds} = w, \tag{2.40}$$

$$\frac{dm_0}{ds} = F_0 \sin\theta_0 - G_0 \cos\theta_0, \tag{2.41}$$

$$\frac{d\theta_0}{ds} = m_0, \tag{2.42}$$

$$\frac{dx_0}{ds} = \cos\theta_0, \tag{2.43}$$

$$\frac{dy_0}{ds} = \sin\theta_0. \tag{2.44}$$

The procedure also results in the following equations for the first-order dynamics:

$$\frac{\partial F_1}{\partial s} = \frac{\partial^2 x_1}{\partial t^2}, \tag{2.45}$$

$$\frac{\partial G_1}{\partial s} = \frac{\partial^2 y_1}{\partial t^2}, \tag{2.46}$$

$$\frac{\partial m_1}{\partial s} = (F_0\theta_1 - G_1)\cos\theta_0 + (G_0\theta_1 + F_1)\sin\theta_0, \tag{2.47}$$

$$\frac{\partial \theta_1}{\partial s} = m_1, \tag{2.48}$$

$$\frac{\partial x_1}{\partial s} = -\theta_1 \sin\theta_0, \tag{2.49}$$

$$\frac{\partial y_1}{\partial s} = \theta_1 \cos\theta_0. \tag{2.50}$$

Equations (2.39) to (2.44) and Eqs. (2.45) to (2.50) are of course the same well-known sets of equations that govern small-on-large vibrations of fixed-length rods [19, 24].

Perturbation Expansion of Boundary Conditions

The appropriate boundary conditions at $s = 0$ are

$$\theta(0,t) = 0, \quad x(0,t) = 0, \quad y(0,t) = 1, \tag{2.51}$$

which are readily linearized to yield

$$\theta_0(0) = 0, \quad x_0(0) = 0, \quad y_0(0) = 1, \tag{2.52}$$

and

$$\theta_1(0,t) = 0, \quad x_1(0,t) = 0, \quad y_1(0,t) = 0. \tag{2.53}$$

Three relatively obvious boundary conditions at the contact point $s = \ell(t)$ are

$$m(\ell(t),t) = M_\ell, \quad \theta(\ell(t),t) = 0, \quad y(\ell(t),t) = 0. \tag{2.54}$$

Equations (2.51) and (2.54) altogether make up six boundary conditions, but seven are required to fully specify a solution. It is not immediately apparent what the seventh condition should be, but a hint is provided by the fact that there was no such confusion in Section 2.2. The essential effect that the foregoing approach neglects, but that is present in the small-on-large case, is horizontal momentum. Thus, it is likely that the missing condition should somehow involve $F(\ell(t),t)$, the axial force in the rod at the contact point.

Indeed, the segment $\ell(t) < s < L$ carries horizontal momentum as it slides left and right along the frictionless substrate, and this must be reflected in the force $F(\ell(t),t)$. A balance of linear momentum quickly yields

$$-F(\ell(t),t) = [L - \ell(t)]\,\frac{\partial^2 x}{\partial t^2}(\ell(t),t) - \dot{\ell}(t)\frac{\partial x}{\partial t}(\ell(t),t), \tag{2.55}$$

which we emphasize is the elusive boundary condition in its dimensionless form. Notice that an additional parameter that was not present in the linear analysis has been introduced, namely the total length of the rod L.[5] There are two important limiting cases for this parameter: $L-\ell(t)\to 0^+$ and $L-\ell(t)\to\infty$. In the former, the rod contacts the substrate only over a very small region such that there is effectively zero axial force to first order acting at $s=\ell(t)$. In the latter, the inertia of the contacting segment is so large that it cannot accelerate along the substrate.

Writing the appropriate variables as regular perturbation series in ϵ, inserting them into Eqs. (2.54) and (2.55), expanding in Taylor series, and grouping like powers of ϵ, it is straightforward to show

$$F_0(\ell_0)=0,\quad m_0(\ell_0)=M_\ell,\quad \theta_0(\ell_0)=0,\quad y_0(\ell_0)=0, \tag{2.56}$$

and

$$\underbrace{\frac{dF_0}{ds}(\ell_0)}_{=0 \text{ by Eq. (2.39)}}\ell_1(t)+F_1(\ell_0,t)+(L-\ell_0)\frac{\partial^2 x_1}{\partial t^2}(\ell_0,t)=0, \tag{2.57}$$

$$\frac{dm_0}{ds}(\ell_0)\ell_1(t)+m_1(\ell_0,t)=0, \tag{2.58}$$

$$\underbrace{\frac{d\theta_0}{ds}(\ell_0)}_{=M_\ell \text{ by Eqs. (2.42) and (2.56)}_2}\ell_1(t)+\theta_1(\ell_0,t)=0, \tag{2.59}$$

$$\underbrace{\frac{dy_0}{ds}(\ell_0)}_{=0 \text{ by Eqs. (2.44) and (2.56)}_3}\ell_1(t)+y_1(\ell_0,t)=0. \tag{2.60}$$

Combining Eqs. (2.58) and (2.59) in order to eliminate $\ell_1(t)$ results in a rotational spring boundary condition:

$$m_1(\ell_0,t)=K\theta_1(\ell_0,t),\quad K=\frac{1}{M_\ell}\frac{dm_0}{ds}(\ell_0). \tag{2.61}$$

The spring constant K can be simplified somewhat by evaluating Eq. (2.41) at $s=\ell_0$ and taking into account Eq. $(2.56)_{1,3}$. Thus

$$K=-\frac{G_0(\ell_0)}{M_\ell}, \tag{2.62}$$

such that the stiffness of the spring is set by the ratio of the static shear force to the static bending moment at $s=\ell_0$.

[5] We reiterate that physically meaningful solutions only exist when $\ell(t)<L$.

To summarize, the boundary conditions for the dynamic variables at $s = \ell_0$ are

$$F_1(\ell_0, t) + (L - \ell_0)\frac{\partial^2 x_1}{\partial t^2}(\ell_0, t) = 0, \quad m_1(\ell_0, t) = K\theta_1(\ell_0, t), \quad y_1(\ell_0, t) = 0, \tag{2.63}$$

with K as in Eq. (2.62). We now have six boundary conditions on the dynamic variables, the correct number required to specify a solution on $0 < s < \ell_0$. However, we have not used all of the information contained in Eqs. (2.57) to (2.60). In particular, we can use Eq. (2.58) to show

$$\ell_1(t) = \frac{m_1(\ell_0, t)}{G_0(\ell_0)}, \tag{2.64}$$

meaning that once the static and dynamic solutions are known, $\ell_1(t)$ can be computed with ease. It should be emphasized that $\ell_1(t)$ does not appear anywhere else in the equations that result from our solution procedure. Furthermore, in contrast to the small-on-small case discussed in Section 2.2, the boundary conditions at the contact point for the small-on-large analysis (i.e., Eq. (2.63)) do *not* in general represent a spatially fixed rotational spring but rather a rotational spring plus an attached mass that is free to slide horizontally.

Determination of Modes of Free Vibration

At this stage the static problem is fully defined by Eqs. (2.39) to (2.44) subject to Eq. (2.52) and Eq. (2.56). The dynamic problem is fully defined by Eqs. (2.45) to (2.50) subject to Eq. (2.53) and Eq. (2.63), and we seek solutions in which each of the *six* dynamic variables F_1, G_1, m_1, θ_1, x_1, and y_1 is separable into a mode shape and a sinusoid of angular frequency ω, e.g., $m_1(s, t) = \hat{m}_1(s)\cos(\omega t)$. Notice that, unlike previous work on similar problems (see [20, 22]), we make absolutely no assumption about the nature of $\ell_1(t)$, most certainly not the severe restriction that it too be sinusoidal with frequency ω.

It is easy to show from Eqs. (2.45) to (2.50) that the ordinary differential equations governing the mode shape are

$$\frac{d\hat{F}_1}{ds} = -\omega^2 \hat{x}_1, \tag{2.65}$$

$$\frac{d\hat{G}_1}{ds} = -\omega^2 \hat{y}_1, \tag{2.66}$$

$$\frac{d\hat{m}_1}{ds} = (F_0\hat{\theta}_1 - \hat{G}_1)\cos\theta_0 + (G_0\hat{\theta}_1 + \hat{F}_1)\sin\theta_0, \tag{2.67}$$

$$\frac{d\hat{\theta}_1}{ds} = \hat{m}_1, \tag{2.68}$$

$$\frac{d\hat{x}_1}{ds} = -\hat{\theta}_1 \sin\theta_0, \tag{2.69}$$

$$\frac{d\hat{y}_1}{ds} = \hat{\theta}_1 \cos\theta_0. \tag{2.70}$$

The corresponding boundary conditions are likewise straightforward to obtain. Equation (2.53) promptly leads to

$$\hat{\theta}_1(0) = 0, \quad \hat{x}_1(0) = 0, \quad \hat{y}_1(0) = 0, \tag{2.71}$$

while Eq. (2.63) yields

$$\hat{F}_1(\ell_0) = \omega^2(L - \ell_0)\hat{x}_1(\ell_0), \quad \hat{m}_1(\ell_0) = K\hat{\theta}_1(\ell_0), \quad \hat{y}_1(\ell_0) = 0. \tag{2.72}$$

Equation $(2.72)_1$, which reflects a sort of spring with frequency-dependent stiffness, makes apparent two interesting limiting behaviors. For low-frequency oscillations ($\omega \to 0^+$), the point $s = \ell_0$ is connected to a rotational spring that is entirely free to move horizontally. By contrast, for high-frequency oscillations ($\omega \to \infty$), the point $s = \ell_0$ is connected to a spatially fixed rotational spring.

Once the static solution, mode shape, and natural frequency have been computed, one can calculate from Eq. (2.64) that

$$\ell_1(t) = \frac{\hat{m}_1(\ell_0)}{G_0(\ell_0)} \cos(\omega t), \tag{2.73}$$

which shows that $m_1(s,t)$ being time-harmonic with angular frequency ω induces the same in $\ell_1(t)$. We emphasize that this was not assumed a priori.

Summary of Equations

To summarize, one must first solve Eqs. (2.39) to (2.44), subject to Eq. (2.52) and Eq. (2.56), for the static solution: the functions $F_0(s)$, $G_0(s)$, $m_0(s)$, $\theta_0(s)$, $x_0(s)$, and $y_0(s)$ on the interval $0 < s < \ell_0$, as well as the constant ℓ_0. Then, using said solution, one solves Eqs. (2.65) to (2.70), subject to Eqs. (2.71) and (2.72), for the mode shape defined by the functions $\hat{F}_1(s)$, $\hat{G}_1(s)$, $\hat{m}_1(s)$, $\hat{\theta}_1(s)$, $\hat{x}_1(s)$, and $\hat{y}_1(s)$ on the (now) fixed interval $0 < s < \ell_0$, as well as for the natural frequency ω. Thereafter $\ell_1(t)$ can be recovered according to Eq. (2.73) if so desired.

Just as in standard linear vibration analysis, the mode shape is only unique up to a scalar multiple; there are seven unknowns but just six boundary conditions. By Eq. (2.73), the amplitude of the contact point oscillations is also indeterminate. For given values of the specific weight w, adhesive moment M_ℓ, and total length L, we use MATLAB's `bvp4c` solver to obtain numerical solutions of the standard boundary-eigenvalue problems for the static configuration, the mode shape, and the natural frequency. Because the amplitude of the mode shape is inherently indeterminate, it is necessary to specify an additional "fake" boundary condition that is independent of the others so as to ensure the numerical problem is not underdetermined.

2.4 Results

We now present the results of an extensive exploration of the parameter space of w, M_ℓ, and L. For the determination of the static configuration, we need not specify the total length L so long as we assume it is large enough that $L > \ell_0$, which we shall do. However, for the determination of the mode shapes and natural frequencies it is in fact necessary to specify a particular value of L. In order to limit the scope of our presentation to the convenient, two-dimensional parameter space (w, M_ℓ), we would like to take the limit $L \to \infty$, in which case we naively expect Eq. $(2.72)_1$ would degenerate to a boundary condition akin to a spatially fixed rotational spring. However, we will demonstrate shortly that said limit is in fact singular in the sense that, if we first take $L \to \infty$ and then take $w \to 0^+$ and $M_\ell \to 0^+$, we obtain natural frequencies that differ by a finite amount from the results of the small-on-small analysis, in which $w \to 0^+$ and $M_\ell \to 0^+$ are assumed at the outset. A related singular limit has been identified in analyzing the vibration of a fixed-length rod about its static configuration [19], so it is not too surprising that one appears here as well.

Static Equilibrium

We first study the simple correspondence between the static non-contacting length ℓ_0 and the parameters w and M_ℓ. (Recall that L does not affect the static equilibrium so long as we take it large enough that $L > \ell_0$.) Figure 2.3 depicts the parametric dependence of ℓ_0 in the gravity-only and adhesion-only cases. We see that the linear analysis of Section 2.2 provides a satisfactory approximation when $w \ll 1$ or $M_\ell \ll 1$, but at the same time $\ell_0 \to \infty$ as $w \to 0^+$ and $M_\ell \to 0^+$, a first sign that we might be facing a problem with a singular limit.

As in the beam-theoretic analysis of Section 2.2, there are only certain regions of the (w, M_ℓ)-plane that the rod can occupy. Perhaps surprisingly, solutions to the nonlinear problem appear only to exist, based purely on our numerical results, subject to the same condition obtained previously, i.e., $M_\ell^2 + 2w \geq 0$. The boundary between the gravity-dominant and adhesion-dominant regions, however, is different, as is easily seen in Fig. 2.4, which depicts the various regions in the plane and introduces a color scheme used in subsequent plots. It also shows how the static non-contacting length ℓ_0 varies according to w and M_ℓ. Notice that the boundary of the "no solution" region can be thought of as the contour corresponding to $\ell_0 \to \infty$.

Mode Shapes and Natural Frequencies

As a first step in understanding the vibration behavior, we focus on the case where $w > 0$ and $M_\ell = 0$, remembering that the parameter L must be reintroduced. We are interested in examining the natural frequencies in the limit $w \to 0^+$ for various L, and determining how they relate to those obtained via the linear analysis presented in Section 2.2 and expounded upon in A.1.

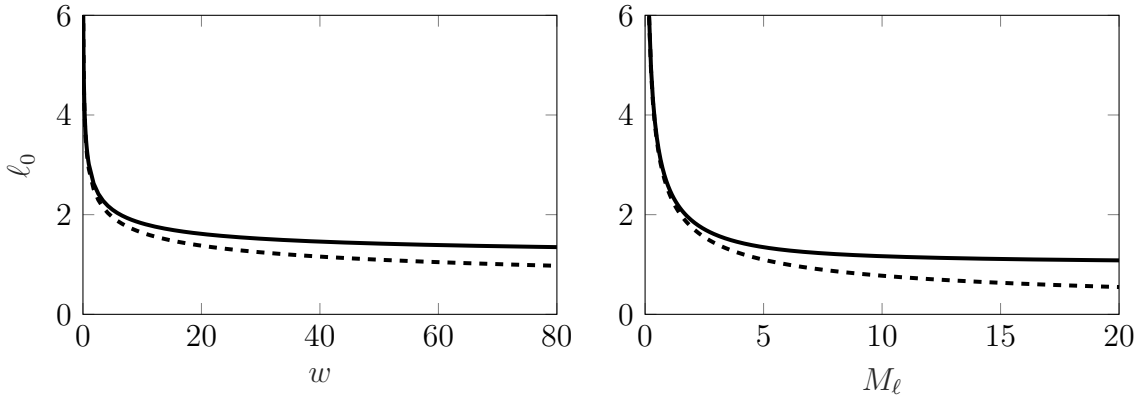

(a) Gravity only.

(b) Adhesion only.

Figure 2.3: Dependence of the static non-contacting length ℓ_0 on the weight per unit length w and adhesive moment M_ℓ when (a) $M_\ell = 0$ and (b) $w = 0$. The dashed lines correspond to the results from the Euler-Bernoulli analysis, Eq. (2.31), when $M_\ell = 0$ and $w = 0$, respectively.

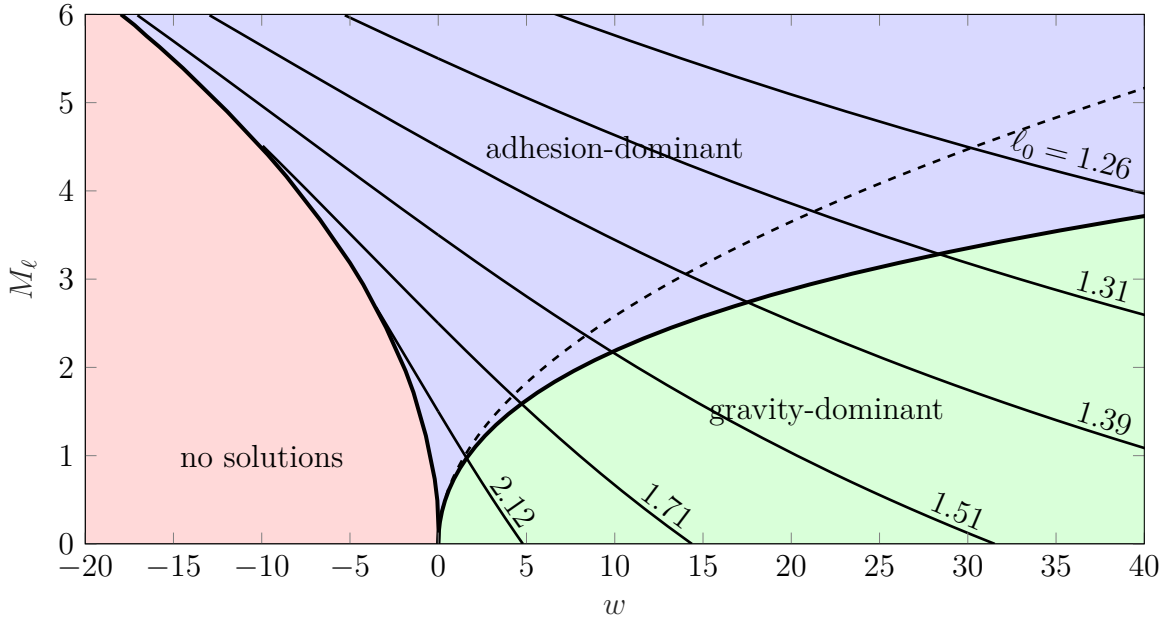

Figure 2.4: Classification of static solutions to the fully nonlinear problem according to the parameters w and M_ℓ and a sample of contours of constant non-contacting length ℓ_0. The dotted line is the boundary determined from the linear analysis of Section 2.2.

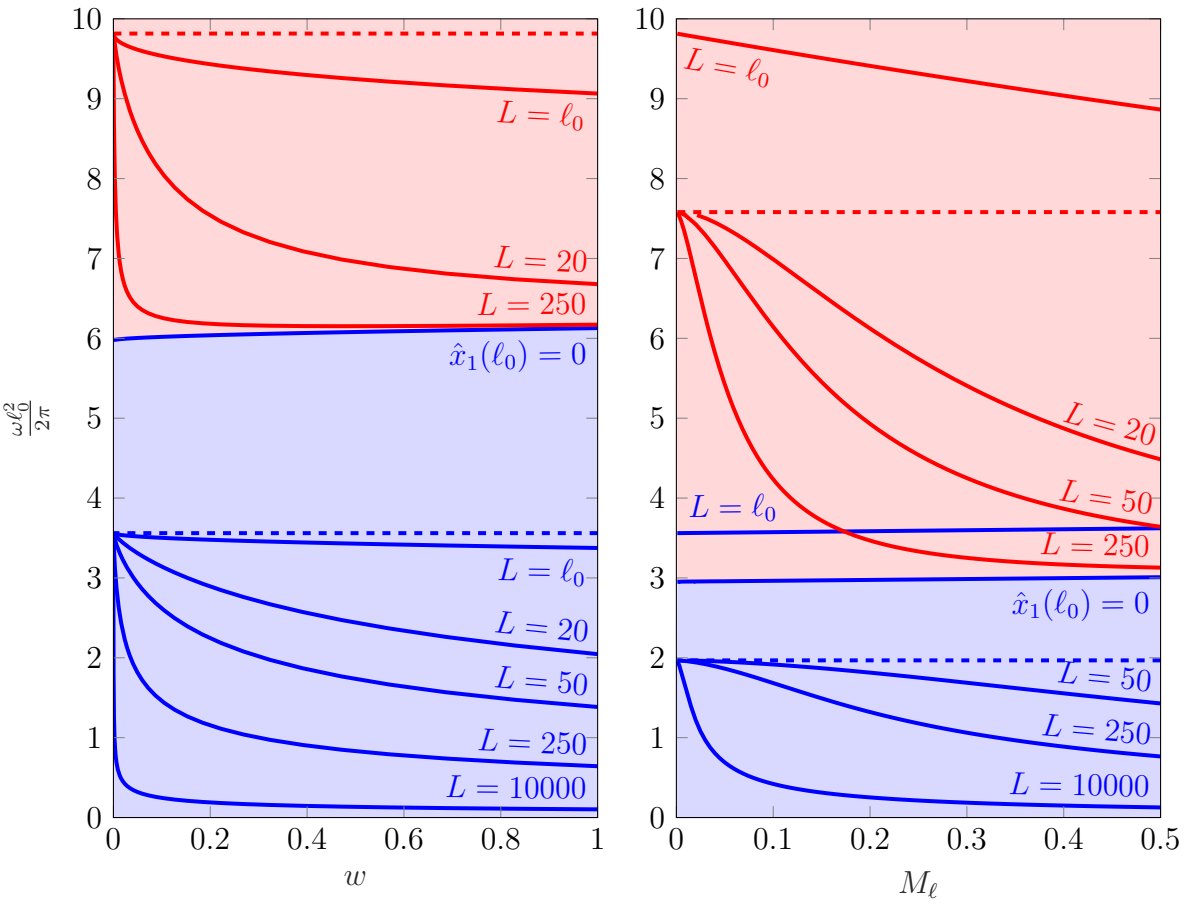

(a) Gravity only.

(b) Adhesion only.

Figure 2.5: Dependence of the first two natural frequencies on the weight per unit length w and adhesive moment M_ℓ when (a) $M_\ell = 0$ and (b) $w = 0$. The dashed lines correspond to the results for the Euler-Bernoulli beam, i.e. the first two roots of Eq. (2.6) and Eq. (A.10), respectively. Blue curves indicate the first natural frequencies and red ones the second.

Recall that $L = \ell_0$ corresponds to a rod whose tip is just barely touching the substrate and, by Eq. $(2.72)_1$, $\hat{F}_1(\ell_0) = 0$. For L very large, on the other hand, we expect (naively) that $\hat{x}_1(\ell_0) = 0$. With reference to Fig. 2.5a, observe that as L is increased, a boundary layer develops in the vicinity of $w = 0$ and, in the limit $L \to \infty$, the first natural frequency appears to tend toward zero for all w. However, if we take the boundary condition $\hat{x}_1(\ell_0) = 0$, then the first natural frequency for any given w is obviously not zero, but rather some finite value, hence the singular nature of the problem. Said finite value then serves as the lower bound for the *second* natural frequency for all L, again shown in Fig. 2.5a.

In a certain sense, the limit $L \to \infty$ causes the first mode to "disappear." Indeed, there is a marked qualitative difference in the mode shape when one takes as a boundary

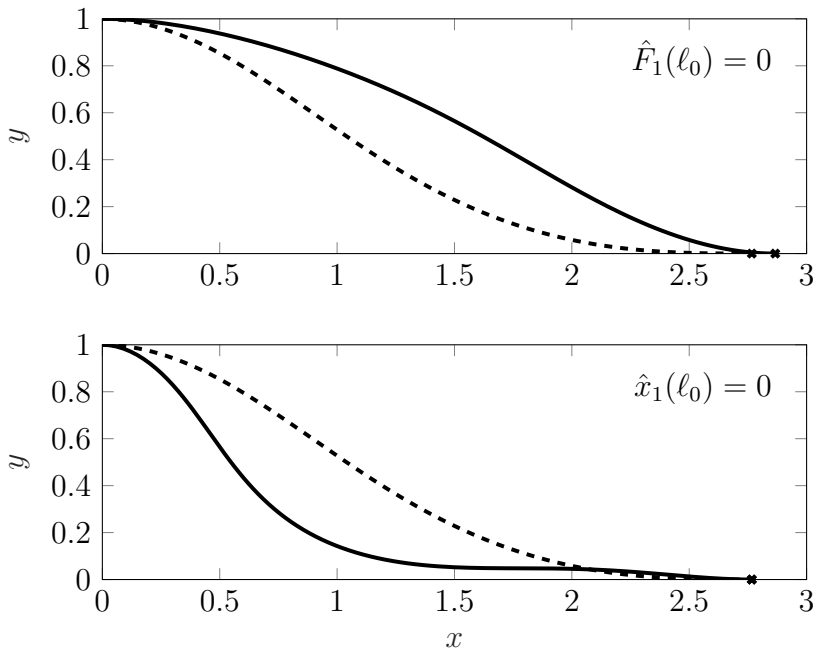

Figure 2.6: Comparison of typical shapes of the first mode of vibration with the distinct boundary conditions $\hat{F}_1(\ell_0) = 0$ and $\hat{x}_1(\ell_0) = 0$. We have taken $w = 1$ and $M_\ell = 0$. The dashed curves represent the static equilibrium and the point $s = \ell_0$ is marked with $\times$.

condition Eq. $(2.72)_1$ with $\ell_0 \leq L < \infty$ as compared to when one replaces it by $\hat{x}_1(\ell_0) = 0$. As illustrated in Fig. 2.6, the mode shape has one inflection point and does not cross the static configuration in the former case, while it has two inflection points and *does* cross the static configuration in the latter. Additionally, the material point $s = \ell_0$ slides along the substrate in the former case while it remains stationary in the latter. A useful heuristic for understanding the singular limit is to envision the vibrating rod as a single-degree-of-freedom mass-spring system in which the contacting segment is the mass $m \propto L$ and the non-contacting segment is the spring with stiffness k. For a fixed k (i.e. fixed static configuration), the natural frequency $\sqrt{k/m}$ tends to zero as $m \to \infty$.

A similar behavior arises when $w = 0$ and $M_\ell > 0$. Referring to Fig. 2.5b, as L is increased, the first natural frequency tends to zero for all M_ℓ, and the first mode "disappears" in the same fashion as before. The adhesion-only case contrasts with its gravity-only counterpart in that the limit $L - \ell_0 \to 0^+$ is *also* singular. To be clear, this means that if one replaces Eq. $(2.72)_1$ with $\hat{F}_1(\ell_0) = 0$, the resulting natural frequencies differ by a finite amount and do not converge as $M_\ell \to 0^+$, a fact that the curves labeled $L = \ell_0$ in Fig. 2.5b clearly demonstrate.

Having highlighted the difficulties than can arise with limiting values of the parameter L, we now present some results in which both gravity and adhesion are considered, taking the boundary condition $\hat{x}_1(\ell_0) = 0$ for specificity. Figures 2.7a and 2.7b show a few contours

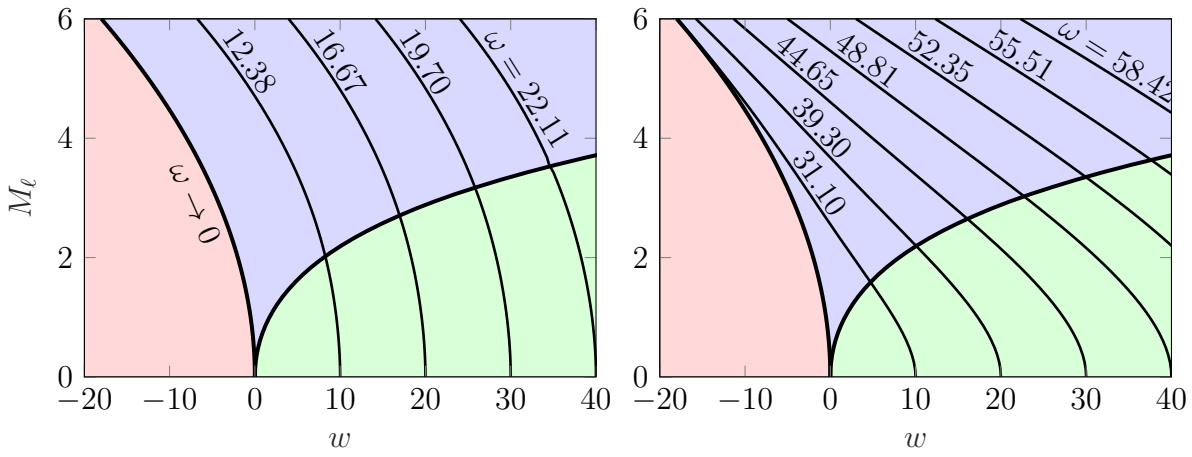

(a) First natural frequency.

(b) Second natural frequency.

Figure 2.7: First two natural frequencies as a function of w and M_ℓ. Contours of constant ω are indicated. See Fig. 2.4 for an interpretation of the colors.

of constant first and second natural frequency, respectively, in the (w, M_ℓ)-plane. In both instances the contours demonstrate a remarkable qualitative similarity. Focusing on Fig. 2.7a, the boundary between where solutions exist and where they do not appears to correspond to $\omega \to 0^+$. Normally such a behavior would be suggestive of a divergence instability, but in our case a more direct interpretation is possible. Figure 2.4 suggests that $\ell_0 \to \infty$ as one approaches the existence boundary such that the rod under consideration is one of semi-infinite length. The natural frequency tending to zero then reflects the well-known fact that a semi-infinite rod can sustain traveling waves.

Stability

All of the computed natural frequencies being real, the preceding linear vibration analysis shows the existence of (linearly) stable modes of vibration everywhere in the phase diagram that a static configuration exists. In other words, the system suffers neither a flutter- nor divergence-type instability. It is nevertheless instructive to apply what is known from the stability theory of elastic rods to the same problem.

An energy-based stability criterion for a statically deformed rod where one end is free to move on a rigid surface was recently formulated [31, 32]. The criterion, summarized in A.2, provides a necessary condition for the nonlinear stability of the system to small perturbations. Application of the criterion shows that configurations where $M_\ell \geq 0$ and $w > 0$ satisfy the necessary condition. However, configurations where $M_\ell \geq 0$ and $w < 0$ do not satisfy the criterion, thereby indicating an instability. However, this conclusion is at odds with the vibration-based analysis and we have been unable to resolve this discrepancy.

2.5 Conclusion

In this chapter we have proposed a systematic method of analyzing small-amplitude vibrations about static equilibria of rods whose length is variable, inspired by several impressive contributions in the existing literature. The essence is to express each quantity as a perturbation series and to expand the boundary conditions in Taylor series about the material points that correspond to the boundaries of the static configuration. We have placed special emphasis on unilateral contact, and in particular on the industrially relevant problem of a heavy rod that is clamped at a certain height at one end and in adhesive contact with a flat, rigid surface at the other. In applying the perturbation method to this problem in both its "small-on-small" and "small-on-large" flavors, we have obtained several counterintuititve results.

It was shown in Section 2.2 that the seemingly mysterious correspondence between the natural frequencies of the aforementioned small-on-small system with zero adhesion and those of a fixed-fixed beam, as first observed by Roy and Chatterjee [22], is not so perplexing after all. Indeed, our method makes it clear that it is not just the natural frequencies that match those of a fixed-fixed beam, but rather the entire leading-order dynamics. When adhesion is included, as discussed in Section 2.2, the leading-order dynamics correspond to those of a beam that is clamped at one end and attached to a spatially fixed rotational spring at the other. (In fact, we showed the more general and apparently novel result that an adhesion boundary condition is equivalent to a spatially fixed rotational spring when the motion of the contact point is small.) Solutions only exist when the dimensionless specific weight w and adhesive moment M_ℓ satisfy a certain necessary condition that leads to a clear classification of solutions in the (w, M_ℓ)-plane.

Sections 2.3 and 2.4 concerned the application of the perturbation method to the corresponding small-on-large problem. A number of new phenomena arise, owing to the inclusion of horizontal momentum. It was shown that the *total* length of the rod L, not just the length ℓ_0 of the non-contacting segment, is a critical parameter in determining the natural frequencies. In fact, the limits $L \to \infty$ and $L - \ell_0 \to 0^+$ can both be singular. Numerical evidence suggests that solutions to the small-on-large problem only exist in the same region of the (w, M_ℓ)-plane as do solutions to the small-on-small problem, an unexpected result. Furthermore, the contour bounding the region where solutions do not exist appears to correspond to a curve of zero natural frequency.

Our results suggest numerous avenues for further research. An exploration of the nonlinear vibration effects that arise when terms are retained to $O(\epsilon^2)$ or higher is of interest [21, 33], as is a generalization of our approach to three dimensions. A particularly intriguing aspect of the problem studied in this chapter is the nature of the boundary of the region of the (w, M_ℓ)-plane where no solutions exist, and we hope to see future work on why it is the same for the small-on-small and small-on-large problems, as well as how it relates to vibration, stability, and existence of static equilibria.

Chapter 3

Pervasive Nonlinear Vibrations Due to Rod-Obstacle Contact

3.1 Introduction

Unilateral contact is a ubiquitous but notoriously difficult feature to model in continuous mechanical systems. Although the state of the art in finite element methods is capable of handling complex contact interactions numerically [8], analytical results are few. Indeed, the general boundary-value problem for contacting continua involves free boundaries that preclude the application of many of the typical mathematical tools. Even the comparatively simple Signorini problem—in which an isotropic, linearly elastic sphere under the action of gravity contacts a rigid plane—is a significant challenge to formulate and solve [34]. Additional concerns arise when dynamics are considered, such as the tendency of even the most basic discrete systems to display chaos or quasiperiodicity upon repeated impact [35, 36].

Theories of deformable bodies with just one dimension of spatial extent such as beams and strings serve as a useful platform for investigating the continuum mechanics of contact. Because the deformation in these theories is parameterized by just one Lagrangian coordinate ξ (and time t), the location of any interface between a region where contact occurs and another where it does not is described by a single, time-dependent scalar $\xi = \gamma(t)$. This is in stark contrast to theories of two- or three-dimensional bodies, in which the interface is generally a time-varying curve or surface.

Due in part to the relative simplicity of tracking the contact interface, a handful of interesting and general theoretical results have actually been obtained for dynamic contact between various kinds of one-dimensional continua and rigid surfaces. For example, it has been shown that an inextensible string can form a kink at a contact interface if the material speed of the interface exceeds the speed of transverse waves in the string [37, 38]. Quasistatic contact has also been found to be intimately related to configurational mechanics [7], but few authors have studied the analogy in a dynamic context, notably Armanini et al. [30].

Very few truly dynamic (i.e., transient) problems in the contact mechanics of one-dimensional continua have been solved analytically, among them the remarkable works by Audoly et al. [39] and Burridge et al. [37]. Researchers have, however, made substantial analytical progress in understanding the role of contact in the vibration of one-dimensional continua. Much of this work has been performed in the context of three engineering applications: cantilevers in microelectromechanical systems (MEMS) [22, 40], marine structures [20, 21, 27, 33, 41], and belt-and-pulley systems [23, 42].

The fundamental hurdle to studying the vibration of one-dimensional continua experiencing contact is the motion of the contact interface. As alluded to by several authors [10, 20, 22, 24, 27, 33, 42], the interface can often be regarded as fixed for the study of linear vibrations superimposed on a static configuration, but the inclusion of effects such as adhesion can lead to unexpected boundary conditions at said point [10]. Approaches that entirely neglect the motion of the contact interface in the presence of adhesion, such as that of Fang et al. [40], lead to asymptotically inconsistent boundary conditions.

This chapter chiefly concerns nonlinear aspects of a prototypical free vibration problem of an elastic beam in unilateral contact with a flat, rigid, and frictionless surface. The linearized version of the problem was first considered by Roy and Chatterjee [22] and has since been expounded upon in our recently published work [10]. In performing a nonlinear finite element simulation to validate their linear analytical analysis, Roy and Chatterjee uncovered evidence of a quadratic nonlinearity in the frequency response. This discovery appears to have been made independently of the earlier analytical discovery by Turnbull et al. [42] that a quadratic nonlinearity exists in a related system. Indeed, several authors have uncovered similar nonlinear-dynamic behavior in problems of contact between one-dimensional continua and surfaces, notably Chatigeorgiou [21] and Demeio et al. [20, 27, 33].

Our goal in studying the aforementioned problem is to gain insight into and develop a comprehensive explanation for, in the simplest possible context, the nonlinear role of contact in the vibration of continuous mechanical systems. We formulate the problem in Section 3.2 and present in Section 3.3 the results of a numerical "experiment" conducted using a non-standard finite element method that is detailed in Appendix B. In Sections 3.5 and 4.3 we apply perturbation methods to reveal the source of the quadratic nonlinearity (see Eq. (3.14b)) and demonstrate excellent agreement with our earlier numerical experiment. In the penultimate section of the chapter, Section 3.6, the more general case of a possibly nonlinear rod contacting a curved surface is considered. We demonstrate that the quadratic nonlinearity (see Eq. (3.51)) persists in this situation and is therefore a purely kinematical result that is independent of the type of one-dimensional continuum considered so long as it does not admit kinks.

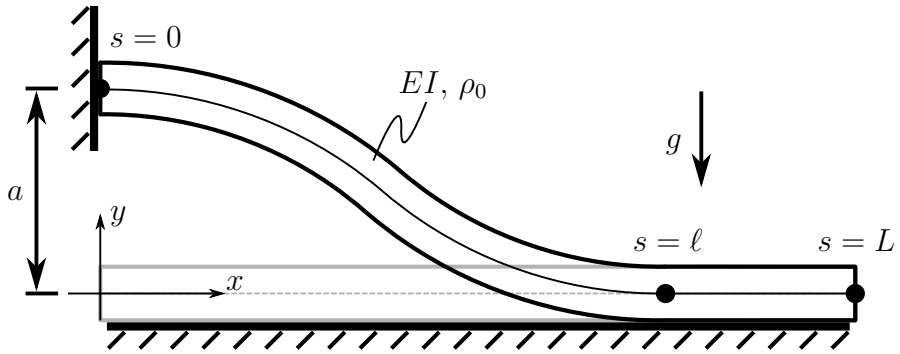

Figure 3.1: Schematic of a beam of length L that is in partial contact with a flat, rigid surface. The free vibration of the beam was first considered by Roy and Chatterjee [22]. If fluid drag and geometric nonlinearity were incorporated, we would have a model of a flexible riser touching the seafloor. Similarly, if electrostatic adhesion were included, we would have a model for stiction between a MEMS cantilever and a substrate.

3.2 Formulation of a Prototypical Problem

Consider the system shown in Fig. 3.1, in which gravity causes the simplest type of one-dimensional continuum with bending stiffness, an inextensible Euler-Bernoulli beam, to come into unilateral contact with the simplest obstacle, a rigid plane, without friction or adhesion.[1] The transverse displacement $y = y(\xi, t)$ of the beam is governed by

$$\mathcal{L}y + \rho_0 g = 0, \tag{3.1}$$

where we employ a compact notation for the linear differential operator

$$\mathcal{L} = \rho_0 \partial^2/\partial t^2 + EI\partial^4/\partial \xi^4. \tag{3.2}$$

Here, ρ_0 is the linear density, EI the flexural rigidity, and g the acceleration due to gravity. We will frequently use $()'$ to denote a partial derivative with respect to ξ and $\dot{()}$ to denote one with respect to t. As we have restricted ourselves to the geometrically linear case, the displacement is purely transverse and thus any material point in the segment $\gamma(t) < \xi < L$ is instantaneously at rest.

Equation (3.1) is to be solved for $0 < \xi < \gamma(t)$ and $t > 0$ subject to the boundary conditions

$$\begin{aligned} y(0,t) = a, \quad y'(0,t) = 0, \\ y(\gamma(t),t) = y'(\gamma(t),t) = y''(\gamma(t),t) = 0. \end{aligned} \tag{3.3}$$

[1] Inherent in using an Euler-Bernoulli beam model of contact is the appearance of a concentrated force exerted by the obstacle on the beam. Some may regard such a force as being unphysical, but such a conundrum can be avoided by using more sophisticated theories of beams [43] or by allowing the obstacle itself to deform [44].

Five boundary conditions are required rather than the usual four because γ is an additional unknown. The associated static equilibrium is described by

$$\begin{aligned} y_0(\xi) &= a\left(1-\frac{\xi}{\gamma_0}\right)^3\left(1+\frac{3\xi}{\gamma_0}\right), \\ \gamma_0 &= a\left(\frac{72EI}{\rho_0 g a^3}\right)^{1/4}. \end{aligned} \tag{3.4}$$

As our interest is in the nonlinear dynamics in the neighborhood of the above equilibrium, we initiate the beam's motion by requiring it to start from rest in a nearby configuration. For specificity we select

$$y(\xi,0) = y_0(\xi) + \frac{3125\epsilon a}{108}\left(1-\frac{\xi}{\gamma_0}\right)^3\left(\frac{\xi}{\gamma_0}\right)^2, \tag{3.5a}$$

$$\dot{y}(\xi,0) = 0, \quad \gamma(0) = \gamma_0, \quad \dot{\gamma}(0) = 0, \tag{3.5b}$$

where the factor of $3125/108$ is included in order to make ϵa the maximum amplitude of the corresponding term, ϵ being a small dimensionless parameter. For the sake of brevity we will subsequently write the second term on the right-hand side of Eq. (3.5a) as $\epsilon a h(\xi)$.

As a brief aside, Eq. (3.5a) has been chosen specifically so that it is compatible with Eq. (3.3), thereby avoiding spurious oscillations due to Gibbs-like phenomena in the coming numerical simulations. Furthermore, homogeneity of the boundary conditions at $\xi = \gamma(t)$ ensures that the total mechanical energy

$$E = \int_0^{\gamma(t)} \left[\frac{1}{2}\rho_0 \dot{y}^2 + \frac{1}{2}EI(y'')^2 + \rho_0 g y\right] \mathrm{d}\xi \tag{3.6}$$

is conserved. Verifying this fact requires use of the Leibniz integral rule due to the time-varying boundary $\xi = \gamma(t)$. If the beam were replaced by a string, the corresponding total mechanical energy would not generally be conserved [38].

3.3 Numerical Evidence of a Quadratic Nonlinearity

Equations (3.1) to (3.5) constitute a well-defined initial-boundary-value problem for the primary variable $y = y(\xi,t)$ and the parameter $\gamma = \gamma(t)$ on a domain that is unknown a priori: $(0,\gamma(t)) \times (0,\infty) \ni (\xi,t)$. Classical numerical techniques are not applicable due to the presence of the free boundary $\xi = \gamma(t)$. We therefore use a non-standard, quasi-Eulerian finite element method based on the idea of applying the stretching transformation $z = \xi/\gamma(t)$ to the spatial domain. Our method is closely related to the one developed by Humer et al. [45, 46] and is detailed in Appendix B.

Figure 3.2 shows a short portion of a numerical "experiment" conducted in accordance with the parameter values specified in Table 3.1. We report only $\gamma(t) - \gamma_0$, which serves as

Quantity	Symbol	Value
Linear density	ρ_0	$0.78\,\mathrm{kg/m}$
Gravitational acceleration	g	$9.8\,\mathrm{m/s^2}$
Flexural rigidity	EI	$166.6\,\mathrm{Nm^2}$
Height of support	a	$6.379 \times 10^{-4}\,\mathrm{m}$
Initialization parameter	ϵ	0.002
Final time	T	$10\,\mathrm{s}$
Number of elements		20
Time step (constant)		$1 \times 10^{-5}\,\mathrm{s}$

Table 3.1: Parameter values used for the numerical experiment. The parameters ρ_0, g, EI, and a match those used by Roy and Chatterjee [22] and lead to $\gamma_0 \approx 1\,\mathrm{m}$.

a convenient scalar quantification of the overall response of the beam. The discrete Fourier transform of the same quantity is shown in Fig. 3.3, which has several interesting features. For one, the peaks of greatest prominence occur almost exactly at the natural frequencies of a fixed-fixed beam of length γ_0, density ρ_0, and flexural rigidity EI, a correspondence that has been reported previously [10, 22]. These frequencies, which we will henceforth refer to as the *linear natural frequencies*, are

$$f_n = \frac{\beta_n^2}{2\pi}\sqrt{\frac{EI}{\rho_0}}, \quad n = 1, 2, 3, \ldots \tag{3.7}$$

where β_n are the roots of (cf. [47])

$$\cos(\beta_n\gamma_0)\cosh(\beta_n\gamma_0) = 1. \tag{3.8}$$

We order β_n in an increasing fashion.

Also intriguing in Fig. 3.3 is the presence of significant secondary peaks, the most prominent of which happens to occur very close to twice the second linear natural frequency: 273 Hz. Other secondary peaks also occur at seemingly miraculous locations, for example the one at 91 Hz, which is remarkably close to the difference between the second and first linear natural frequencies. In fact, almost all the secondary peaks occur at sums or differences of the linear natural frequencies, as indicated in Fig. 3.3 by the dashed and dash-dotted lines, respectively. We should note that the peak at 273 Hz was previously discovered by Roy and Chatterjee, who used a commercial finite element software with the ability to handle generic contact [22]. No other secondary peaks are visible in their frequency response, however, which could be due to the fact that the standard finite element implementation of contact is poorly suited to handling impact phenomena [9].

The pattern described above is no miracle; it is instead indicative of the presence of a rich set of *superharmonic* and *combination resonances* (sometimes called *combination tones*).

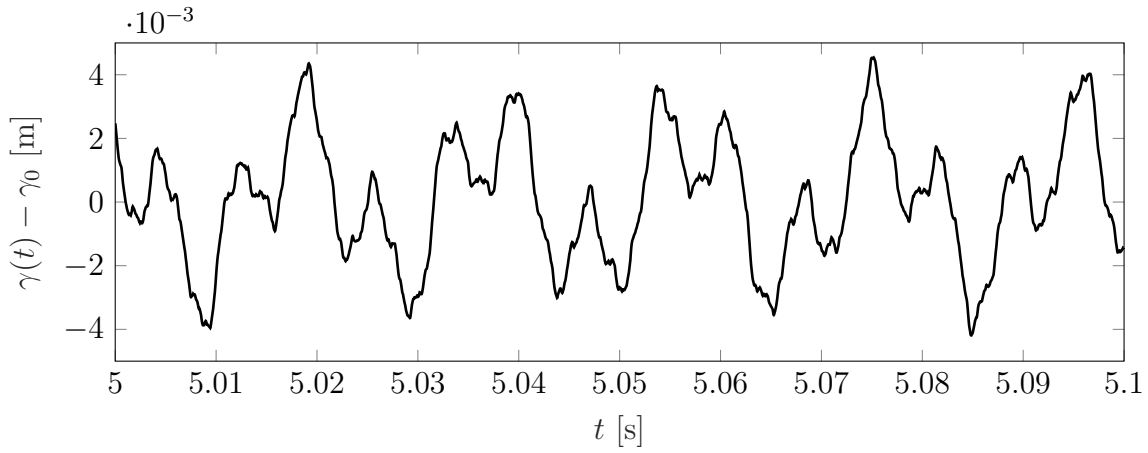

Figure 3.2: An excerpt of $\gamma(t) - \gamma_0$ versus t from the numerical experiment conducted according to the parameter values in Table 3.1.

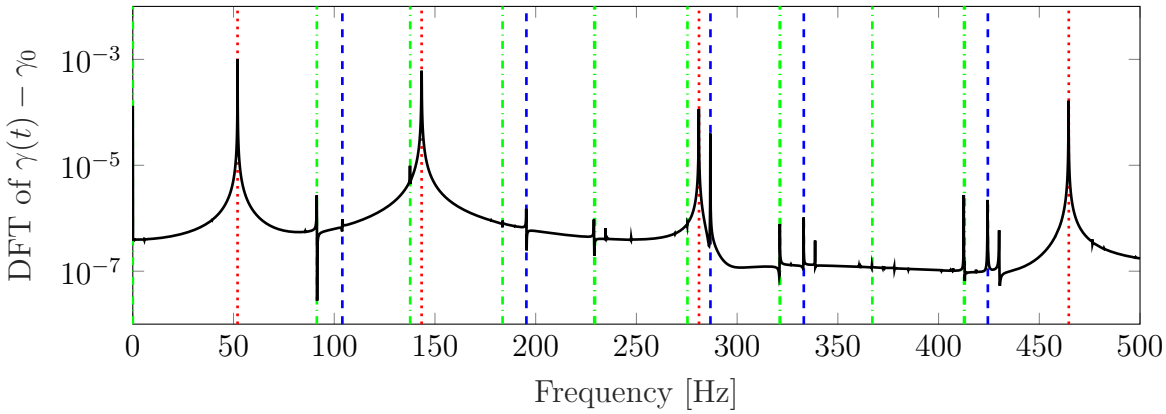

Figure 3.3: Discrete Fourier transform of $\gamma(t) - \gamma_0$ (in black) as obtained from the non-standard finite element simulation conducted according to the parameters in Table 3.1. The dotted lines (red) indicate the linear natural frequencies f_n, while the dashed lines (blue) correspond to the sums of said frequencies, and the dash-dotted lines (green) to their absolute differences. Only the sums and differences produced from the first eight of f_n are shown. The peaks at 104 Hz and 287 Hz both occur at twice a linear natural frequency (52 Hz and 143 Hz, respectively).

The superharmonic resonances we have discovered are of the $2:1$ variety, meaning that they appear at twice the linear natural frequencies f_n. Likewise, we might call the combination resonances $1:1$ in the sense that they are of the form $f_n \pm f_m$ rather than, for example, $3f_n \pm f_m$, which might well be called $3:1$ combination resonances.

The well-established theory of weakly nonlinear vibrations suggests that the $2:1$ superharmonic and $1:1$ combination resonances could arise from a nonlinearity somewhere in the problem that is quadratic in one of the dependent variables [4, 48]. However, the classical results on nonlinear vibrations are confined to cases where the nonlinearity occurs in the differential equation. In our case the differential equation, Eq. (3.1), is entirely linear (albeit inhomogeneous) and the sole source of the nonlinearity is the fact that the contact interface $\xi = \gamma(t)$ is free to move back and forth. It is hard to imagine how such a feature would lead to a quadratic nonlinearity. We seek to resolve this conundrum in the remainder of the chapter.

3.4 Derivation of Perturbation Equations

The only hope for studying the present problem analytically is by way of perturbation methods. Taking inspiration from work on related problems [33, 42], we begin our analytical study by assuming the existence of sufficiently term-by-term differentiable perturbation expansions of the form

$$y(\xi, t) = y_0(\xi) + \sum_{k=1}^{\infty} \epsilon^k y_k(\xi, t), \tag{3.9a}$$

$$\gamma(t) = \gamma_0 + \sum_{k=1}^{\infty} \epsilon^k \gamma_k(t), \tag{3.9b}$$

with the goal of obtaining a sequence of boundary-value problems for y_1 and γ_1, y_2 and γ_2, and so on. We reiterate that ϵ is a small parameter that specifies the amplitude of the initial displacement away from the static equilibrium, as per Eq. (3.5a). Inserting Eq. (4.31) into Eq. (3.1) implies $\mathcal{L}y_k = 0$ for all $k \in \mathbb{Z}^+$. The boundary conditions for y_k at $\xi = 0$ are straightforward to infer from Eq. (3.3). However, it is less clear what to do with the boundary conditions at $\xi = \gamma(t)$.

The natural approach is to expand the boundary conditions about the initial location $\xi = \gamma_0$, but this must be done without neglecting powers of ϵ in an ad hoc manner, lest the boundary conditions at varying orders be inconsistent [42]. Recall the boundary condition $y(\gamma(t), t) = 0$, for example. We obtain from Eq. (3.9) the following:

$$y_0\left(\gamma_0 + \sum_{k=1}^{\infty} \epsilon^k \gamma_k(t)\right) + \sum_{k=1}^{\infty} \epsilon^k y_k\left(\gamma_0 + \sum_{j=1}^{\infty} \epsilon^j \gamma_j(t), t\right) = 0, \tag{3.10}$$

which can then be expanded in Taylor series about $\epsilon = 0$. Upon equating each of the coefficients of the Taylor series to zero, one obtains a set of relations among γ_k, y_k at $\xi = \gamma_0$,

and the ξ-derivatives of y_k at $\xi = \gamma_0$. The same procedure can be applied to $y'(\gamma(t), t) = 0$ and $y''(\gamma(t), t) = 0$. After doing so and then making all possible simplifications, we obtain a sequence of linear initial-boundary-value problems for y_k on the (fixed rather than variable) domain $(0, \gamma_0) \times (0, \infty) \ni (\xi, t)$, as well as a sequence of algebraic expressions for γ_k.

The first-order problem we find as a result of the aforementioned method is to solve $\mathcal{L}y_1 = 0$ subject to the boundary conditions

$$y_1(0,t) = y_1'(0,t) = y_1(\gamma_0,t) = y_1'(\gamma_0,t) = 0, \tag{3.11}$$

and the initial conditions

$$y_1(\xi,0) = ah(\xi), \quad \dot{y}_1(\xi,0) = 0. \tag{3.12}$$

Thus y_1 can be regarded as the displacement of a fixed-fixed beam of length γ_0. This analogy has been developed extensively elsewhere [10]. Once y_1 is known, we can compute

$$\gamma_1(t) = -\frac{y_1''(\gamma_0,t)}{y_0'''(\gamma_0)}. \tag{3.13}$$

The second-order problem is to solve $\mathcal{L}y_2 = 0$ subject to the boundary conditions

$$y_2(0,t) = y_2'(0,t) = y_2(\gamma_0,t) = 0, \tag{3.14a}$$

$$y_2'(\gamma_0,t) = \frac{1}{2}y_0'''(\gamma_0)[\gamma_1(t)]^2, \tag{3.14b}$$

and the initial conditions

$$y_2(\xi,0) = \dot{y}_2(\xi,0) = 0. \tag{3.15}$$

Here, y_2 can be regarded as the displacement of a beam of length γ_0, fixed at both ends, whose support at $\xi = \gamma_0$ has a prescribed angle of rotation. After obtaining y_2, we can compute

$$\begin{aligned}\gamma_2(t) = &-[y_0'''(\gamma_0)]^{-1}\left\{\frac{1}{2}y_0'''(\gamma_0)[\gamma_1(t)]^2\right.\\ &\left.+\, y_1'''(\gamma_0,t)\gamma_1(t) + y_2''(\gamma_0,t)\right\}.\end{aligned} \tag{3.16}$$

One can in principle continue to identify the higher-order boundary-value problems to be solved, but we limit our discussion to second order as we are interested in the dominant nonlinear dynamics only.

The quadratic nonlinearity we have been seeking occurs in Eq. (3.14b), whereby the first-order system feeds into the second-order system through a boundary forcing proportional to γ_1^2. For illustrative purposes we can define the displacement from the static equilibrium $u = \epsilon y_1 + \epsilon^2 y_2 + \ldots$ and use Eq. (3.13) to expand Eq. (3.14b). Neglecting terms of order higher than ϵ, u can be shown to solve $\mathcal{L}u = 0$ subject to

$$u(0,t) = u'(0,t) = u(\gamma_0,t) = 0, \tag{3.17a}$$

$$u'(\gamma_0,t) = \epsilon\frac{[u''(\gamma_0,t)]^2}{2y_0'''(\gamma_0)}, \tag{3.17b}$$

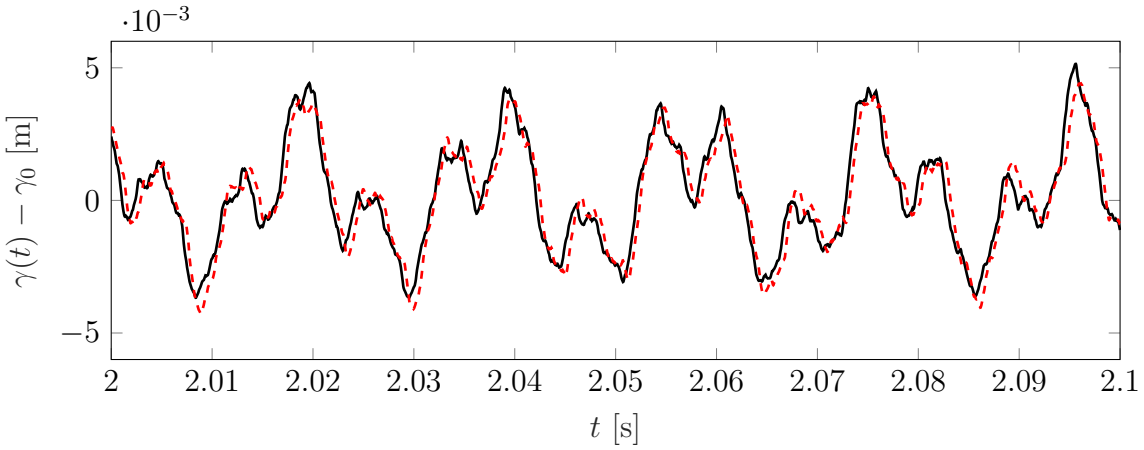

Figure 3.4: Comparison between a portion of $\epsilon\gamma_1(t) + \epsilon^2\gamma_2(t)$ (solid black line) and of the numerical solution to the fully nonlinear problem (dashed red line). Both solutions correspond to the parameter values in Table 3.1.

and appropriate initial conditions. Hence we have a standard boundary-value problem for u on a fixed spatial domain $(0, \gamma_0) \ni \xi$ with a weak, quadratic nonlinearity in the boundary conditions, namely Eq. (3.17b). With u' being the angular displacement and u'' proportional to the bending moment, Eq. (3.17b) is mechanically equivalent to a nonlinear spring attached to the boundary $\xi = \gamma_0$.

3.5 Solution of the Perturbation Equations

Quantitative Study via Numerical Method

The static solution being known from Eq. (3.4), the first- and second-order dynamic problems formulated in Section 4.3 constitute canonical initial-boundary-value problems that can be solved sequentially by any number of semi-analytical or numerical methods. In this section use a standard finite element method with isoparametric elements, cubic Hermite shape functions, and implicit Newmark time integration to obtain the perturbation solution through second order according to the parameters in Table 3.1. Though this approach has the benefit of faithfully representing wave propagation and other high-frequency effects, it is not useful for developing a qualitative understanding of how the solution should behave. For this reason we investigate the analytical solution in the following section.

Figure 3.4 shows the close correspondence between $\gamma(t) - \gamma_0$ from the earlier numerical experiment and $\epsilon\gamma_1(t) + \epsilon^2\gamma_2(t)$ as obtained by the method described above. The agreement between the two deteriorates to some extent at later times, but not nearly to a degree that would suggest non-uniform validity of the perturbation expansions, Eqs. (3.9b) and (4.31). The discrete Fourier transform of our numerical approximation to $\epsilon\gamma_1(t) + \epsilon^2\gamma_2(t)$ is shown in

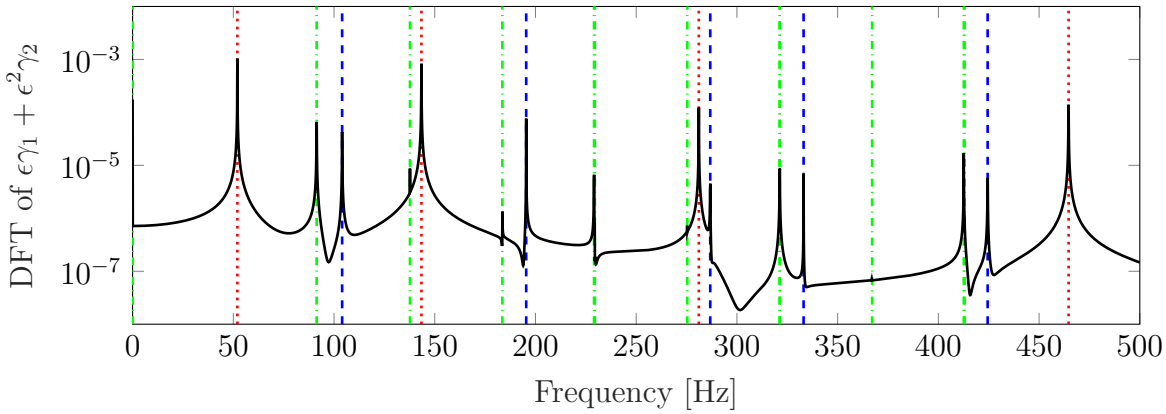

Figure 3.5: Discrete Fourier transform of the numerical approximation of $\epsilon\gamma_1(t) + \epsilon^2\gamma_2(t)$ as obtained by a finite element solution of the perturbative equations. Notice the close correspondence with Fig. 3.3, which is generated from a nonlinear finite element solution of the original problem.

Fig. 3.5, which faithfully reproduces the key features of Fig. 3.3, namely the location of the primary and secondary resonances. The minor disparities in the amplitudes between the two response spectra are to be expected as the vertical scale is logarithmic and small differences due to numerical inaccuracy, the absence of higher-order contributions to the perturbative solution, or other factors can appear amplified. Figure 3.5 also shows that a handful of the small peaks in Fig. 3.3, for example the ones at 339 Hz and 430 Hz, are not accounted for in the first- or second-order dynamics. It is likely that these peaks are third-order effects.

Qualitative Study via Analytical Method

More instructive than the precise quantitative solution of the perturbation equations is a qualitative look at how the contact nonlinearity gives rise to superharmonic and combination resonances. To investigate this issue we solve the perturbation equations analytically by way of a modal superposition method. We verify in the process that our regular perturbation expansions do not contain any secular terms through second order and are therefore uniformly valid.

The unique solution of the first-order problem is

$$y_1(\xi, t) = \sum_{n=1}^{\infty} A_n X_n(\xi) \cos(\omega_n t) \tag{3.18}$$

where

$$A_n = a \int_0^{\gamma_0} h(\xi) X_n(\xi) \, \mathrm{d}\xi. \tag{3.19}$$

Furthermore,

$$X_n(\xi) = \frac{1}{\sqrt{\gamma_0}}\Bigg\{ \cos(\beta_n\xi) - \cosh(\beta_n\xi) - [\sin(\beta_n\xi) - \sinh(\beta_n\xi)]\frac{\cos(\beta_n\gamma_0) - \cosh(\beta_n\gamma_0)}{\sin(\beta_n\gamma_0) - \sinh(\beta_n\gamma_0)}\Bigg\} \tag{3.20}$$

are the mode shapes of a fixed-fixed beam of length γ_0, and $\omega_n = \beta_n^2\sqrt{EI/\rho_0}$ are its angular natural frequencies. The modes are orthonormal in the sense that $\int_0^{\gamma_0} X_m(\xi)X_n(\xi)\,\mathrm{d}\xi = \delta_{mn}$. Taking Eqs. (3.4) and (3.13) into account,

$$\gamma_1(t) = \frac{\gamma_0^3}{24a}\sum_{n=1}^{\infty} A_n X_n''(\gamma_0)\cos(\omega_n t). \tag{3.21}$$

Equation (3.21) may appear at first to fail to satisfy the initial condition $\gamma_1(0) = 0$ but actually does so upon summing the infinite series. This is because Eq. $(3.12)_1$ implies

$$\sum_{n=1}^{\infty} A_n X_n''(\xi) = ah''(\xi), \tag{3.22}$$

and our particular choice of initial condition, Eq. (3.5a) means that $h''(\gamma_0) = 0$, hence $\gamma_1(0) = 0$.

To solve the second-order system we introduce a new variable

$$v(\xi,t) = y_2(\xi,t) - \frac{12a}{\gamma_0^2}\left(\frac{\xi}{\gamma_0}\right)^2\left(1 - \frac{\xi}{\gamma_0}\right)[\gamma_1(t)]^2, \tag{3.23}$$

which can be shown to satisfy

$$\mathcal{L}v = \rho_0 f, \tag{3.24a}$$
$$v(0,t) = v'(0,t) = v(\gamma_0,t) = v'(\gamma_0,t) = 0, \tag{3.24b}$$
$$v(\xi,0) = \dot{v}(\xi,0) = 0, \tag{3.24c}$$

where

$$f(\xi,t) = -\frac{24a}{\gamma_0^2}\left(\frac{\xi}{\gamma_0}\right)^2\left(1 - \frac{\xi}{\gamma_0}\right)\left(\dot{\gamma}_1^2 + \gamma_1\ddot{\gamma}_1\right). \tag{3.25}$$

The variable v can be regarded as the transverse displacement of a fixed-fixed beam of length γ_0, initially straight and at rest, that is subjected to a time-dependent body force (per unit mass) $f = f(\xi,t)$. Following the well-established method of modal superposition [47], we assume a solution of the form

$$v(\xi,t) = \sum_{n=1}^{\infty} X_n(\xi)T_n(t), \tag{3.26}$$

where $T_n(t)$ are to be determined. Inserting Eq. (3.26) into Eq. (3.24a), multiplying by an arbitrary X_m, integrating in ξ from 0 to γ_0, and performing some simplifications, we find a series of ordinary differential equations for the modal amplitudes T_m, $m \in \mathbb{Z}^+$:

$$\ddot{T}_m + \omega_m^2 T_m = \int_0^{\gamma_0} f(\xi, t) X_m(\xi) \, \mathrm{d}\xi, \tag{3.27}$$

where $T_m(0) = \dot{T}_m(0) = 0$ by Eq. (3.24c). The solution to Eq. (3.27) can be written as

$$T_m(t) = \frac{1}{\omega_m} \int_0^t \int_0^{\gamma_0} f(\xi, t) X_m(\xi) \sin(\omega_m(t - \tau)) \, \mathrm{d}\xi \, \mathrm{d}\tau \tag{3.28}$$

and y_2 can be reconstructed from Eqs. (3.23) and (3.26). Finally, γ_2 can be found from Eq. (3.16).

It is crucial to investigate the nature of f. If it were to contain frequency content at any of the (angular) natural frequencies ω_m, secular terms that grow linearly in t would arise in y_2 by way of T_m and thus our regular perturbation expansions, Eqs. (3.9b) and (4.31), would furnish satisfactory approximations only for $t = O(\epsilon)$. (Unbounded growth in the solution is inconsistent with physical intuition and conservation of the energy in Eq. (3.6).) It is well-known that when secular terms are present, one must typically resort to more sophisticated tools such as averaging methods, the Linstedt-Poincaré method, or the method of multiple scales [4, 48]. The essence of each of these methods is that one can "cancel" secular terms by choosing appropriate corrections to the linear natural frequencies. If no secular terms arise at a given order, the frequency correction at that order is zero.

Fortunately for us, f happens not to have frequency content at any ω_m, meaning that the regular perturbation expansions are uniformly valid and no correction to the natural frequencies occurs through second order in ϵ. The latter fact comports with the results of an investigation of a closely related problem [42]. As a proof of sorts, notice that the time-dependence of f is entirely determined by the quantity $\dot{\gamma}_1^2 + \gamma_1 \ddot{\gamma}_1$, as per Eq. (3.25). In view of Eq. (3.21), $\dot{\gamma}_1^2 + \gamma_1 \ddot{\gamma}_1$ contains terms of just two kinds. First are the terms proportional to $\cos^2(\omega_n t)$ or $\sin^2(\omega_n t)$ that, by the half-angle formulas, provide constant forcing as well as harmonic forcing at frequency $2\omega_n$. Then there are terms that are proportional to $\sin(\omega_m t)\sin(\omega_n t)$ and $\cos(\omega_m t)\cos(\omega_n t)$, where $m \neq n$. The product-to-sum identity

$$\begin{aligned} &\sin(\omega_m t)\sin(\omega_n t) \\ &\quad = \frac{1}{2}[\cos((\omega_m - \omega_n)t) - \cos((\omega_m + \omega_n)t)] \end{aligned} \tag{3.29}$$

and similar for $\cos(\omega_m t)\cos(\omega_n t)$ show that terms of the second type force the second-order system at all possible sums and absolute differences of the linear natural frequencies. By virtue of the fact that the linear natural frequencies are derived from a transcendental characteristic equation, no simple algebraic relationships exist among them. Therefore none of $2\omega_n$, $\omega_m + \omega_n$, or $|\omega_m - \omega_n|$ is exactly equal to a particular ω_p, and no secular terms arise in any T_m.

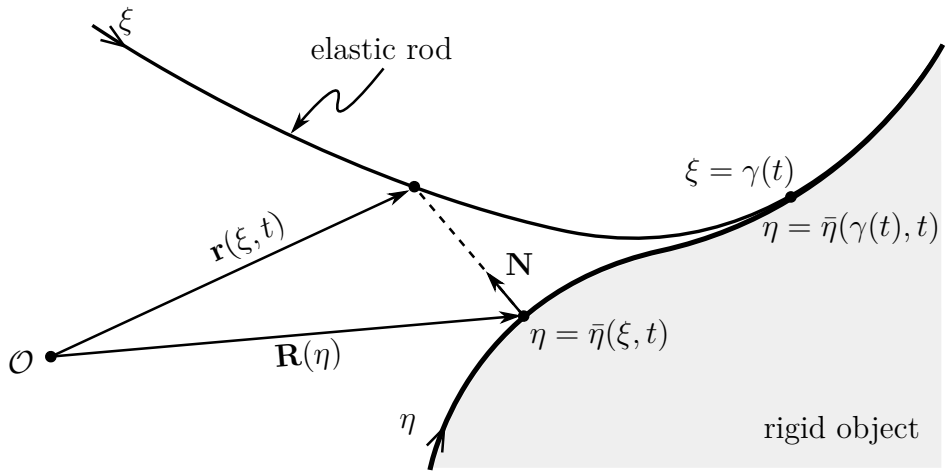

Figure 3.6: Kinematics of contact and interpretation of the gap function.

The above analysis of the frequency content of f is key to understanding how the quadratic nonlinearity gives rise to the secondary resonances shown in Figs. 3.3 and 3.5. Terms like $\cos^2(\omega_n t)$, which force the second-order system at $2\omega_n$, lead to the superharmonic resonances, while terms like $\cos(\omega_m t)\cos(\omega_n t)$, which force the second-order system at $\omega_m + \omega_n$ and $|\omega_m - \omega_n|$, lead to the combination resonances. If higher-order terms were included we would expect additional nonlinear resonances to appear, and such resonances are indeed seen in Fig. 3.3, but is is unlikely that they would be observable in any practical system due to the presence of damping.

3.6 Kinematics of Contact

Our previous analysis pertains to the simplest beam model and a flat surface. It is natural to question if the quadratic nonlinearity persists or is altered if a more general rod theory is employed and if the contacting surface is curved. We do not invoke the balance laws, the constitutive law, or any other aspect of the governing equations for the rod theory in this entire section. In fact, we require virtually nothing of the rod other than that it be (1) inextensible and (2) free of kinks in the neighborhood of the contact interface. The entirely kinematic analysis that follows demonstrates that the quadratic nonlinearity of Sections 3.2 to 3.5 does indeed persist in these far more general circumstances.

Conditions on the Gap Function

Consider Fig. 3.6, wherein a portion of rod is in contact with a rigid surface. The current placement of the material curve constituting the lateral surface of the rod is described by the vector-valued function $\mathbf{r}(\xi, t)$ where ξ is the arc-length coordinate. A portion of the

curve is unconstrained along a segment of finite length $a < \xi < \gamma(t)$ and another portion is unilaterally constrained to conform to the boundary of a rigid object along another segment of finite length $\gamma(t) < \xi < b$. The unit tangent vector to the material curve at the point ξ at time t is denoted by $\mathbf{e}_t(\xi, t)$. A normal vector to the curve is defined by the product $\mathbf{e}_n(\xi, t) = \mathbf{E}_3 \times \mathbf{e}_t(\xi, t)$ where $\mathbf{E}_3$ is the unit vector normal to the plane of contact. The curvature of the material curve is computed from the identity $\kappa(\xi, t) = \mathbf{r}''(\xi, t) \cdot \mathbf{e}_n(\xi, t)$.

The boundary of the rigid object with which contact occurs is described by the parameterization $\mathbf{R}(\eta)$, with η being an arc-length parameter chosen (without loss of generality) so that it is increasing in the same direction as ξ. We shall assume the surface to be such that $\mathbf{R}(\cdot)$ is at least twice continuously differentiable. Analogously to the rod, $\mathbf{T}(\eta) = \mathbf{R}'(\eta)$ is the unit tangent of the surface, $\mathbf{N}(\eta) = \mathbf{E}_3 \times \mathbf{T}(\eta)$ the unit normal, and $K(\eta) = \mathbf{R}''(\eta) \cdot \mathbf{N}(\eta)$ the curvature.

Following Wriggers [8], we can concisely encode the necessary conditions for contact with the *gap function*

$$u(\xi, t) = \min_{\eta} \|\mathbf{r}(\xi, t) - \mathbf{R}(\eta)\|, \tag{3.30}$$

which is the minimum distance between the location of the material point ξ at time t and the rigid surface described by $\mathbf{R}(\eta)$. The value of η at which said minimum occurs is

$$\bar{\eta}(\xi, t) = \arg\min_{\eta} \|\mathbf{r}(\xi, t) - \mathbf{R}(\eta)\|. \tag{3.31}$$

As a necessary condition for the minimization,

$$\frac{\partial}{\partial \eta} \|\mathbf{r}(\xi, t) - \mathbf{R}(\eta)\| = 0 \quad \text{when} \quad \eta = \bar{\eta}(\xi, t), \tag{3.32}$$

meaning that

$$\frac{\mathbf{r}(\xi, t) - \mathbf{R}(\bar{\eta}(\xi, t))}{\|\mathbf{r}(\xi, t) - \mathbf{R}(\bar{\eta}(\xi, t))\|} \cdot \mathbf{T}(\bar{\eta}(\xi, t)) = 0. \tag{3.33}$$

The leftmost term in the product of Eq. (3.33) lies in the plane with normal $\mathbf{E}_3$ and, by virtue of being orthogonal to the unit tangent and having unit magnitude, must be equal to $\pm\mathbf{N}(\bar{\eta}(\xi, t))$. Our stipulation that ξ and η increase in the same direction means that the aforementioned term is equal to $\mathbf{N}(\bar{\eta}(\xi, t))$. Accordingly,

$$\mathbf{r}(\xi, t) = \mathbf{R}(\bar{\eta}(\xi, t)) + u(\xi, t)\mathbf{N}(\bar{\eta}(\xi, t)), \tag{3.34}$$

which gives rise to an additional representation of the gap function:

$$u(\xi, t) = [\mathbf{r}(\xi, t) - \mathbf{R}(\bar{\eta}(\xi, t))] \cdot \mathbf{N}(\bar{\eta}(\xi, t)). \tag{3.35}$$

Equation (3.34) shows that, with the exception of certain degenerate cases, the placement of a material point at a given time can be specified completely by the pair (η, u). It is this coordinate system that will prove most convenient for our purposes.

We now proceed to derive three conditions that the gap function must necessarily satisfy at $\xi = \gamma(t)^-$. These will serve as boundary conditions for the free-boundary-value problem that determines the shape of the rod in the segment $a < \xi < \gamma(t)$. The first and most obvious condition is that

$$u(\gamma(t)^-, t) = 0. \tag{3.36}$$

The second condition relates to the first spatial derivative of the gap function. By direct calculation from Eq. (3.35), taking Eq. (3.34) into account, we see that

$$u'(\xi, t) = \mathbf{e}_t(\xi, t) \cdot \mathbf{N}(\bar{\eta}(\xi, t)). \tag{3.37}$$

As kinks incur an infinite energetic penalty in elastic rods, we exclude them by demanding that $\mathbf{e}_t(\cdot, t)$ be everywhere continuous.[2] This assumption implies that $\mathbf{e}_n(\cdot, t)$ is also continuous.[3] As such,

$$u'(\gamma(t)^-, t) = 0, \tag{3.38}$$

which is the second condition.

The final condition, perhaps predictably, involves the second spatial derivative of the gap function. Accordingly, by differentiating Eq. (3.37), we see that

$$\begin{aligned} u''(\xi, t) =& \kappa(\xi, t)\mathbf{e}_n(\xi, t) \cdot \mathbf{N}(\bar{\eta}(\xi, t)) \\ &- \mathbf{e}_t(\xi, t) \cdot K(\bar{\eta}(\xi, t))\bar{\eta}'(\xi, t)\mathbf{T}(\bar{\eta}(\xi, t)). \end{aligned} \tag{3.39}$$

The no-kink assumption also tells us that, upon differentiation of Eq. (3.34) with respect to ξ and evaluation at $\xi = \gamma(t)$, $\bar{\eta}'(\gamma(t), t) = 1$. Hence Eq. (3.39) yields

$$u''(\gamma(t)^-, t) = \kappa(\gamma(t)^-, t) - K(\bar{\eta}(\gamma(t)^-, t)). \tag{3.40}$$

Here arises our purpose for being careful with the continuity of various quantities at $\xi = \gamma(t)$: it is possible in certain applications for $\kappa(\cdot, t)$ to be discontinuous, for example when the rod-surface interaction is characterized by a JKR-type adhesion energy.[4] In that case the jump in the curvature across the contact point is a certain prescribed quantity:

$$\Delta\kappa_\gamma = \kappa(\gamma(t)^+, t) - \kappa(\gamma(t)^-, t). \tag{3.41}$$

Because the rod perfectly conforms to the surface and the surface has a continuous curvature, $\kappa(\gamma(t)^+, t) = K(\bar{\eta}(\gamma(t)^-, t))$, and therefore Eqs. (3.40) and (3.41) give rise to the third and final condition,

$$u''(\gamma(t)^-, t) = -\Delta\kappa_\gamma. \tag{3.42}$$

[2]Such an exclusion is not warranted in the case of one-dimensional continua that have no bending energy. For the simplest such object, the inextensible string, a kink can in fact occur at $\xi = \gamma(t)$ if the material speed of the discontinuity $|\dot{\gamma}(t)|$ exceeds the speed of propagation of transverse waves [37, 38].

[3]Recall that the continuity of $\mathbf{T}(\cdot)$ and $\mathbf{N}(\cdot)$ was assumed from the outset.

[4]For examples of the analysis of rods in dry (or JKR-type) adhesion to surfaces, see O'Reilly [7] and Majidi et al. [31] and references therein.

Equations (3.36), (3.38) and (3.42) are the three conditions that must hold at $\xi = \gamma(t)$. They could alternatively be stated in terms of the position vector $\mathbf{r}$ and its derivatives $\mathbf{r}'$ and $\mathbf{r}''$, but the gap function u provides the most succinct expressions. Unfortunately, it is very rare in solving actual problems that η and u provide a convenient parameterization of the motion of the rod, so in practice Eqs. (3.36), (3.38) and (3.42) must be translated into equivalent expressions in whichever particular coordinate system is used for a given problem. The remainder of Section 3.6 involves applying asymptotic methods to Eqs. (3.36), (3.38) and (3.42). The reader should keep in mind that the same exact approach can be applied to the contact conditions as expressed in any chosen coordinate system. However, considerable simplifications take place when u is used.

Perturbation Analysis of the Contact Point

As with our earlier work in this chapter, our interest is in small excursions of the rod from a static configuration described by $\mathbf{r}_0(\xi)$ for $a < \xi < \gamma_0$. The section $\gamma_0 < \xi < b$ that conforms perfectly to the rigid surface has a known shape and is therefore not of any particular interest as far as kinematics is concerned. We assume the existence of perturbation expansions of the form

$$u(\xi, t) = u_0(\xi) + \sum_{k=1}^{\infty} \epsilon^k u_k(\xi, t), \tag{3.43a}$$

$$\gamma(t) = \gamma_0 + \sum_{k=1}^{\infty} \epsilon^k \gamma_k(t), \tag{3.43b}$$

where $\epsilon \ll 1$ is a small bookkeeping parameter. In order to consistently expand Eqs. (3.36), (3.38) and (3.42) in Taylor series about the static configuration, consider $g(\gamma(t), t)$, where g stands for u, u', or u''. Defining

$$\begin{aligned} h(t;\epsilon) = {} & g_0\left(\gamma_0 + \sum_{k=1}^{\infty} \epsilon^k \gamma_k(t)\right) \\ & + \sum_{k=1}^{\infty} \epsilon^k g_k\left(\gamma_0 + \sum_{j=1}^{\infty} \epsilon^j \gamma_j(t), t\right). \end{aligned} \tag{3.44}$$

and expanding in Taylor series about $\epsilon = 0$ leads to, after some delicate computations,

$$\begin{aligned} h(t;\epsilon) = {} & g_0(\gamma_0) + \epsilon[g_0'(\gamma_0)\gamma_1 + g_1(\gamma_0, t)] \\ & + \epsilon^2\left[\frac{1}{2}g_0''(\gamma_0)\gamma_1^2 + g_0'(\gamma_0)\gamma_2\right. \\ & \left. + g_1'(\gamma_0, t)\gamma_1 + g_2(\gamma_0, t)\right] + O(\epsilon^3). \end{aligned} \tag{3.45}$$

Applying Eq. (3.45) to Eqs. (3.36), (3.38) and (3.42), isolating the coefficients of ϵ^k for $k \geq 0$, and making all possible simplifications gives

$$u_0(\gamma_0) = 0, \quad u_0'(\gamma_0) = 0, \quad u_0''(\gamma_0) = -\Delta\kappa_\gamma, \tag{3.46}$$

to order zero,

$$u_1(\gamma_0, t) = 0, \quad u_1'(\gamma_0, t) = -\frac{\Delta\kappa_\gamma}{u_0'''(\gamma_0)} u_1''(\gamma_0, t), \tag{3.47}$$

to order one, and

$$u_2(\gamma_0, t) = 0, \quad u_2'(\gamma_0, t) = \frac{1}{2} u_0'''(\gamma_0)[\gamma_1(t)]^2, \tag{3.48}$$

to order two. Additionally, we see the counterpart to Eq. (3.13),

$$\gamma_1(t) = -\frac{u_1''(\gamma_0, t)}{u_0'''(\gamma_0)}, \tag{3.49}$$

and the counterpart to Eq. (3.16),

$$\begin{aligned} \gamma_2(t) = -[u_0'''(\gamma_0)]^{-1} \Big\{ &\frac{1}{2} u_0'''(\gamma_0)[\gamma_1(t)]^2 \\ &+ u_1'''(\gamma_0, t)\gamma_1(t) + u_2''(\gamma_0, t) \Big\}. \end{aligned} \tag{3.50}$$

We have assumed in deriving Eqs. (3.46) to (3.50) that $\Delta\kappa_\gamma = O(1)$, which need not necessarily be the case, for example when the jump in curvature is due to very weak adhesion. As in Sections 3.5 and 4.3, we consider the dynamics only through second order in ϵ.

Referring to Eq. (3.17b), observe that when $\Delta\kappa_\gamma = 0$, Eq. $(3.47)_2$ resembles the "clamped" boundary condition for an Euler-Bernoulli beam if u_1 is the transverse displacement (and thus u_1' the angular displacement). When $\Delta\kappa_\gamma \neq 0$, the same equation resembles the boundary condition for a spatially fixed rotational spring since the moment in an Euler-Bernoulli beam is proportional to u_1''. By inserting Eq. (3.49) into Eq. $(3.48)_2$, we arrive at

$$u_2'(\gamma_0, t) = \frac{1}{2u_0'''(\gamma_0)}[u_1''(\gamma_0, t)]^2, \tag{3.51}$$

which is identical to the quadratic nonlinearity obtained in our study of the prototypical problem (cf. Eq. (3.14b)).

3.7 Conclusion

We have studied a simple example of dynamic contact in a continuous mechanical system. In a numerical "experiment" performed using a bespoke finite element method, we observed

the presence of a number of nonlinear resonances of both the superharmonic and combination varieties. We used a perturbation method to show that these resonances are due to a dominantly quadratic nonlinearity in the boundary conditions of the governing initial-boundary-value problem. Furthermore, we found excellent agreement between the fully nonlinear numerical results and those obtained from the second-order perturbation analysis.

Though our initial analysis was presented in a highly restricted context, we demonstrated that the quadratic nature of the contact nonlinearity is actually a kinematic phenomenon that can hold in a very broad class of problems. We anticipate similar effects to arise in contact-induced nonlinear vibrations of two- and three-dimensional continua, but significant research remains to be conducted in this area. Future work could also consider the higher-order perturbation equations, investigate the effect of adhesion, or study the interaction between contact and geometric or material nonlinearities in the beam or rod itself.

Chapter 4

Electrostatically Actuated MEMS in the Post-Touchdown Regime

4.1 Introduction

Many microelectromechanical systems (MEMS) incorporate beam- or plate-like structures that deflect in the lateral direction due to applied electrostatic forces between the structure and a stationary electrode, such as the device illustrated in Fig. 4.1. The canonical model of such systems, sometimes known as *the* MEMS equation, exhibits a so-called "pull-in" instability after the applied voltage exceeds a critical value. Being critically important for the design of practical devices, pull-in has been the subject of countless studies, and the reader is encouraged to consult Zhang et al. [49] for an authoritative review, Batra et al. [50] for a mechanics-focused summary of the literature, or Laurençot and Walker [51] for a mathematically oriented discussion.

If the voltage continues to be increased beyond pull-in, the beam or plate can come into contact with the electrode, an event known as "touchdown." When the actuating structure and the electrode are bare conductors, touchdown leads to a short-circuit, and is therefore often regarded as a failure mode. In other cases, such as when the electrode is coated with an insulating dielectric layer, touchdown can be instead exploited to augment the functionality of the device (see, e.g., work by Kafumbe et al. [52] or Li et al. [53]). Under certain circumstances, touchdown can lead to stiction, in which surface forces between the actuator and the dielectric layer prevent the actuator from returning to its undeformed position. Several different physical phenomena can contribute to stiction, including van der Waals forces [54], quantum-mechanical Casimir forces [50], and capillary adhesion [55, 56], the latter being more important in the context of manufacturing rather than device operation.

While there exists a vast literature on predicting the onset of pull-in, a comparatively small body of work focuses on the mechanics after touchdown, especially with regard to dynamics. The earliest work relevant for our purposes is that of Kafumbe et al. [52], who used

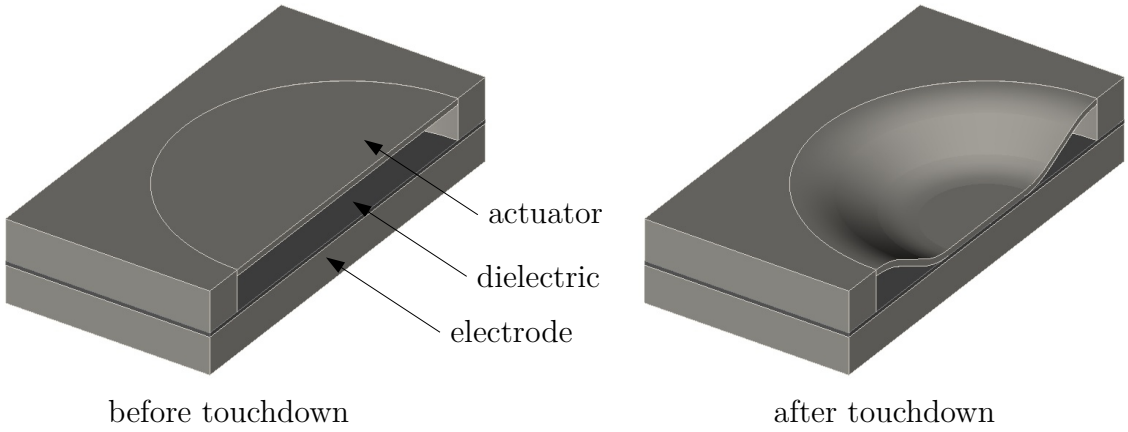

Figure 4.1: Schematic of a plate-based electrostatic actuator prior to touchdown (left) and after touchdown (right).

a vibration method to assess the linear stability of a beam-based electrostatic actuator, as did Gorthi et al. [57] some time later. Zhang and Zhao [58] studied the transient dynamics of an analogous system with periodic forcing and emphasized the importance of the motion of the contact nonlinearity. Savkar et al. [59] demonstrated theoretically the use of vibrations to initiate stiction repair and Savkar and Murphy [60] extended this work to demonstrate complete stiction repair. In the process these researchers brought useful concepts from dynamic fracture mechanics into the MEMS literature. More recent studies involving transient dynamics include those by Vyasarayani et al. [61] and Li et al. [53].

All of the papers mentioned in the paragraph above pertain to beam-based actuators. Very little appears to have been written about the post-touchdown dynamics of plate-based actuators. The most notable work is that of Lindsay et al. [62, 63] and Lindsay [64] who presented and analyzed in depth a partial differential equation inspired by the MEMS equation. While their impressive work spans a wide range of mathematical issues, it is ultimately not of particular relevance for our purposes as the differential equation they consider does not contain an inertial term. Mathematical results on similar so-called "obstacle problems" are numerous [65, 66], but are unfortunately not directly relevant to understanding the mechanics of any practical device.

Aside from the obvious engineering applications, the problem of touchdown in electrostatic MEMS actuators is also of interest from the perspective of fundamental mechanics, owing to the presence of a contact interface, i.e., a boundary in the domain between material points that are in contact with the dielectric and points that are not. The contact interface is actually a *free* boundary in the mathematical sense, meaning that it is unknown a priori and must be determined as part of the solution of the problem. Because free boundaries are a nonlinearity in their own right, they can induce nonlinear dynamics in systems that are governed by linear differential equations. For beams, where the spatial domain is a line

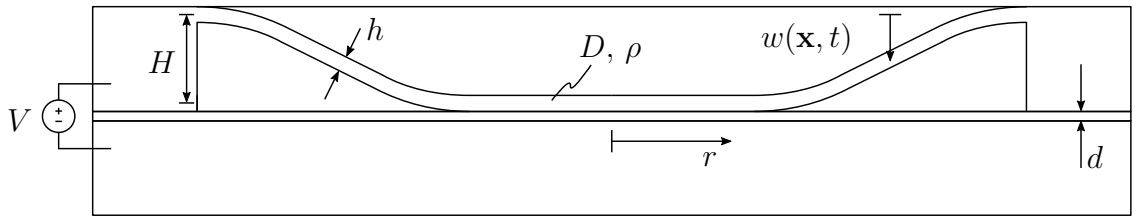

Figure 4.2: Schematic cutaway of the post-touchdown configuration of the actuator with various quantities indicated.

segment, contact interfaces are simply points. For plates, on the other hand, the spatial domain is a planar region and contact interfaces are curves. In either case, as discussed by Goldberg and O'Reilly [11], the presence of contact poses unique analytical and computational challenges, especially in the dynamic setting, where the use of standard numerical techniques can lead to non-physical spectral content in the solution.

The purpose of the present work is to demonstrate procedures for formulating and analyzing models of post-touchdown dynamics in electrostatic plate actuators. In order to focus on the essential mechanics associated with the motion of the contact interface, we consider an idealized model that neglects several effects important in real devices, among them the electrical fringing field, mid-plane stretching of the plate, and squeeze-film damping. Amending our work to include these effects (and others) is an incremental task, and the lessons learned throughout this chapter are not altered significantly by their omission.

The organization of the chapter is as follows. Section 4.2 outlines the basic problem to be solved. In Section 4.3 we use a variational principle to derive the governing differential equations and formulate the linear stability problem. We briefly characterize the pre-touchdown equilibrium solutions in Section 4.4 and then proceed to characterizing the post-touchdown equilibrium solutions in Section 4.5. Finally, in Section 4.6, a reduced-order model of the dynamics is introduced and then briefly applied to the problem of stiction repair, making use of basic techniques from nonlinear dynamics. Concluding remarks are contained in Section 4.7.

4.2 Problem Description

Referring to Figs. 4.1 and 4.2, consider an initially flat plate of thickness h, volumetric density ρ, and flexural rigidity D clamped at a height H above a rigid dielectric layer of thickness d and permittivity ϵ_d, beneath which is an electrode that interacts with the plate via Coulomb forces. The simply connected planar domain that describes the plate in its reference configuration is denoted Ω. (Later on we will take Ω to be a disk, but little additional effort is required for us to consider a more general domain here.) For h small, the transverse deflection w—chosen to be positive toward the dielectric—is governed to a reasonable approximation by Kirchhoff-Love plate theory, which assumes the kinetic and

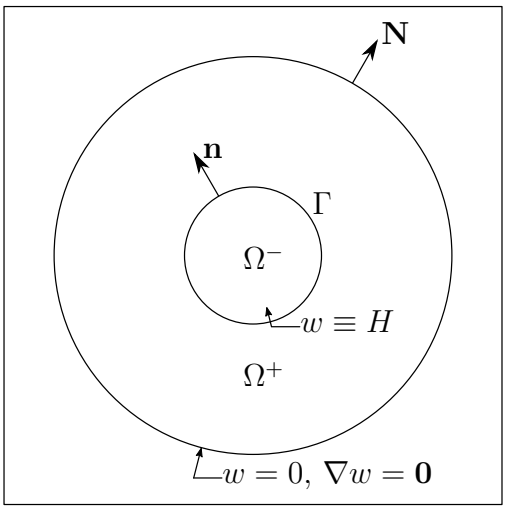

Figure 4.3: Top view of the actuator indicating the contact interface Γ.

strain energies

$$T = \int_\Omega \frac{1}{2}\rho h \dot{w}^2 \,\mathrm{d}S \quad \text{and} \quad W = \int_\Omega \frac{1}{2} D\big(\nabla^2 w\big)^2 \,\mathrm{d}S\,, \tag{4.1}$$

respectively. In Eq. (4.1), ∇ is the two-dimensional gradient on Ω, ∇^2 the Laplacian, and $\mathrm{d}S$ the infinitesimal area element. Letting V be the voltage applied across the plate and electrode, ϵ_0 the permittivity of free space (the permittivity of air being neglected), and $\epsilon_r = \epsilon_d/\epsilon_0$ the relative permittivity of the dielectric, we adopt the approximate electric potential

$$U = \int_\Omega \frac{\epsilon_0 V^2}{2(H + d/\epsilon_r - w)} \,\mathrm{d}S\,, \tag{4.2}$$

which several authors have used previously [52, 58, 67]. A derivation of Eq. (4.2) with $d = 0$ from Maxwell's equations can be found in the work of Pelesko and Bernstein [68]. Finally, the clamped boundary conditions read

$$w = 0 \quad \text{and} \quad \nabla w = \mathbf{0} \quad \text{on} \quad \partial\Omega. \tag{4.3}$$

There are many different ways the plate could feasibly come into contact with the dielectric layer. The contact could occur at a single point, along a curve, or over an area. There could be several separate regions of contact. The contact regions could have smooth boundaries, or highly geometrically irregular ones. Due to the abundance of possibilities, we must limit ourselves to a very particular case. The most practically relevant situation, illustrated in Fig. 4.3, is when contact occurs over a single, finitely sized region $\Omega^- \subset \Omega$, in which $w = H$ identically. The complementary region is denoted by Ω^+ and the boundary between the two, which is assumed to be smooth, by Γ. On physical grounds we require w

and ∇w to be continuous across Γ, leading to the following interfacial conditions:

$$w = H \quad \text{and} \quad \nabla w = \mathbf{0} \quad \text{on} \quad \Gamma. \tag{4.4}$$

Although we have not explicitly indicated so with our notation, Ω^+ and Ω^- (and therefore Γ) vary with time. The contact interface Γ is not merely a moving boundary, but rather a *free* boundary that is unknown a priori. A complete solution of the governing equations will therefore consist of *both* a time-dependent displacement field w and curve Γ.

Because our system contains only conservative forces, we find it convenient to use a variational principle to derive the governing equations. The Lagrangian $L = T - W + U$ can be partitioned according to

$$L = \int_{\Omega^-} \mathcal{L}^- \, \mathrm{d}S + \int_{\Omega^+} \mathcal{L}^+ \, \mathrm{d}S \tag{4.5}$$

where

$$\mathcal{L}^- = \frac{\epsilon_0 V^2}{2d} \tag{4.6}$$

is the density associated with the $(-)$ "phase" of the plate, and

$$\mathcal{L}^+ = \frac{1}{2}\rho h \dot{w}^2 - \frac{1}{2} D\big(\nabla^2 w\big)^2 + \frac{\epsilon_0 V^2}{2(H + d/\epsilon_r - w)} \tag{4.7}$$

is the density for the $(+)$ phase. For now, the energy density of the $(-)$ phase is simply the same as that of the $(+)$ phase, but evaluated at $w = H$ and $\dot{w} = 0$. However, because we will shortly introduce an approximation that makes the two densities differ, it is expedient to distinguish between them from the outset. Given an initial state $\{w(\mathbf{x}, 0), \Gamma(0)\}$ and final state $\{w(\mathbf{x}, T), \Gamma(T)\}$, the plate-electrode system is assumed to take some path in the solution space such that the action

$$\mathcal{A} = \int_0^T L \, \mathrm{d}t \tag{4.8}$$

is rendered stationary among all sufficiently smooth displacement fields $w : \Omega^+ \to \mathbb{R}$ satisfying Eqs. (4.3) and (4.4), and all smooth contact interfaces $\Gamma \subset \Omega$.

4.3 Derivation of Governing Equations

In this section we deduce necessary conditions that follow from $\delta\mathcal{A} = 0$. These will consist of an Euler-Lagrange equation holding in Ω^+ and a Weierstrass-Erdmann corner condition holding on Γ. Because the dielectric layer can be very thin in a practical device, we develop the governing equations for two separate cases: one in which the dimensionless thickness $\epsilon = d/(H\epsilon_r)$ is finite, and another in which $\epsilon \to 0$. It will be shown that the latter case has the same variational structure as a plate with JKR-type adhesion in Ω^- and no electrical potential in Ω^+, a correspondence that has been found in the context of a related problem involving beams by Gorthi et al. [57], but not rigorously justified. Before proceeding to obtain necessary conditions, however, we must first develop a handful of intermediate results.

Intermediate Results

Denoting the variation of the free interface Γ by $\delta\mathbf{x}$, Eq. (4.4) yields the compatibility conditions

$$\delta w + \nabla w \cdot \delta\mathbf{x} = 0 \quad \text{and} \quad \nabla\delta w + \nabla(\nabla w)\delta\mathbf{x} = \mathbf{0} \quad \text{on} \quad \Gamma^+. \tag{4.9}$$

Both conditions in Eq. (4.9) should be interpreted as holding in a limiting sense as Γ is approached from the side of Ω^+. Owing to the constancy of $w = H$ and $\nabla w = \mathbf{0}$ on Γ, the only non-zero component of $\nabla(\nabla w)$ on Γ^+ is $\mathbf{n} \cdot \nabla(\nabla w)\mathbf{n}$, and thus Eq. (4.9) yields

$$\delta w = 0 \quad \text{and} \quad \nabla\delta w \cdot \mathbf{n} + \nabla^2 w\, \delta x = 0 \quad \text{on} \quad \Gamma^+, \tag{4.10}$$

where $\delta x = \delta\mathbf{x} \cdot \mathbf{n}$. The same argument can be used to deduce that

$$\dot{w} = 0 \quad \text{on} \quad \Gamma. \tag{4.11}$$

Reynolds' transport theorem can be used to show

$$\frac{\mathrm{d}}{\mathrm{d}t}\left(\int_{\Omega^-} f \,\mathrm{d}S + \int_{\Omega^+} g \,\mathrm{d}S\right) = \int_{\Omega^-} \dot{f} \,\mathrm{d}S + \int_{\Omega^+} \dot{g} \,\mathrm{d}S + \int_\Gamma (g - f) v \,\mathrm{d}s\,, \tag{4.12}$$

where v is the normal velocity of Γ as it evolves in the reference configuration (*not* the velocity of a material point) and $\mathrm{d}s$ is the infinitesimal line element on Γ. Equation (4.12) yields, in light of Eq. (4.11),

$$\frac{\mathrm{d}}{\mathrm{d}t}\int_{\Omega^+} \rho h \dot{w} \,\mathrm{d}S = \int_{\Omega^+} \rho h \ddot{w} \,\mathrm{d}S\,. \tag{4.13}$$

If we regard the time derivatives in Eq. (4.12) as variations instead, it follows immediately that

$$\delta L = \int_{\Omega^-} \delta\mathcal{L}^- \,\mathrm{d}S + \int_{\Omega^+} \delta\mathcal{L}^+ \,\mathrm{d}S + \int_\Gamma (\mathcal{L}^+ - \mathcal{L}^-)\delta x \,\mathrm{d}s\,. \tag{4.14}$$

Observe that the normal velocity v is replaced by the normal variation δx in this interpretation of the transport theorem.

Governing Equations for a Thick Dielectric Layer

When the dielectric layer is not thin (i.e., $\epsilon = d/(H\epsilon_r) > 0$), the variational problem is exactly as stated in Section 4.2. Inserting the Lagrangian densities, Eqs. (4.6) and (4.7), into Eq. (4.14) and integrating by parts both spatially and temporally, we obtain

$$\begin{aligned} \delta L = &- \int_{\Omega^+} \left[\rho h \ddot{w} + D\nabla^4 w - \frac{\epsilon_0 V^2}{2H^2(1 + \epsilon - w/H)^2}\right]\delta w \,\mathrm{d}S \\ &+ \int_{\Gamma^+} D(\nabla^2 w)^2 \delta x \,\mathrm{d}s + \frac{\mathrm{d}}{\mathrm{d}t}\int_{\Omega^+} \rho h \dot{w}\, \delta w \,\mathrm{d}S\,, \end{aligned} \tag{4.15}$$

where Eqs. (4.3), (4.10) and (4.13) have been invoked. The variation $\delta\mathcal{A}$ is obtained by integrating Eq. (4.15) from $t = 0$ to $t = T$. Then, setting $\delta\mathcal{A} = 0$ and making judicious choices of δw and δx, we deduce the Euler-Lagrange equation

$$\rho h\ddot{w} + D\nabla^4 w = \frac{\epsilon_0 V^2}{2H^2(1+\epsilon - w/H)^2} \quad \text{in} \quad \Omega^+ \tag{4.16}$$

and the Weierstrass-Erdmann corner condition

$$D(\nabla^2 w)^2 = 0 \quad \text{or} \quad \nabla^2 w = 0 \quad \text{on} \quad \Gamma^+. \tag{4.17}$$

The time-integral of the last term in Eq. (4.15) vanishes because $\delta w = 0$ at $t = 0$ and $t = T$, and therefore yields no additional necessary conditions.

Governing Equations for a Vanishingly Thin Dielectric Layer

As discussed previously, we would like to obtain the governing equations in the limit $\epsilon = d/(H\epsilon_r) \to 0$. A naive approach might be to simply set $\epsilon = 0$ in Eq. (4.16), but this is problematic, for then the right-hand side is singular when $w = H$, which holds on Γ. We must instead return to the original variational statement of the problem and make adjustments to the electrical potential energy U before again deducing the boundary-value problem from the stationarity of the action.

The electrical potential energy can be written

$$U = \int_{\Omega^-} \frac{\epsilon_d V^2}{2d}\,\mathrm{d}S + \int_{\Omega^+} \frac{\epsilon_0 V^2}{2H(1+\epsilon - w/H)}\,\mathrm{d}S\,, \tag{4.18}$$

or, introducing A as the (constant) area of Ω,

$$U = \frac{\epsilon_d V^2}{2d}\left[A - \int_{\Omega^+}\left(1 + \frac{\epsilon}{1-w/H}\right)^{-1}\mathrm{d}S\right]. \tag{4.19}$$

The integrand in Eq. (4.19) has a convergent geometric series

$$\left(1 + \frac{\epsilon}{1-w/H}\right)^{-1} = 1 - \frac{\epsilon}{1-w/H} + \left(\frac{\epsilon}{1-w/H}\right)^2 - \ldots \tag{4.20}$$

so long as $w/H < 1 - \epsilon$. However, $w/H = 1$ must be satisfied on Γ, so we can only use the geometric series outside of a thin boundary layer B_ϵ that is adjacent to Γ. We partition the integral in Eq. (4.19) accordingly:

$$\begin{aligned}\int_{\Omega^+}\left(1 + \frac{\epsilon}{1-w/H}\right)^{-1}\mathrm{d}S &= \int_{B_\epsilon}\left(1 + \frac{\epsilon}{1-w/H}\right)^{-1}\mathrm{d}S \\ &+ \int_{\Omega^+\setminus B_\epsilon}\left[1 - \frac{\epsilon}{1-w/H} + \left(\frac{\epsilon}{1-w/H}\right)^2 - \ldots\right]\mathrm{d}S\end{aligned} \tag{4.21}$$

In B_ϵ, we have $w/H \leq 1$, with equality as $\epsilon \to 0$, meaning that the integral over B_ϵ in Eq. (4.21) vanishes, and therefore

$$U \to \frac{\epsilon_d V^2}{2d} A^-, \tag{4.22}$$

where A^- is the (time-dependent) area of Ω^-.

On account of Eq. (4.22), the Lagrangian can be cast in the form

$$L = \int_{\Omega^-} \frac{\epsilon_d V^2}{2d} \,\mathrm{d}S + \int_{\Omega^+} \left[\frac{1}{2}\rho h \dot{w}^2 - \frac{1}{2} D(\nabla^2 w)^2\right] \mathrm{d}S\,, \tag{4.23}$$

which is exactly equivalent to the Lagrangian for a plate with no electrostatic forces but instead a (reversible) JKR-type adhesion acting on the contacting region, where the driving force

$$\mathcal{G} = \frac{\epsilon_d V^2}{2d} \tag{4.24}$$

can be regarded as the work of adhesion, or the fracture toughness, of an imaginary adhesive produced by the electric field in the infinitesimal region above the dielectric. The variation of L is

$$\begin{aligned} \delta L = &- \int_{\Omega^+} \left(\rho h \ddot{w} + D\nabla^4 w\right) \delta w \,\mathrm{d}S + \int_{\Gamma^+} \left[\frac{1}{2} D(\nabla^2 w)^2 - \frac{\epsilon_d V^2}{2d}\right] \delta x \,\mathrm{d}s \\ &+ \frac{\mathrm{d}}{\mathrm{d}t} \int_{\Omega^+} \rho h \dot{w}\, \delta w \,\mathrm{d}S\,. \end{aligned} \tag{4.25}$$

By the same procedure employed in the previous section, Eq. (4.25) allows us to deduce from $\delta \mathcal{A} = 0$ the Euler-Lagrange equation

$$\rho h \ddot{w} + D\nabla^4 w = 0 \quad \text{in} \quad \Omega^+ \tag{4.26}$$

and the Weierstrass-Erdmann corner condition

$$\frac{1}{2} D(\nabla^2 w)^2 = \mathcal{G} \quad \text{on} \quad \Gamma^+. \tag{4.27}$$

Equation (4.27) has the same form as the adhesion-moment boundary condition encountered in studies of beams and plates in contact with rigid surfaces endowed with JKR adhesion.[1] It should be emphasized that there is no initiation criterion associated with delamination for this special adhesive, and Eq. (4.27) holds whether the contact interface is locally retreating or advancing. Indeed, the entire system is conservative and the "adhesion" reversible.

[1] See, e.g., the work of O'Reilly [7], Mastrangelo and Hsu [56], Majidi and Adams [69], or Hure and Audoly [70]. As discussed by Goldberg and O'Reilly [71], the condition could also be established using a configurational force balance for the plate.

Summary of the Governing Equations

To summarize, we have deduced in either case a free boundary-value problem of the following form:

$$\rho h\ddot{w} + D\nabla^4 w = F(w) \qquad \text{in } \Omega^+ \tag{4.28a}$$
$$w = 0 \qquad \text{on } \partial\Omega \tag{4.28b}$$
$$\nabla w = \mathbf{0} \qquad \text{on } \partial\Omega \tag{4.28c}$$
$$w = H \qquad \text{on } \Gamma \tag{4.28d}$$
$$\nabla w = \mathbf{0} \qquad \text{on } \Gamma \tag{4.28e}$$
$$\nabla^2 w = -C \qquad \text{on } \Gamma^+ \tag{4.28f}$$

subject to appropriate initial conditions. For the case of a dielectric of finite thickness, i.e., $\epsilon > 0$,

$$F(w) = \frac{\epsilon_0 V^2}{2H^2(1+\epsilon - w/H)^2} \quad \text{and} \quad C = 0, \tag{4.29}$$

while for the case of a dielectric of vanishingly small thickness, i.e., $\epsilon \to 0$,

$$F(w) = 0 \quad \text{and} \quad C = \sqrt{\frac{2\mathcal{G}}{D}}, \tag{4.30}$$

where $\mathcal{G} = \epsilon_d V^2/(2d)$ (cf. Eq. (4.24)). The parameters ρ, h, D, ϵ_0, ϵ_d, V, H, and ϵ are treated as given data.

Linear Vibration and Stability

We can assess the stability of static configurations of the plate (i.e., solutions of Eq. (4.28) with no dependence on time t) by linearizing the dynamics about such a configuration and seeking solutions that grow in time. This method of stability analysis, though lacking rigorous mathematical justification for PDE systems, is widely used in engineering applications. It is important to realize that because we are dealing with a free-boundary problem, we must do more than simply linearize the differential equation, Eq. (4.28a). Since the contact interface Γ can vary with time, we must also linearize the domain Ω^+ over which the boundary-value problem is defined.

To begin the process of linearizing the dynamics about $\{w_0(\mathbf{x}), \Gamma_0\}$, we assume

$$w = w_0 + \varepsilon w_1, \tag{4.31}$$

where ε is a small bookkeeping parameter (not to be confused with $\epsilon = d/(H\epsilon_r)$, the dimensionless dielectric thickness). Inserting Eq. (4.31) into Eq. (4.28a) and retaining only terms linear in ε, we obtain

$$\rho h\ddot{w}_1 + D\nabla^4 w_1 = F'(w_0)w_1, \tag{4.32}$$

where $F' = \mathrm{d}F/\mathrm{d}w$. Equations (4.28b) and (4.28c), the two boundary conditions on $\partial\Omega$, yield

$$w_1 = 0 \quad \text{and} \quad \nabla w_1 = \mathbf{0} \quad \text{on} \quad \partial\Omega_0. \tag{4.33}$$

Moving on to the linearization of the conditions at the contact interface, let $\mathbf{X}$ be an arbitrary point on Γ at time t. Because Γ is close to Γ_0, the interface in the static configuration, we can always find a corresponding point $\mathbf{X}_0 \in \Gamma_0$ by following the unit normal $\mathbf{n}_0$ to Γ_0 that satisfies the following relation:

$$\mathbf{X} = \mathbf{X}_0 + \varepsilon X_1 \mathbf{n}_0, \tag{4.34}$$

where X_1 is the "displacement" of the contact boundary from its location in the static configuration.

Each of the interface conditions, Eqs. (4.28d) to (4.28f), is an expression of the form

$$f(\mathbf{X}, t) = 0 \quad \text{for} \quad \mathbf{X} \in \Gamma. \tag{4.35}$$

Writing $f = f_0 + \varepsilon f_1$, using Eq. (4.34), and isolating the coefficients of ε^0 and ε^1, we obtain

$$f_1(\mathbf{X}_0, t) + f_{0,n}(\mathbf{X}_0) X_1 = 0 \quad \text{for} \quad \mathbf{X}_0 \in \Gamma_0, \tag{4.36}$$

where the shorthand $()_{,n} = \nabla() \cdot \mathbf{n}_0$ has been employed. Applying Eq. (4.36) to Eqs. (4.28d) to (4.28f) and making some simplifications produces the following boundary conditions on Γ_0^+:

$$w_1 = 0, \qquad w_{1,n} = C X_1, \qquad \nabla^2 w_1 + \left(\nabla^2 w_0\right)_{,n} X_1 = 0. \tag{4.37}$$

Equation (4.37) can be rearranged to eliminate X_1, yielding the following boundary-value problem for w_1:

$$\rho h \ddot{w}_1 + D\nabla^4 w_1 = F'(w_0) w_1 \qquad \text{in } \Omega_0^+ \tag{4.38a}$$

$$w_1 = 0 \qquad \text{on } \partial\Omega_0 \tag{4.38b}$$

$$w_{1,n} = 0 \qquad \text{on } \partial\Omega_0 \tag{4.38c}$$

$$w_1 = 0 \qquad \text{on } \Gamma_0 \tag{4.38d}$$

$$\left(\nabla^2 w_0\right)_{,n} w_{1,n} + C\nabla^2 w_1 = 0 \qquad \text{on } \Gamma_0^+ \tag{4.38e}$$

After solving Eq. (4.38) subject to initial conditions on w_1 and $\dot{w}_1$, one can compute $X_1 = -\nabla^2 w_1 / (\nabla^2 w_0)_{,n}$ a posteriori for all points on Γ_0.

Some comments are in order about Eq. (4.38). In the thin-dielectric model, $C = 0$ and therefore Eq. (4.38e) reduces to $w_{1,n} = 0$ on Γ_0^+. Also, $F = 0$ identically, so the right-hand side of Eq. (4.38a) becomes zero. The dynamics are then equivalent to those of a plate occupying Ω_0^+ that is clamped on its inner and outer boundaries. In the thick-dielectric model, the dynamics are also equivalent to a plate occupying Ω_0^+ with its outer

boundary clamped, but with some important differences: the equivalent plate rests on a non-uniform elastic foundation with stiffness $-F'(w_0)$ and its inner boundary Γ_0 is connected to a distributed torsional spring with stiffness $-D(\nabla^2 w_0)_{,n}/C$.[2]

We assess stability by seeking solutions to Eq. (4.38) of the form

$$w_1(\mathbf{x}, t) = \phi(\mathbf{x}) e^{\Lambda t}, \tag{4.39}$$

where $\phi : \Omega_0^+ \to \mathbb{C}$ and $\Lambda \in \mathbb{C}$ are to be determined. The eigenfunctions $\{\phi_n\}$ are the complex mode shapes and the imaginary part of the eigenvalues $\{\Lambda_n\}$ are the corresponding natural frequencies. The general response of the linearized system is a superposition of all the modes, so if any one of the eigenvalues has $\operatorname{Re}\Lambda_n > 0$, then the n-th component of the superposition can be expected initially to grow in time if the system is perturbed slightly away from equilibrium (i.e., if $w_1(\mathbf{x}, 0) \neq 0$ and/or $\dot{w}_1(\mathbf{x}, 0) \neq 0$). Thus if we can find at least one solution with $\operatorname{Re}\Lambda > 0$, we refer to the underlying equilibrium state as *linearly unstable*. Inserting Eq. (4.39) into Eq. (4.38) leads to the following eigenvalue problem:

$$\rho h \Lambda^2 \phi + D\nabla^4 \phi = F'(w_0)\phi \qquad \text{in } \Omega_0^+ \tag{4.40a}$$
$$\phi = 0 \qquad \text{on } \partial\Omega_0 \tag{4.40b}$$
$$\phi_{,n} = 0 \qquad \text{on } \partial\Omega_0 \tag{4.40c}$$
$$\phi = 0 \qquad \text{on } \Gamma_0 \tag{4.40d}$$
$$\left(\nabla^2 w_0\right)_{,n} \phi_{,n} + C\nabla^2 \phi = 0 \qquad \text{on } \Gamma_0^+ \tag{4.40e}$$

The eigenvalue problem defined by Eq. (4.40) is homogeneous in the mode shape ϕ (i.e., any scalar multiple of ϕ is also a solution), so an additional normalization condition must be used when obtaining numerical solutions in order to close the system of equations.

Axisymmetric Problem

From here to the end of the chapter we limit ourselves to studying axisymmetric solutions for circular actuators. In this case, Ω is a disk of radius b and Γ a circle of radius a. Letting r be a radial coordinate emanating from the center of Ω, solutions consist of $w = w(r, t)$ and $a = a(t)$, and the governing two-point boundary-value problem reads:

$$\rho h \ddot{w} + D\nabla^4 w = F(w) \tag{4.41a}$$
$$w(b, t) = 0 \tag{4.41b}$$
$$w'(b, t) = 0 \tag{4.41c}$$
$$w(a(t), t) = H \tag{4.41d}$$
$$w'(a(t), t) = 0 \tag{4.41e}$$
$$w''(a(t), t) = -C \tag{4.41f}$$

[2] The (scalar) bending moment is $M = -D\nabla^2 w$ [72, Section 1.4.1].

where

$$\nabla^4 w = w'''' + \frac{2}{r}w''' - \frac{1}{r^2}w'' + \frac{1}{r^3}w', \tag{4.42}$$

the shorthand $()' = \partial()/\partial r$ being employed throughout. Initial conditions should be specified on $w(r,0)$, $\dot{w}(r,0)$, and $a(0)$. The linear stability problem defined by Eq. (4.40) becomes as follows:

$$\left[D\nabla^4 + \rho h\Lambda^2 - F'(w_0)\right]\phi = 0 \tag{4.43a}$$
$$\phi(b) = 0 \tag{4.43b}$$
$$\phi'(b) = 0 \tag{4.43c}$$
$$\phi(a_0) = 0 \tag{4.43d}$$
$$C\phi''(a_0) + w_0'''(a_0)\phi'(a_0) = 0 \tag{4.43e}$$

In the following sections, we use the solver `bvp4c` in MATLAB to solve Eq. (4.41) for the static equilibria and Eq. (4.43) to assess their stability.

4.4 Static Equilibria Before Touchdown

No matter whether we are considering a thick or thin dielectric layer, it is prudent to investigate the static equilibria of the plate prior to touchdown before moving on to studying equilibria post-touchdown. Fortunately, the pre-touchdown problem is straightforward to formulate: simply replace Eqs. (4.41d) to (4.41f) with the requirement that $w(0,t)$ be bounded and let $F(w)$ be given by the expression in Eq. (4.29). With a suitable nondimensionalization, it can be shown that static solutions depend only on the dimensionless parameters

$$\epsilon = \frac{d}{H\epsilon_r} \quad \text{and} \quad \lambda = \frac{\epsilon_0 V^2 b^4}{DH^3}. \tag{4.44}$$

Thus, all solutions can be classified in the (λ,ϵ)-plane. In the sequel, we limit discussion to cases where $\epsilon > 0$ (since the dielectric thickness cannot be negative) and $\lambda > 0$ (since the electrode must attract the plate rather than repel it if touchdown is to occur for sufficiently large voltages).

A bifurcation diagram of the static equilibria for several fixed ϵ is shown in Fig. 4.4. Special attention should be paid to the curve corresponding to $\epsilon = \epsilon_c \approx 1.16$. For $0 \le \epsilon < \epsilon_c$, there can be zero, one, or two physically meaningful equilibria, depending on the value of λ. For $\epsilon > \epsilon_c$, however, there can be only zero or one, and the pull-in instability is absent. Any solutions violating the constraint $w/H \le 1$ are unphysical, so the vertical axis of the figure ranges only from 0 to 1. The dash-dotted line in Fig. 4.4 connects the turning points of the curves for varying ϵ. It intersects $w_0(0)/H = 1$ at $\lambda = \lambda_c \approx 280$.

By translating the results of Fig. 4.4 into the (λ,ϵ)-plane, we obtain a full characterization of various solution regimes and the bifurcations that occur between them. Referring to

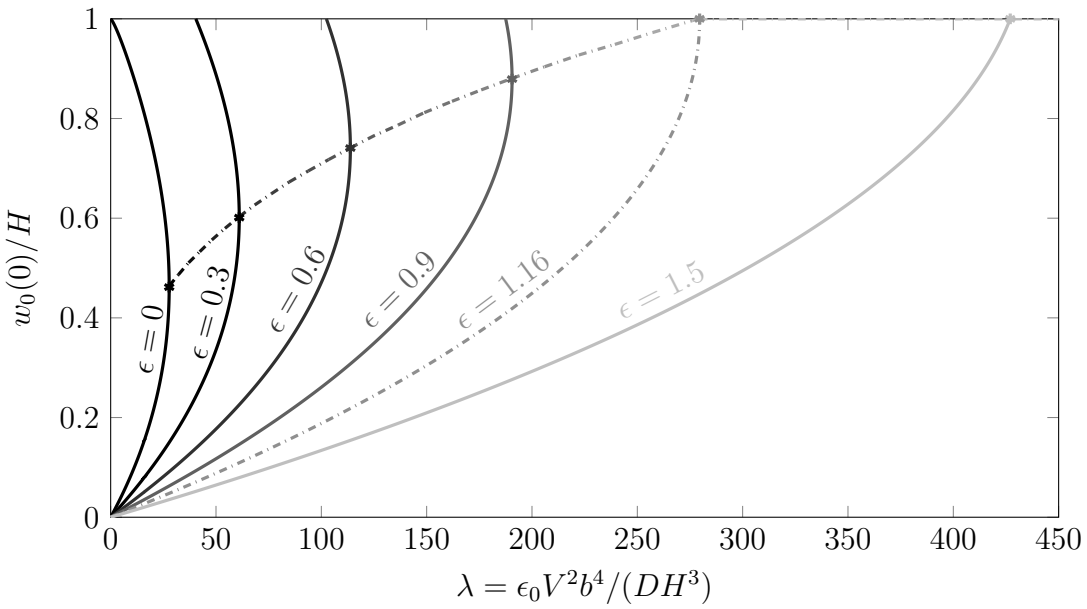

Figure 4.4: Bifurcation diagram for the pre-touchdown equilibria when ϵ takes on several different values. The pull-in instability does not occur for $\epsilon > \epsilon_c \approx 1.16$.

Fig. 4.5, passing from the two-solution zone to the zero-solution zone, a saddle-node bifurcation occurs. The boundary of the one-solution zone, which corresponds to $w_0(0)/H = 1$, can be shown to approach $\lambda = 128\epsilon^2$ as $\epsilon \to \infty$.

4.5 Static Equilibria After Touchdown

The solution space of the post-touchdown equilibrium problem is markedly more difficult to characterize than that of the pre-touchdown problem, and this is for two reasons. First, a distinction must be made between the thick-dielectric ($\epsilon > 0$) and thin-dielectric ($\epsilon \to 0$) models that need not be made in the pre-touchdown problem. Second, as we demonstrate in the sequel, the structure of the equilibria as λ and ϵ are varied can be quite complex. We therefore do not attempt to provide a comprehensive characterization of the solutions in the (λ, ϵ)-plane akin to Fig. 4.5, but instead focus on demonstrating the numerical convergence of the thick-dielectric solutions to the thin-dielectric solution as ϵ is decreased.

As a point of clarification, it is not hard to show that solutions to the post-touchdown equilibrium problem, like those of the pre-touchdown equilibrium problem, depend only on the parameters λ and ϵ. However, since $w(0)/H = 1$ by definition in the post-touchdown problem, we must use a different quantity to characterize solutions when constructing an analogue of Fig. 4.4. A natural choice is the dimensionless (static) contact radius $\alpha_0 = a_0/b$.

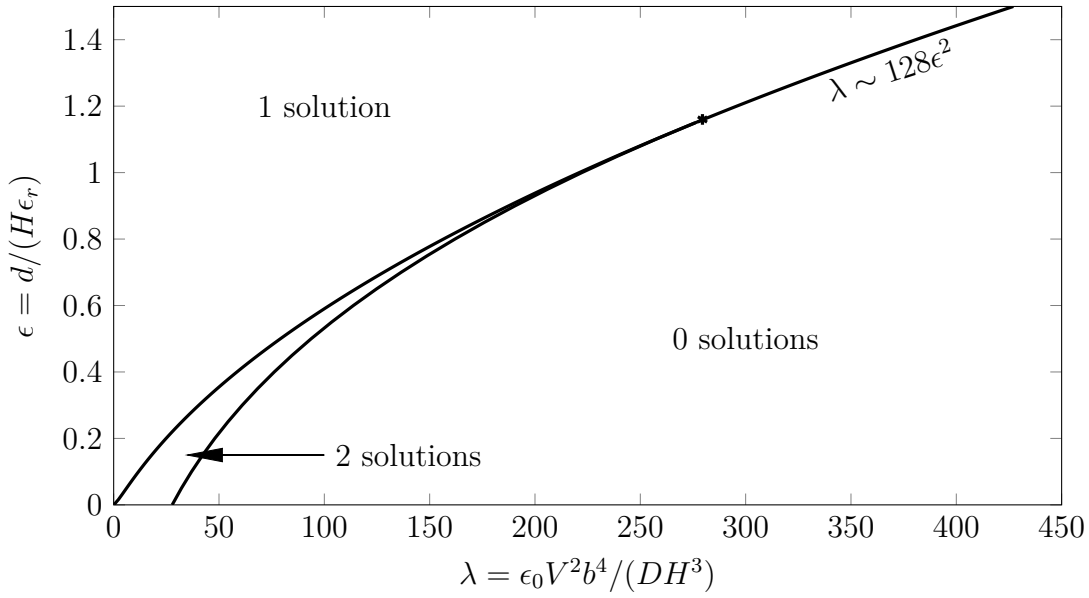

Figure 4.5: Characterization of the pre-touchdown equilibria in terms of the control parameters λ and ϵ. There is exactly one solution at any point on the curves separating the three regions. The critical triple-point marked by the asterisk corresponds to $\lambda = \lambda_c \approx 280$ and $\epsilon = \epsilon_c \approx 1.16$.

Thick Dielectric

Figure 4.6 shows a bifurcation diagram constructed for various $\epsilon > 0$, with λ being the control parameter and α_0 the response variable. We clearly see that there can be zero, one, two, or three equilibria depending on the values of ϵ and λ. Furthermore, unstable equilibria appear only to exist when $\epsilon \lesssim 0.01105$. One shortcoming of this plot is that it does not clearly display a limiting behavior as $\epsilon \to 0$, a matter that will be remedied shortly. It is also unclear whether or not, for fixed ϵ, λ approaches some finite value as $\alpha_0 \to 0$.

Thin Dielectric

In the thin-dielectric case ($\epsilon \to 0$), it is actually possible to solve for the equilibria semi-analytically. Many of the results we recount here have been obtained in the literature for the equivalent adhesion problem [56, 73], so some details are omitted. The displacement field is

$$\frac{w_0(r;a_0)}{H} = c_1\left(\frac{r}{b}\right)^2 + c_2\left(\frac{r}{b}\right)^2 \ln\left(\frac{r}{b}\right)^2 + c_3 \ln\left(\frac{r}{b}\right)^2 + c_4 \tag{4.45}$$

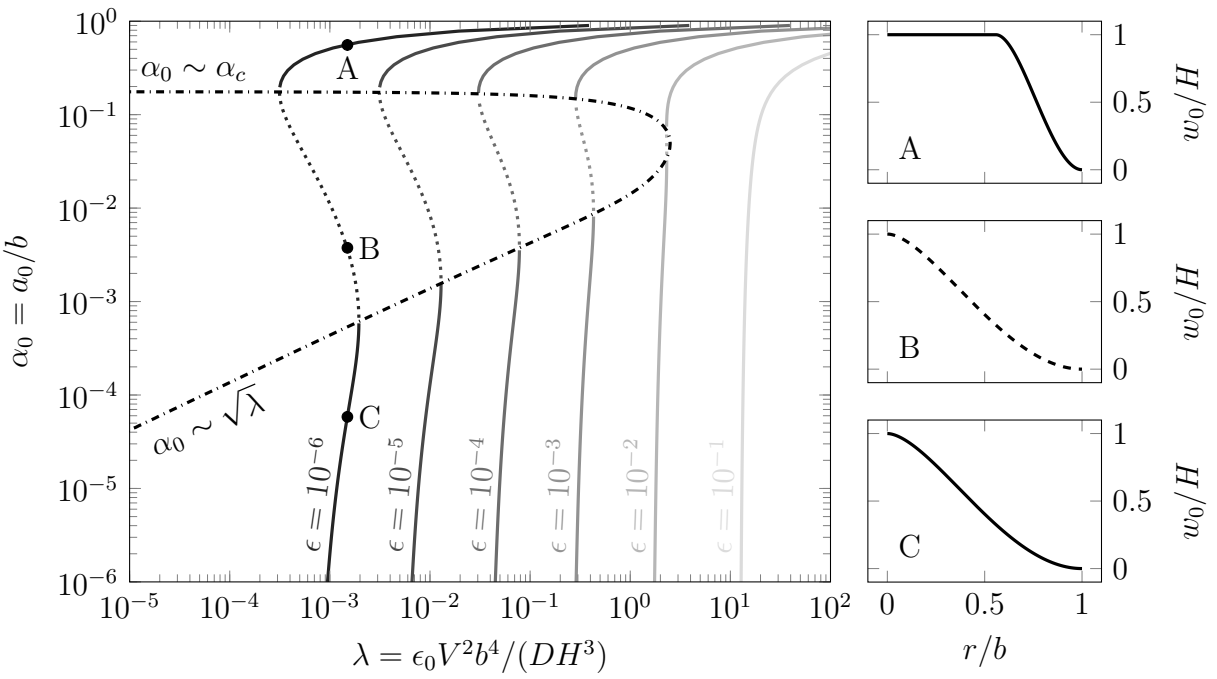

Figure 4.6: Bifurcation diagram of post-touchdown equilibria for various finite ϵ in the thick-dielectric model. The dotted segments correspond to solutions that are unstable as determined by the method outlined in Section 4.3. The dash-dotted curve marks the boundary of the unstable regime, and its limiting behaviors are indicated. As discussed in Section 4.5, $\alpha_c \approx 0.176$ is the boundary between stable and unstable solutions in the thin-dielectric model. The critical thickness below which unstable equilibria appear possible is $\epsilon \approx 0.01105$.

with coefficients

$$c_1 = \frac{1 - \alpha_0^2 - \alpha_0^2 \ln \alpha_0^2}{Q(\alpha_0)} = -c_4 \tag{4.46a}$$

$$c_2 = -\frac{1 - \alpha_0^2}{Q(\alpha_0)} \tag{4.46b}$$

$$c_3 = \frac{\alpha_0^2 \ln \alpha_0^2}{Q(\alpha_0)} \tag{4.46c}$$

where $Q(\alpha) = (\alpha \ln \alpha^2)^2 - (1 - \alpha^2)^2$. The quantity $\alpha_0 = a_0/b$ is unknown a priori and must be determined from the solvability condition

$$\gamma = 8\left[\frac{1 - \alpha_0^2 + \ln \alpha_0^2}{Q(\alpha_0)}\right]^2 \tag{4.47}$$

where $\gamma = \mathcal{G}b^4/(DH^2) = \lambda/(2\epsilon)$ is a dimensionless measure of the strength of the fictitious adhesive in the thin-dielectric model.

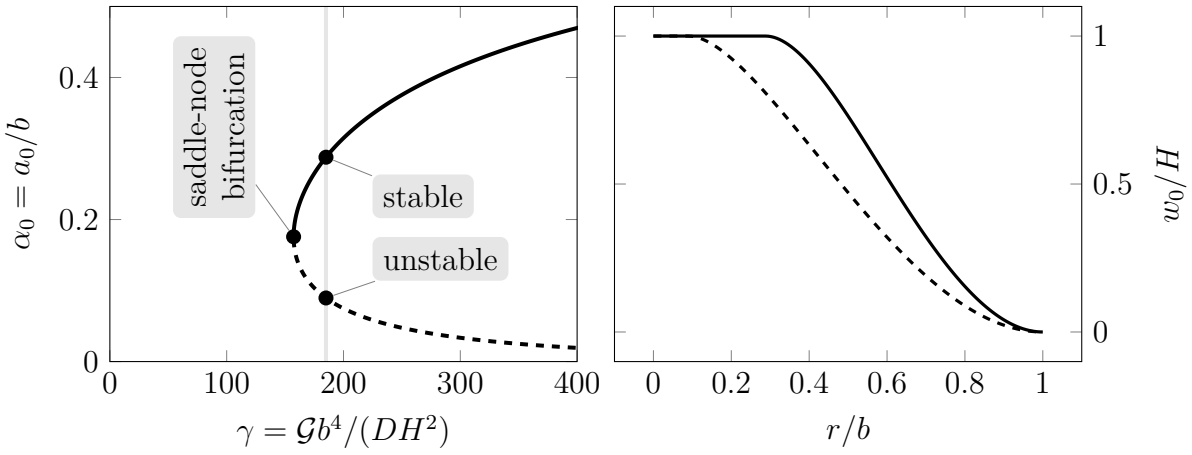

Figure 4.7: Bifurcation diagram for post-touchdown equilibrium solutions of the thin-dielectric model (left) and the stable and unstable solutions at $\gamma = 185$ (right).

Equation (4.47) possesses no solutions when $\gamma < \gamma_c \approx 157.3$, one solution when $\gamma = \gamma_c$ (in which case $\alpha_0 = \alpha_c \approx 0.176$), and two when $\gamma > \gamma_c$. These facts are reflected in the bifurcation diagram in Fig. 4.7. Energetic considerations readily show that, when $\gamma > \gamma_c$, the equilibrium corresponding to the larger value of α_0 is stable while that corresponding to the smaller α_0 is unstable [55]. Thus a saddle-node bifurcation takes place at $\gamma = \gamma_c$. Another important observation from Eq. (4.47) is that point-adhesion is not possible in the thin-dielectric model. That is to say, there does not exist any finite γ for which $\alpha_0 = 0$ is an equilibrium, even in a limiting sense.

In light of Eqs. (4.1), (4.22), and (4.45) to (4.47), the total potential energy of the plate-electrode system in the thin-dielectric model is, in dimensionless terms,

$$\frac{\Pi b^2}{DH^2} = -\frac{8\pi}{Q(\alpha_0)}\left[1 - \alpha_0^2 + \frac{\alpha_0^2}{Q(\alpha_0)}\left(1 - \alpha_0^2 + \ln \alpha_0^2\right)^2\right]. \tag{4.48}$$

Equation (4.48) is remarkably simple. For any valid equilibrium with $0 < \alpha_0 < 1$, it tells us exactly the total potential energy without the need for any intermediate calculations. It is worthwhile noting, however, that setting $\mathrm{d}\Pi/\mathrm{d}\alpha_0 = 0$ from Eq. (4.48) is *not* a statement of the principle of stationary potential energy. This is because the "load" γ is not fixed in Eq. (4.48), but rather varies as necessary according to Eq. (4.47) in order to ensure that a solution exists.

Comparison Between Thick- and Thin-Dielectric Models

The thick- and thin-dielectric models can be compared by plotting the total potential energy Π versus α as in Fig. 4.8. In that figure, the solid lines correspond to solutions of the thick-dielectric model with various values of ϵ, the lightest gray being $\epsilon = 10^{-1}$ and the black

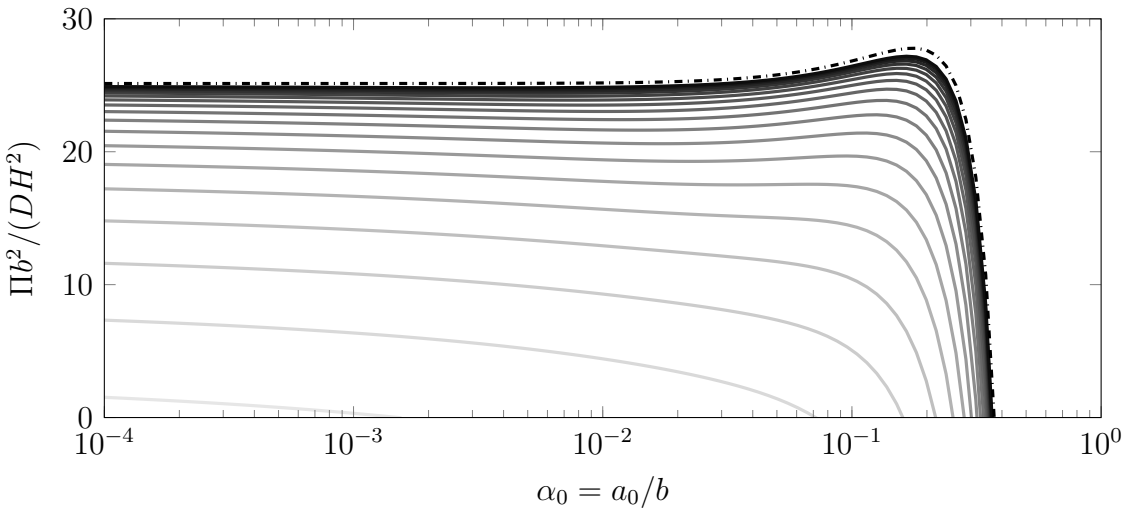

Figure 4.8: Comparison between post-touchdown equilibrium solutions to the thick-dielectric equations ($\epsilon > 0$, solid curves) and the thin-dielectric equations ($\epsilon \to 0$, dash-dotted curve). The nineteen solid curves correspond to thick-dielectric solutions ranging from $\epsilon = 10^{-1}$ in the lightest gray to $\epsilon = 10^{-3}$ in black, with the intermediate values being logarithmically spaced.

being $\epsilon = 10^{-3}$. Each solid line was generated under "displacement" control, i.e., for a given ϵ, we swept through a range of values of α_0, leaving λ to be determined. The dashed line represents Eq. (4.48), the result from the thin-dielectric model. Because the thick-dielectric results so clearly converge to the thin-dielectric result, we can be confident in the usefulness of the latter model as an approximation to the former for ϵ small. Indeed, when we move on to study the dynamics of this system in subsequent sections of the chapter, our focus will be on the thin-dielectric model.

A method of comparing the thick- and thin-dielectric models that incorporates some elements of the system's dynamics is to record how the first eigenvalue $\Lambda_1 = \mu_1 + i\omega_1$ of the linearized dynamics as per Section 4.3 varies as ϵ and α are varied. (Recall that ω_1 is also the natural frequency.) This comparison is made in Fig. 4.9. It should be noted that the values of α for which $\mu_1 > 0$ correspond exactly to the regimes of instability marked by the dotted segments in Fig. 4.6.

4.6 Dynamics of the Thin-Dielectric Model

Having shown that the thin-dielectric model is a good approximation to the thick-dielectric model for $\epsilon = d/(H\epsilon_r)$ small, we now turn our attention entirely to the former and investigate the post-touchdown dynamics.

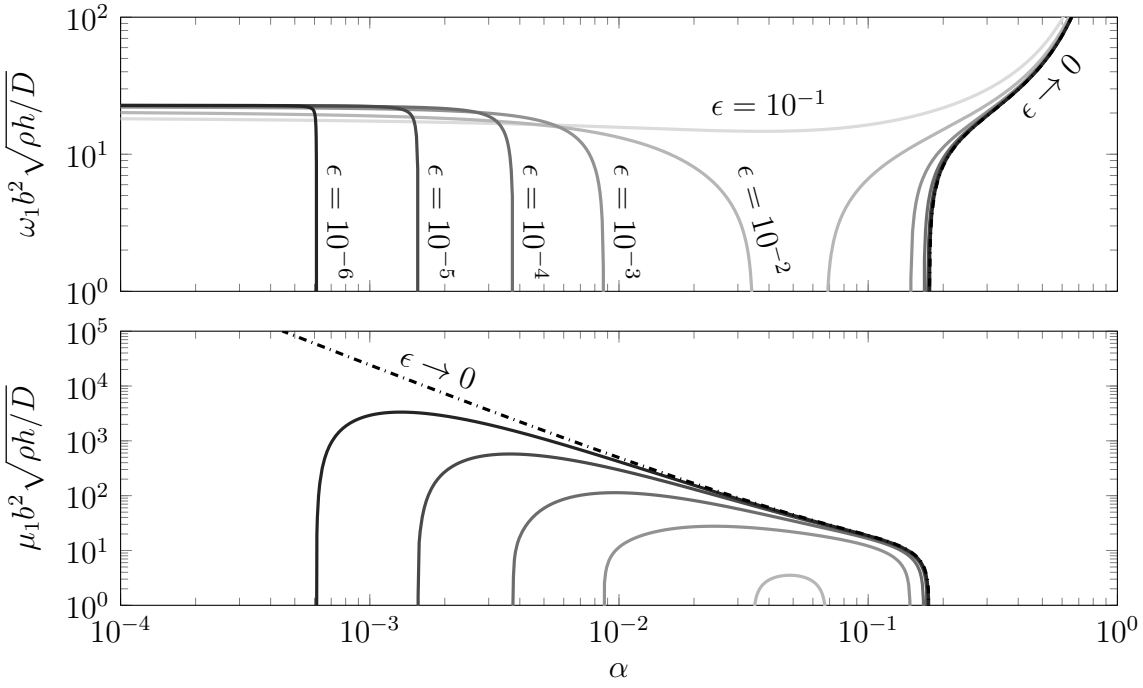

Figure 4.9: Evolution of the first eigenvalue $\Lambda_1 = \mu_1 + i\omega_1$ of the linearized dynamics for both the thick-dielectric model (with various ϵ) and the thin-dielectric model. The dash-dotted curves correspond to the thin-dielectric model. Note that the curve in the upper panel is somewhat obscured due to the rapid convergence of the thick-dielectric solutions as ϵ is decreased. The instability is of the divergence type, as is expected in the case of a conservative, non-gyroscopic system.

The free boundary $r = a(t)$ makes analytical solution of the exact dynamics practically impossible, so we must resort to approximate techniques. One possibility is to use a finite element code with an algorithm that accounts for contact between the plate and the dielectric. While such a model may be relatively straightforward to implement, it has the fundamental limitation that the resolution of $a(t)$ is set by the mesh size, not the time step and wave speed. It is known that the motion of contact interfaces has a strong influence on the dynamics of the overall system [11], so we can expect large changes in $a(t)$ over the course of a single time step to introduce spurious frequency content in the overall response. Indeed, exactly this setback has been observed in a very similar contact problem [22, Fig. 2].

A remedy to the issue of spurious spectral content is to use a sort of arbitrary Lagrangian-Eulerian (ALE) method in which the time-varying spatial domain $a(t) < r < b$ is mapped to a fixed spatial domain $a_0 < R < b$. The simplest mapping that accomplishes this is the linear one:

$$R(r,t) = \frac{b-r}{b-a(t)}a_0 + \frac{r-a(t)}{b-a(t)}b. \tag{4.49}$$

Recognizing that any function $f = f(r,t)$ can also be written $f = \bar{f}(R,t)$, we have $f(r,t) = \bar{f}(R(r,t),t)$. Differentiating with respect to r and t, respectively,

$$f' = \frac{\partial f}{\partial r} = \frac{\partial \bar{f}}{\partial R}\frac{\partial R}{\partial r} \quad \text{and} \quad \dot{f} = \frac{\partial f}{\partial t} = \frac{\partial \bar{f}}{\partial t} + \frac{\partial \bar{f}}{\partial R}\frac{\partial R}{\partial t}. \tag{4.50}$$

These formulas allow us to transform the original problem, Eq. (4.41), which was posed on the time-varying spatial domain, to one posed on the fixed spatial domain. The new problem can then be solved by any number of standard numerical techniques, such as finite elements [11, 46] or modal superposition [74]. The downside to this approach is that it introduces new terms to the PDE that are highly nonlinear in a.

A third numerical technique is based on the assumption

$$w(r,t) = w_0(r;a(t)) + \sum_{n=1}^{N} \phi_n(r;a(t))q_n(t) \tag{4.51}$$

where $\phi_n(r;a)$ are the axisymmetric vibration modes of a plate with inner radius a (and density ρ, flexural rigidity D, etc.). Equation (4.51), which automatically satisfies the requisite kinematic boundary conditions, is inserted into the Lagrangian to obtain $L = L(a, q_1, q_2, \ldots, q_N, \dot{a}, \dot{q}_1, \dot{q}_2, \ldots, \dot{q}_N)$, from which $N+1$ Euler-Lagrange equations for (a, q_i) follow. Approaches of this type have been employed in several applications, including axially moving media [75, 76], contact [77], and fracture mechanics [78, 79]. One shortcoming, noted by Abdelmoula and Debruyne [79], is that this method can lead to violation of the impenetrability constraint $w \leq H$. However, the same authors do mention that said violation is small and does not significantly affect the overall dynamics in their application.

The three methods outlined above are entirely numerical and provide no insight into the fundamental dynamics of the system, not to mention that they all have unique challenges in computational implementation. It is therefore desirable to have some approximate analytical tools available to gain at least a qualitative understanding of the dynamics. Perturbation theory has proven successful in analyzing small vibrations about equilibria in similar problems [10, 11, 33, 42], but this approach has the major downside of not being able to accommodate large deviations of $a(t)$ from a_0, such as occur in a dynamic release of the actuator. For this purpose it is useful to borrow an approach commonly used in dynamic fracture mechanics [78] and employed on a handful occasions in the context of MEMS adhesion [22, 59, 60]. We assume Eq. (4.51) holds with $N = 0$, i.e.,

$$w(r,t) = w_0(r;a(t)). \tag{4.52}$$

In similar fashion to the previously described numerical method, Eq. (4.52) is inserted into the Lagrangian to obtain $L = L(a, \dot{a})$, from which follows a single Euler-Lagrange equation known in the fracture literature as a "crack tip equation of motion." While this method does neglect the small-scale vibrations that occur as the plate moves, it has the distinct advantage of capturing the underlying bulk motion all the while enabling the application of many standard analytical tools.

Equation of Motion

Under the assumption of Eq. (4.52), the kinetic energy is

$$\frac{T}{2\pi} = \frac{1}{2}\rho h H^2 m\Big(\frac{a}{b}\Big)\dot{a}^2 \quad \text{where} \quad m(\alpha) = \int_\alpha^1 \left(\frac{\partial \bar{w}_0}{\partial \alpha}\right)^2 \bar{r}\,\mathrm{d}\bar{r}\,. \tag{4.53}$$

The quantity $m(\alpha)$, the meaning of which will be discussed momentarily, has a lengthy expression that we omit here. With the strain energy being

$$\frac{W}{2\pi} = \frac{DH^2}{b^2}\frac{4(\alpha^2-1)}{Q(\alpha)}. \tag{4.54}$$

and recalling that $U = \epsilon_d V^2/(2d)$ in the thin-dielectric model, the Lagrangian is given by $L(a,\dot{a}) = T(a,\dot{a}) - W(a) + U$. Introducing the following dimensionless quantities,

$$\bar{r} = \frac{r}{b}, \quad \tau = \frac{t}{b^2\sqrt{\rho h/D}}, \quad \bar{w} = \frac{w}{H}, \quad \bar{L} = \frac{Lb^2}{2\pi D H^2}, \tag{4.55}$$

and using $\dot{\alpha}$ to denote $\mathrm{d}\alpha/\mathrm{d}\tau$ rather than $\mathrm{d}\alpha/\mathrm{d}t$ as used previously, the dimensionless Lagrangian can be expressed as

$$\bar{L}(\alpha,\dot{\alpha}) = \frac{1}{2}m(\alpha)\dot{\alpha}^2 - v(\alpha) \quad \text{where} \quad v(\alpha) = \frac{4(\alpha^2-1)}{Q(\alpha)} - \frac{1}{2}\gamma\alpha^2, \tag{4.56}$$

which reflects a particle of position-dependent mass $m(\alpha)$ in a one-dimensional potential $V(\alpha)$. It should be noted that the condition of equilibrium, $\mathrm{d}V/\mathrm{d}\alpha = 0$, is equivalent to Eq. (4.47).

The equation of motion associated with Eq. (4.56) can be written in several insightful forms, one being

$$m(\alpha)\ddot{\alpha} = F(\alpha,\dot{\alpha}) \quad \text{where} \quad F(\alpha,\dot{\alpha}) = -\frac{\partial}{\partial\alpha}\left[\frac{1}{2}m(\alpha)\dot{\alpha}^2 + v(\alpha)\right], \tag{4.57}$$

which bears a superficial similarity to Newton's second law. A consequence of Eq. (4.57) is the conservation of the (dimensionless) total mechanical energy

$$e = \frac{1}{2}m(\alpha)\dot{\alpha}^2 + v(\alpha). \tag{4.58}$$

Phase Portraits

The equation of motion, Eq. (4.57), describes a single-degree-of-freedom system whose solutions depend on a single parameter γ. A great deal of insight can therefore be gained by investigating how the $(\alpha,\dot{\alpha})$-phase portrait changes as γ is varied. Figure 4.10 shows three

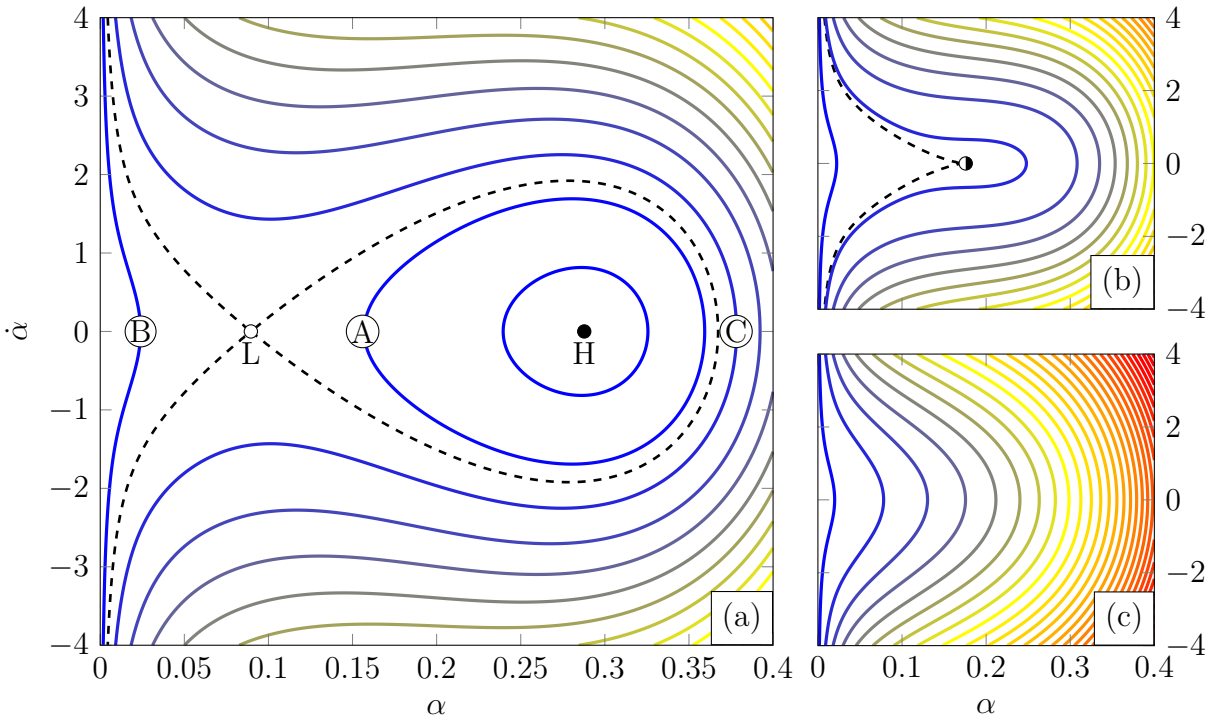

Figure 4.10: Phase portraits for (a) $\gamma = 185$, (b), $\gamma = \gamma_c \approx 157.3$, and (c) $\gamma = 100$. Where present, the dashed curves are the separatrices that form the boundary between closed and non-closed trajectories of the system. The direction of the closed trajectories is clockwise, and the non-closed trajectories run from top to bottom. "Warmer" colors correspond to larger e, while "cooler" colors correspond to smaller e.

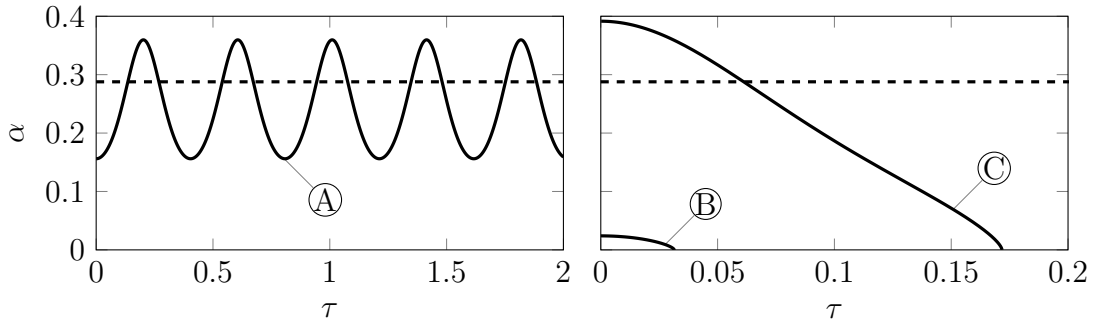

Figure 4.11: Time series of a typical closed trajectory (left) and typical non-closed trajectories (right) corresponding to the labels A, B, and C in Fig. 4.10(a). The dashed line in each plot indicates the stable equilibrium.

phase portraits, one where $\gamma > \gamma_c$, another where $\gamma = \gamma_c$, and a third where $\gamma < \gamma_c$. The direction of the non-closed trajectories is from top to bottom, while the direction of the closed orbits is clockwise.

Several interesting features can be gleaned from the phase portraits. For one, when $\gamma > \gamma_c$, closed orbits around the stable equilibrium $\alpha(t) = \alpha_H$ exist. What's more, these orbits are asymmetric, meaning that the plate's excursion from equilibrium is greater when it is lifting off of the dielectric ($\alpha(t) > \alpha_H$) than when it is pushing down onto the dielectric ($\alpha(t) < \alpha_H$). Another interesting feature is that all of the non-closed trajectories are asymptotic to $\alpha = 0$, but $\alpha(t) \to 0$ in finite time from any initial condition outside of the separatrix. (This is *finite-time blow up* in mathematical terms.) Physically speaking, $\alpha = 0$ means that the plate has released from the dielectric. A real-world MEMS device of the sort being considered here can, of course, achieve release in finite time. It is remarkable that our qualitative model, with its many drastic simplifying assumptions, still reflects this behavior. Numerical solutions starting from the points labeled A, B, and C in Fig. 4.10(a) are illustrated in Fig. 4.11, clearly demonstrating the asymmetry of the closed orbits and the finite-time blow-up of the non-closed trajectories.

Parametric Excitation and Application to Stiction Repair

We now briefly apply our model to the problem of vibration-assisted stiction repair, a topic that has been studied previously [59, 60]. Consider the following idealized case: a certain voltage V_0 has been applied that is large enough to cause stiction, meaning that the actuator is "stuck" at the stable fixed point $\alpha = \alpha_H$ (cf. Fig. 4.10(a)). If we only have control over small dynamic deviations from V_0, can the actuator be released from the initial conditions $\alpha(0) = \alpha_H$ and $\dot{\alpha}(0) = 0$? This is a problem of parametric excitation in a strongly nonlinear system, a complete treatment of which would require its own full-length chapter. Here we merely demonstrate the ability of our model to capture the qualitatively correct dynamics.

Recall that γ is proportional to the *squared* voltage. It is therefore somewhat more useful, though we are still dealing with a purely qualitative model, to replace $\gamma = \nu^2$. We can accomplish stiction repair by superposing a small linear chirp of amplitude δ on top of the static ν_0:

$$\nu(\tau) = \nu_0 + \delta \sin\left(\Omega(\tau)\tau\right), \quad \Omega(\tau) = (1 - \beta\tau)\omega_H. \tag{4.59}$$

Here, ω_H is the linearized natural frequency about the stable fixed point. Savkar and Murphy [60] investigated a similar excitation technique for releasing a stiction-failed MEMS beam, and found that a decreasing chirp was more effective than an increasing one, motivating our choice of the former. Figure 4.12 shows the response of a system with $\gamma_0 = 160$ to a chirp of amplitude $\delta = 0.01$ and decay rate $\beta = 0.002$, suggesting that the strategy of applying a small-amplitude decreasing voltage chirp may be a feasible technique to use in a real device.

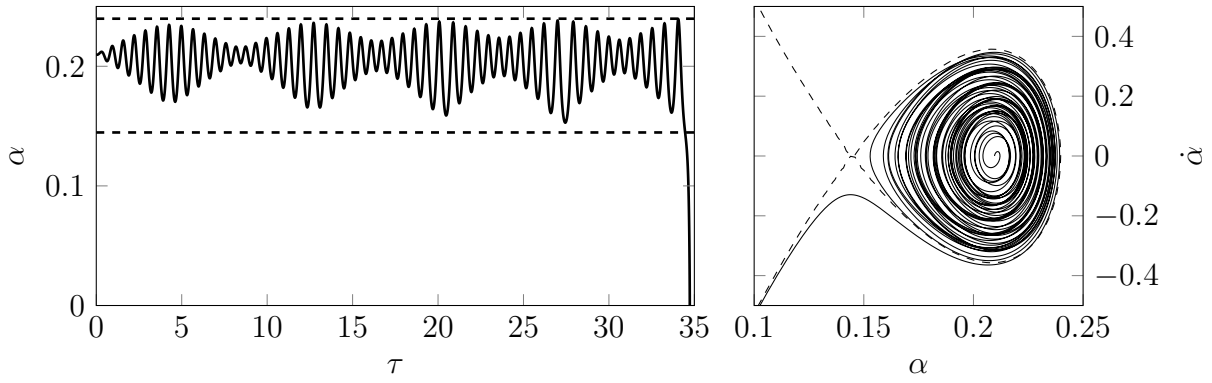

Figure 4.12: Response of the reduced-order dynamics with $\gamma_0 = 160$ due to the voltage chirp given by Eq. (4.59) with $\delta = 0.01$ and $\beta = 0.002$: time series (left) and phase plane trajectory (right). The dashed lines in the time series represent the maximum and minimum values of α for orbits within the separatrix indicated by the dashed curve in the phase plane.

4.7 Conclusion

In this chapter, we studied the fundamental mechanics of contact in plate-based electrostatic actuators, with a special interest in the nonlinear effects induced by the motion of the contact interface. Using a variational principle, we derived two models: one in which a certain dimensionless parameter was finite (what we called the thick-dielectric model) and another where the parameter was vanishingly small (the thin-dielectric model). After characterizing the equilibrium solutions to the axisymmetric problem for both models, we discussed the challenges associated with solving the transient dynamics before applying a simplifying approximation to the thin-dielectric model to obtain a single second-order ordinary differential equation for the location of the contact interface. The solutions of this differential equation were studied in the phase plane and the relevance of the model to the problem of vibration-assisted stiction repair was discussed briefly.

There are a number of aspects of touchdown dynamics that deserve further study. One is the issue of nonlinear vibrations. As suggested by previous work on problems involving rods and beams [11], the leading-order nonlinear effect of the contact interface should be to induce superharmonic and combination resonances. It may be possible to exploit these resonances to accelerate stiction repair. Another avenue of research would be to study the comparative advantages of the various numerical methods discussed in Section 4.6 and to extend them to non-axisymmetric solutions. Finally, it would be useful for the design of practical MEMS devices to extend the models proposed in this chapter to incorporate the effects of several physical phenomena we omitted, including the electrical fringing field, mid-plane stretching of the plate, and squeeze-film damping.

Chapter 5

Concluding Remarks

In this dissertation we have explored several topics in the dynamics of structures with unilateral contact constraints by way of example. After having presented some basic ideas in Chapter 1, we proceeded to study in Chapter 2 the linearized dynamics of a system that models microelectromechanical cantilevers and flexible risers. Then, in Chapter 3, we investigated the nonlinear dynamics of the same system and discovered a pattern in the nonlinear resonances induced by the constraint of contact. A generalization of this result led us to the conclusion that similar patterns would likely arise in a wide array of structural systems with contact, a result with implications for the design of vibration-critical systems. While Chapters 2 and 3 concerned only problems of beams moving in the plane, we studied in Chapter 4 a problem of a plate in three dimensions. Despite the fact that the plate problem was significantly more involved to formulate, its dynamics had many similarities to the beam problems, in large part due to both beams and plates being governed by a spatially fourth-order partial differential equation.

Chapters 2 and 3 suggest a number of avenues for future research on the problem of the contacting cantilever. One direction could be to apply similar methods of analysis to more sophisticated models of MEMS cantilevers and flexible risers and determine the extent to which the nonlinear resonances are important for realistic parameter values. Another direction could be to continue to study our simplistic model but with a handful of added features. For example, a natural question is whether contact can generate chaotic motions, especially in the presence of forcing. The conditions under which the beam can sustain multiple regions of contact may also be interesting. The beam could hypothetically eject pulses into the contacting region that then travel off to infinity, thereby dissipating energy from the initial non-contacting region. It would also be interesting from a theoretical point-of-view to investigate how the dynamics differ when a rod theory that accounts for additional effects such as extension, shear, cross-sectional deformation, and warping is employed. Indeed, it is well-known that inextensible, unshearable rod theories (such as Euler-Bernoulli beam theory) fail to capture the correct three-dimensional deformation fields in the vicinity of contact interfaces.

The plate problem from Chapter 4 provides countless opportunities for future research.

There is a wide variety of rich behaviors that can arise due to the fact that the contact interface is a curve rather than a point. As an example, it could be the case that certain non-axisymmetric perturbations to an axisymmetric motion are unstable in a manner that is geometrically similar to the fingering instability in Hele-Shaw cells [80]. Studying this sort of problem would necessitate the development of numerical techniques that can track the non-axisymmetric contact interface, which is no small task in and of itself. One promising method might involve regarding the current domain as a conformal mapping of a simple reference domain, such as a sphere. The mapping could then be approximated by some means and then introduced into the governing equations. The advantage of using a conformal mapping is that it would preserve the biharmonic operator in the differential equation. In addition to non-axisymmetric motions, one could also study the dynamics of the transition from pre-touchdown to post-touchdown configurations, especially the moment at which the plate impacts the substrate. There are also several additional nonlinear-dynamical matters worth pursuing, such as a detailed analysis of the periodic motions the plate can execute after touchdown and the implications of the saddle-node bifurcation in the static equilibria of the thin-dielectric model for bottlenecking.

There are countless technological applications where a proper modeling of contact dynamics using the principles from this dissertation would be beneficial. One mentioned briefly in Chapter 1 is vibration-mediated adhesion, in which small-amplitude, high-frequency vibrations can be used to greatly enhance the pull-off force of an adhesive contact, or reduce it to zero. Recent research has shown that this technique can outperform the well-known "gecko" adhesion technology by certain metrics [5]. Mechanical metamaterials are another potential application; contact interactions between cells could be used to tune exotic dynamics in the bulk "material." Vibration-induced loosening of bolted joints, a major nuisance across countless industries, also poses several opportunities for contact dynamicists, as analyses are typically limited to the case where a bolt is sufficiently tight that the contact surface (often called the bearing surface in this context) is fixed. During incipient loss of bolt tension, however, the bearing surface can change size and shape. Taking this into account would be an especially challenging, but rewarding, application of the sort of analysis conducted in this dissertation.

Bibliography

[1] P. G. Hodge. *Plastic Analysis of Structures*. McGraw-Hill, 1959.

[2] P. Rosenau. On essential nonlinearities emerging from linear systems. *Wave Motion*, 110:102881, 2022. DOI: 10.1016/j.wavemoti.2022.102881.

[3] V. F. Nesterenko. Propagation of nonlinear compression pulses in granular media. *Journal of Applied Mechanics and Technical Physics*, 24(5):733–743, 1983. DOI: 10.1007/BF00905892.

[4] A. H. Nayfeh and D. T. Mook. *Nonlinear Oscillations*. Wiley Classics Library. Wiley, New York, 1995. DOI: 10.1002/9783527617586.

[5] L. Shui, L. Jia, H. Li, J. Guo, Z. Guo, Y. Liu, Z. Liu, and X. Chen. Rapid and continuous regulating adhesion strength by mechanical micro-vibration. *Nature Communications*, 11(1):1583, 1, 2020. DOI: 10.1038/s41467-020-15447-x.

[6] C. Y. Wang. Lifting of Heavy Elastic Sheet. *Journal of Engineering Mechanics*, 109(1):47–53, 1983. DOI: 10.1061/(ASCE)0733-9399(1983)109:1(47).

[7] O. M. O'Reilly. *Modeling Nonlinear Problems in the Mechanics of Strings and Rods*. Interaction of Mechanics and Mathematics. Springer International Publishing AG, Cham, CH, 2017. DOI: 10.1007/978-3-319-50598-5.

[8] P. Wriggers. *Computational Contact Mechanics*. Springer-Verlag Berlin Heidelberg, 2nd edition, 2006. DOI: 10.1007/978-3-540-32609-0.

[9] R. L. Taylor and P. Papadopoulos. On a finite element method for dynamic contact/impact problems. *International Journal for Numerical Methods in Engineering*, 36(12):2123–2140, 1993. DOI: 10.1002/nme.1620361211.

[10] N. N. Goldberg and O. M. O'Reilly. On contact point motion in the vibration analysis of elastic rods. *Journal of Sound and Vibration*, 487:115579, 2020. DOI: 10.1016/j.jsv.2020.115579.

[11] N. N. Goldberg and O. M. O'Reilly. Pervasive nonlinear vibrations due to rod-obstacle contact. *Nonlinear Dynamics*, 103:2169–2181, 2021. DOI: 10.1007/s11071-021-06245-1.

[12] N. N. Goldberg and O. M. O'Reilly. Electrostatically actuated MEMS in the post-touchdown regime: The thin-dielectric limit and a novel reduced-order model for release dynamics. *International Journal of Solids and Structures*, 252:111812, 2022. DOI: 10.1016/j.ijsolstr.2022.111812.

[13] L. Vu-Quoc and S. Li. Dynamics of sliding geometrically-exact beams: large angle maneuver and parametric resonance. *Computer Methods in Applied Mechanics and Engineering*, 120(1-2):65–118, 1995. DOI: 10.1016/0045-7825(94)00051-N.

[14] N. Singh, I. Sharma, and S. S. Gupta. Dynamics of variable length geometrically exact beams in three-dimensions. *International Journal of Solids and Structures*, 191-192:614–627, 2019. DOI: 10.1016/j.ijsolstr.2019.11.005.

[15] L. Mansfield and J. G. Simmonds. The Reverse Spaghetti Problem: Drooping Motion of an Elastica Issuing from a Horizontal Guide. *Journal of Applied Mechanics*, 54(1):147, 1987. DOI: 10.1115/1.3172949.

[16] D. Vella, A. Boudaoud, and M. Adda-Bedia. Statics and Inertial Dynamics of a Ruck in a Rug. *Physical Review Letters*, 103(17):174301, 2009. DOI: 10.1103/PhysRevLett.103.174301.

[17] G. Napoli and A. Goriely. A tale of two nested elastic rings. *Proceedings of the Royal Society A: Mathematical, Physical and Engineering Sciences*, 473(2204):20170340, 2017. DOI: 10.1098/rspa.2017.0340.

[18] N. N. Goldberg and O. M. O'Reilly. Mechanics-based model for the cooking-induced deformation of spaghetti. *Physical Review E*, 101(1):013001, 2020. DOI: 10.1103/PhysRevE.101.013001.

[19] S. Neukirch, J. Frelat, A. Goriely, and C. Maurini. Vibrations of post-buckled rods: The singular inextensible limit. *Journal of Sound and Vibration*, 331(3):704–720, 2012. DOI: 10.1016/j.jsv.2011.09.021.

[20] L. Demeio and S. Lenci. Forced nonlinear oscillations of semi-infinite cables and beams resting on a unilateral elastic substrate. *Nonlinear Dynamics*, 49(1-2):203–215, 2007. DOI: 10.1007/s11071-006-9122-0.

[21] I. K. Chatjigeorgiou. Second-order nonlinear dynamics of catenary pipelines: A frequency domain approach. *Computers & Structures*, 123:1–14, 2013. DOI: 10.1016/j.compstruc.2013.04.006.

[22] A. Roy and A. Chatterjee. Vibrations of a Beam in Variable Contact With a Flat Surface. *Journal of Vibration and Acoustics*, 131(4):041010, 2009. DOI: 10.1115/1.3086930.

[23] Y. Vetyukov, E. Oborin, J. Scheidl, M. Krommer, and C. Schmidrathner. Flexible belt hanging on two pulleys: Contact problem at non-material kinematic description. *International Journal of Solids and Structures*, 168:183–193, 2019. DOI: 10.1016/j.ijsolstr.2019.03.034.

[24] R. H. Plaut and L. N. Virgin. Deformation and vibration of upright loops on a foundation and of hanging loops. *International Journal of Solids and Structures*, 51(18):3067–3075, 2014. DOI: 10.1016/j.ijsolstr.2014.05.003.

[25] L. N. Virgin, J. V. Giliberto, and R. H. Plaut. Deformation and vibration of compressed, nested, elastic rings on rigid base. *Thin-Walled Structures*, 132:167–175, 2018. DOI: 10.1016/j.tws.2018.08.015.

[26] A. Humer and H. Irschik. Large deformation and stability of an extensible elastica with an unknown length. *International Journal of Solids and Structures*, 48(9):1301–1310, 2011. DOI: 10.1016/j.ijsolstr.2011.01.015.

[27] L. Demeio and S. Lenci. Second-order solutions for the dynamics of a semi-infinite cable on a unilateral substrate. *Journal of Sound and Vibration*. EUROMECH Colloquium 483, Geometrically Non-Linear Vibrations of Structures, 315(3):414–432, 2008. DOI: 10.1016/j.jsv.2008.03.010.

[28] W.-C. Ro, J.-S. Chen, and S.-Y. Hong. Vibration and stability of a constrained elastica with variable length. *International Journal of Solids and Structures*, 47(16):2143–2154, 2010. DOI: 10.1016/j.ijsolstr.2010.04.015.

[29] S. Chucheepsakul and T. Monprapussorn. Divergence instability of variable-arc-length elastica pipes transporting fluid. *Journal of Fluids and Structures*, 14(6):895–916, 2000. DOI: 10.1006/jfls.2000.0301.

[30] C. Armanini, F. D. Corso, D. Misseroni, and D. Bigoni. Configurational forces and nonlinear structural dynamics. *Journal of the Mechanics and Physics of Solids*, 130:82–100, 2019. DOI: 10.1016/j.jmps.2019.05.009.

[31] C. Majidi, O. M. O'Reilly, and J. A. Williams. On the stability of a rod adhering to a rigid surface: Shear-induced stable adhesion and the instability of peeling. *Journal of the Mechanics and Physics of Solids*, 60(5):827–843, 2012. DOI: 10.1016/j.jmps.2012.01.015.

[32] C. Majidi, O. M. O'Reilly, and J. A. Williams. Bifurcations and instability in the adhesion of intrinsically curved rods. *Mechanics Research Communications*, 49:13–16, 2013. DOI: 10.1016/j.mechrescom.2013.01.004.

[33] L. Demeio, G. Lancioni, and S. Lenci. Nonlinear resonances in infinitely long 1D continua on a tensionless substrate. *Nonlinear Dynamics*, 66(3):271–284, 2011. DOI: 10.1007/s11071-011-0016-4.

[34] G. Fichera. Problemi elastostatici con vincoli unilaterali: il problema di Signorini con ambigue condizioni al contorno. *Atti dell'Accademia Nazionale dei Lincei*, 7(8):91–140, 1964.

[35] P. J. Holmes. The dynamics of repeated impacts with a sinusoidally vibrating table. *Journal of Sound and Vibration*, 84(2):173–189, 1982. DOI: 10.1016/S0022-460X(82)80002-3.

[36] J. M. T. Thompson and R. Ghaffari. Chaotic dynamics of an impact oscillator. *Physical Review A*, 27(3):1741–1743, 1983. DOI: 10.1103/PhysRevA.27.1741.

[37] R. Burridge, J. Kappraff, and C. Morshedi. The Sitar String, a Vibrating String with a One-Sided Inelastic Constraint. *SIAM Journal on Applied Mathematics*, 42(6):1231–1251, 1982. DOI: 10.1137/0142086.

[38] H. Singh and J. A. Hanna. Pick-up and impact of flexible bodies. *Journal of the Mechanics and Physics of Solids*, 106:46–59, 2017. DOI: 10.1016/j.jmps.2017.04.019.

[39] B. Audoly, A. Callan-Jones, and P.-T. Brun. Dynamic curling of an Elastica: a nonlinear problem in elastodynamics solved by matched asymptotic expansions. In D. Bigoni, editor, *Extremely Deformable Structures*, CISM International Centre for Mechanical Sciences, pages 137–155. Springer Vienna, Vienna, 2015. DOI: 10.1007/978-3-7091-1877-1_3.

[40] W. Fang, J. Mok, and H. Kesari. Effects of geometric nonlinearity in an adhered microbeam for measuring the work of adhesion. *Proceedings of the Royal Society A: Mathematical, Physical and Engineering Sciences*, 474(2211):20170594, 2018. DOI: 10.1098/rspa.2017.0594.

[41] M. S. Triantafyllou, A. Bliek, and H. Shin. Dynamic analysis as a tool for open-sea mooring system design. *Transactions of the Society of Naval Architects and Marine Engineers*, 93:303–324, 1985.

[42] P. Turnbull, N. Perkins, and W. Schultz. Contact-Induced Nonlinearity in Oscillating Belts and Webs. *Journal of Vibration and Control*, 1(4):459–479, 1995. DOI: 10.1177/107754639500100404.

[43] P. Naghdi and M. Rubin. On the significance of normal cross-sectional extension in beam theory with application to contact problems. *International Journal of Solids and Structures*, 25(3):249–265, 1989. DOI: 10.1016/0020-7683(89)90047-4.

[44] S. Lenci and M. Callegari. Simple analytical models for the J-lay problem. *Acta Mechanica*, 178(1):23–39, 2005. DOI: 10.1007/s00707-005-0239-x.

[45] A. Humer. Dynamic modeling of beams with non-material, deformation-dependent boundary conditions. *Journal of Sound and Vibration*, 332(3):622–641, 2013. DOI: 10.1016/j.jsv.2012.08.026.

[46] A. Humer, I. Steinbrecher, and L. Vu-Quoc. General sliding-beam formulation: A non-material description for analysis of sliding structures and axially moving beams. *Journal of Sound and Vibration*, 480:115341, 2020. DOI: 10.1016/j.jsv.2020.115341.

[47] S. S. Rao. *Vibration of Continuous Systems*. Wiley, Hoboken, N.J, 2007. DOI: 10.1002/9780470117866.

[48] N. Minorsky. *Nonlinear Oscillations*. R. E. Krieger, Malabar, Florida, 1987.

[49] W.-M. Zhang, H. Yan, Z.-K. Peng, and G. Meng. Electrostatic pull-in instability in MEMS/NEMS: A review. *Sensors and Actuators A: Physical*, 214:187–218, 2014. DOI: 10.1016/j.sna.2014.04.025.

[50] R. Batra, M. Porfiri, and D. Spinello. Reduced-order models for microelectromechanical rectangular and circular plates incorporating the Casimir force. *International Journal of Solids and Structures*, 45(11-12):3558–3583, 2008. DOI: 10.1016/j.ijsolstr.2008.02.019.

[51] P. Laurençot and C. Walker. Some singular equations modeling MEMS. *Bulletin of the American Mathematical Society*, 54(3):437–479, 2016. DOI: 10.1090/bull/1563.

[52] S. M. M. Kafumbe, J. S. Burdess, and A. J. Harris. Frequency adjustment of microelectromechanical cantilevers using electrostatic pull down. *Journal of Micromechanics and Microengineering*, 15(5):1033–1039, 2005. DOI: 10.1088/0960-1317/15/5/020.

[53] Y. Li, S. A. Meguid, Y. Fu, and D. Xu. Unified nonlinear quasistatic and dynamic analysis of RF-MEMS switches. *Acta Mechanica*, 224(8):1741–1755, 2013. DOI: 10.1007/s00707-013-0831-4.

[54] R. Batra, M. Porfiri, and D. Spinello. Effects of van der Waals Force and Thermal Stresses on Pull-in Instability of Clamped Rectangular Microplates. *Sensors*, 8(2):1048–1069, 2008. DOI: 10.3390/s8021048.

[55] C. Mastrangelo and C. Hsu. Mechanical stability and adhesion of microstructures under capillary forces. I. Basic theory. *Journal of Microelectromechanical Systems*, 2(1):33–43, 1993. DOI: 10.1109/84.232593.

[56] C. H. Mastrangelo and C. H. Hsu. Mechanical stability and adhesion of microstructures under capillary forces. II. Experiments. *Journal of Microelectromechanical Systems*, 2(1):44–55, 1993. DOI: 10.1109/84.232594.

[57] S. Gorthi, A. Mohanty, and A. Chatterjee. Cantilever beam electrostatic MEMS actuators beyond pull-in. *Journal of Micromechanics and Microengineering*, 16(9):1800–1810, 2006. DOI: 10.1088/0960-1317/16/9/007.

[58] Y. Zhang and Y.-P. Zhao. Vibration of an adhered microbeam under a periodically shaking electrical force. *Journal of Adhesion Science and Technology*, 19(9):799–815, 2005. DOI: 10.1163/1568561054867864.

[59] A. A. Savkar, K. D. Murphy, Z. C. Leseman, T. J. Mackin, and M. R. Begley. On the Use of Structural Vibrations to Release Stiction Failed MEMS. *Journal of Microelectromechanical Systems*, 16(1):163–173, 2007. DOI: 10.1109/JMEMS.2006.885986.

[60] A. Savkar and K. Murphy. The evolution of stiction repair for microelectromechanical system cantilevers using periodic excitation. *Journal of Sound and Vibration*, 329(2):189–201, 2010. DOI: 10.1016/j.jsv.2009.09.003.

[61] C. P. Vyasarayani, E. M. Abdel-Rahman, J. McPhee, and S. Birkett. Modeling MEMS Resonators Past Pull-In. *Journal of Computational and Nonlinear Dynamics*, 6(3):031008, 2011. DOI: 10.1115/1.4002835.

[62] A. Lindsay, J. Lega, and K. Glasner. Regularized model of post-touchdown configurations in electrostatic MEMS: Equilibrium analysis. *Physica D: Nonlinear Phenomena*, 280–281:95–108, 2014. DOI: 10.1016/j.physd.2014.04.007.

[63] A. E. Lindsay, J. Lega, and K. B. Glasner. Regularized model of post-touchdown configurations in electrostatic MEMS: interface dynamics. *IMA Journal of Applied Mathematics*, 80(6):1635–1663, 2015. DOI: 10.1093/imamat/hxv011.

[64] A. E. Lindsay. Regularized model of post-touchdown configurations in electrostatic MEMS: bistability analysis. *Journal of Engineering Mathematics*, 99(1):65–77, 2016. DOI: 10.1007/s10665-015-9820-z.

[65] G. Duvaut and J. L. Lions. *Inequalities in Mechanics and Physics*, volume 219 of *Grundlehren Der Mathematischen Wissenschaften*. Springer-Verlag Berlin Heidelberg, 1976. DOI: 10.1007/978-3-642-66165-5.

[66] M. Shillor, M. Sofonea, and J. J. Telega. *Models and Analysis of Quasistatic Contact: Variational Methods*. Lecture Notes in Physics. Springer-Verlag Berlin Heidelberg, 1st edition, 2004. DOI: 10.1007/b99799.

[67] F. Yang. Electromechanical instability of microscale structures. *Journal of Applied Physics*, 92(5):2789–2794, 2002. DOI: 10.1063/1.1496123.

[68] J. A. Pelesko and D. H. Bernstein. *Modeling MEMS and NEMS*. CRC Press, 2002. DOI: 10.1201/9781420035292.

[69] C. Majidi and G. G. Adams. Adhesion and delamination boundary conditions for elastic plates with arbitrary contact shape. *Mechanics Research Communications*, 37(2):214–218, 2010. DOI: 10.1016/j.mechrescom.2010.01.002.

[70] J. Hure and B. Audoly. Capillary buckling of a thin film adhering to a sphere. *Journal of the Mechanics and Physics of Solids*, 61(2):450–471, 2013. DOI: 10.1016/j.jmps.2012.09.016.

[71] N. N. Goldberg and O. M. O'Reilly. A Material Momentum Balance Law for Shells and Plates with Application to Phase Transformations and Adhesion. *Acta Mechanica*, In press.

[72] E. H. Mansfield. *The Bending and Stretching of Plates*. Cambridge University Press, New York, 2nd edition, 1989. DOI: 10.1017/CBO9780511525193.

[73] J. L. Liu. Theoretical analysis on capillary adhesion of microsized plates with a substrate. *Acta Mechanica Sinica*, 26(2):217–223, 2010. DOI: 10.1007/s10409-009-0318-7.

[74] P. Wang and J.-D. Wei. Vibrations in a moving flexible robot arm. *Journal of Sound and Vibration*, 116(1):149–160, 1987. DOI: 10.1016/S0022-460X(87)81326-3.

[75] J. Yuh and T. Young. Dynamic Modeling of an Axially Moving Beam in Rotation: Simulation and Experiment. *Journal of Dynamic Systems, Measurement, and Control*, 113(1):34–40, 1991. DOI: 10.1115/1.2896355.

[76] W. D. Zhu and J. Ni. Energetics and Stability of Translating Media with an Arbitrarily Varying Length. *Journal of Vibration and Acoustics*, 122(3):295–304, 2000. DOI: 10.1115/1.1303003.

[77] R.-F. Fung and C.-C. Chen. Free and forced vibration of a cantilever beam contacting with a rigid cylindrical foundation. *Journal of Sound and Vibration*, 202(2):161–185, 1997. DOI: 10.1006/jsvi.1996.0831.

[78] L. B. Freund. *Dynamic Fracture Mechanics*. Cambridge University Press, 1st edition, 1990. DOI: 10.1017/CBO9780511546761.

[79] R. Abdelmoula and G. Debruyne. Modal analysis of the dynamic crack growth and arrest in a DCB specimen. *International Journal of Fracture*, 188(2):187–202, 2014. DOI: 10.1007/s10704-014-9954-4.

[80] L. Paterson. Radial fingering in a Hele Shaw cell. *Journal of Fluid Mechanics*, 113:513–529, 1981. DOI: 10.1017/S0022112081003613.

Appendix A

Details on the Linear Rod Vibration Problem

A.1 Small-on-Small Vibrations with Combined Gravity and Adhesion

Recall that the leading-order dynamics of the linearized system are governed by Eqs. (2.21) to (2.24) and Eq. (2.29), except with the rotational spring stiffness K given by Eq. (2.32). Following the standard procedure, we seek solutions of the form $y_1(x,t) = Y(x)\sin(\omega t)$ with the goal of determining the admissible natural frequencies ω. We then must solve

$$-\omega^2 Y + \frac{d^4Y}{dx^4} = 0 \tag{A.1}$$

subject to

$$Y(0) = 0\,, \quad \frac{dY}{dx}(0) = 0\,, \quad Y(\ell_0) = 0\,, \quad \frac{d^2Y}{dx^2}(\ell_0) = K\frac{dY}{dx}(\ell_0)\,. \tag{A.2}$$

Introducing $\beta = \sqrt{\omega}$, the general solution of Eq. (A.1) is

$$Y(x) = A\cos(\beta x) + B\sin(\beta x) + C\cosh(\beta x) + D\sinh(\beta x)\,. \tag{A.3}$$

Applying Eq. $(A.2)_{1,2}$ leads to

$$Y(x) = A\left[\cos(\beta x) - \cosh(\beta x)\right] + B\left[\sin(\beta x) - \sinh(\beta x)\right]\,. \tag{A.4}$$

Equation $(A.2)_{3,4}$ give rise to an algebraic system of the form

$$\begin{bmatrix} c_1 & c_2 \\ c_3 & c_4 \end{bmatrix}\begin{bmatrix} A \\ B \end{bmatrix} = \begin{bmatrix} 0 \\ 0 \end{bmatrix}\,, \tag{A.5}$$

where

$$c_1(\beta; w, M_\ell) = K\left[\sin(\beta\ell_0) + \sinh(\beta\ell_0)\right] - \beta\left[\cos(\beta\ell_0) + \cosh(\beta\ell_0)\right]\,, \tag{A.6}$$

$$c_2(\beta; w, M_\ell) = -K\left[\cos(\beta\ell_0) - \cosh(\beta\ell_0)\right] - \beta\left[\sin(\beta\ell_0) + \sinh(\beta\ell_0)\right]\,, \tag{A.7}$$

$$c_3(\beta; w, M_\ell) = \cos(\beta\ell_0) - \cosh(\beta\ell_0)\,, \tag{A.8}$$

$$c_4(\beta; w, M_\ell) = \sin(\beta\ell_0) - \sinh(\beta\ell_0)\,. \tag{A.9}$$

In order for non-trivial solutions of Eq. (A.5) to exist, we must have

$$c_1c_4 - c_2c_3 = 0\,. \tag{A.10}$$

Given the parameters w and M_ℓ as well as ℓ_0 from the corresponding static solution, Eq. (A.10) is a transcendental equation for $\beta = \sqrt{\omega}$ that is readily solved with a numerical root-finding method.

A.2 Nonlinear Stability

For completeness, we present a nonlinear stability criterion for the static equilibrium configuration of a heavy elastic rod with one end fixed and the other end contacting a smooth surface with the possible presence of dry adhesion. The criterion was developed by Majidi et al. [31, 32] and is based on establishing conditions by which the potential energy functional is minimized with respect to perturbations in $\theta_0(s)$ and ℓ_0 that preserve the boundary conditions. The version of the criterion for the problem of interest here is discussed by O'Reilly [7, Section 4.7.2].

For a given static configuration of the rod, $\theta_0(s)$ and ℓ_0 are known. There are two parts to the criterion. The first part verifies that the rod has not buckled by finding a bounded solution $r(s)$ to a Ricatti equation:

$$\frac{dr}{ds} + P_0 - \frac{r^2}{EI} = 0\,, \qquad r(0) = 0\,, \qquad s \in [0, \ell_0)\ , \tag{A.11}$$

where $P_0 = P_0(s)$ is the tangential component of the contact force (or tension) in the rod:

$$P_0 = F_0 \cos\theta_0 + G_0 \sin\theta_0\,. \tag{A.12}$$

The second part captures stability with respect to perturbations to ℓ_0:

$$S_0 \frac{d\theta_0}{ds}(\ell_0^-) - \rho_0 g \sin\theta_0(\ell_0^-) \geq \left[\frac{d\theta_0}{ds}\left(\ell_0^-\right)\right]^2 r(\ell_0^-)\,, \tag{A.13}$$

where

$$S_0 = -EI\frac{d^2\theta_0}{ds^2}(\ell_0^-)\,, \tag{A.14}$$

and, for any function $f(x)$,

$$f(\ell_0^-) = \lim_{\sigma\to 0} f(\ell_0 - \sigma)\,, \qquad \sigma > 0\,. \tag{A.15}$$

For a given static configuration of the rod, if a bounded solution $r = r(s)$ to Eq. (A.11) can be found and Eq. (A.13) is satisfied, then the static configuration is said to be nonlinearly stable.

For the problem at hand $\theta_0(\ell_0) = 0$ and we can use Eq. (2.41) to simplify the expression for S_0: $S_0 = G_0$. Thus, Eq. (A.13) simplifies to

$$G_0 \geq \left[\frac{d\theta_0}{ds}(\ell_0^-)\right] r(\ell_0^-). \tag{A.16}$$

While G_0 is the vertical component of the contact force in the rod, the inequality Eq. (A.16) has no obvious physical interpretation.

Appendix B

Details on the Nonlinear Rod Vibration Problem

Here we describe the numerical method used in Section 3.2 to solve Eqs. (3.1) to (3.5). A similar approach for a more general class of problems has been developed by Humer et al. [45, 46], motivated by the earlier method of Vu-Quoc and Li [13]. The first step is to introduce the stretching transformation $z = \xi/\gamma(t)$, which maps the variable spatial domain $[0, \gamma(t)]$ to the fixed one $[0, 1]$. By writing $y = y(\xi, t) = \tilde{y}(\gamma(t)\xi, t)$ and then applying the chain rule, Eq. (3.1) becomes

$$\begin{aligned}\rho_0 \Bigg[&\frac{\partial^2 \tilde{y}}{\partial t^2} + \left(\frac{2\dot{\gamma}^2}{\gamma} - \ddot{\gamma} \right) \frac{z}{\gamma} \frac{\partial \tilde{y}}{\partial z} - \frac{2\dot{\gamma} z}{\gamma} \frac{\partial^2 \tilde{y}}{\partial t \partial z} \\ &+ \left(\frac{\dot{\gamma} z}{\gamma} \right)^2 \frac{\partial^2 \tilde{y}}{\partial z^2} \Bigg] + \frac{1}{\gamma^4} \frac{\partial^2}{\partial z^2} \left(EI \frac{\partial^2 \tilde{y}}{\partial z^2} \right) = -\rho_0 g \,.\end{aligned} \tag{B.1}$$

The appropriate boundary conditions are $\tilde{y} = a$ and $\partial \tilde{y}/\partial z = 0$ at $z = 0$, and $\tilde{y} = \partial \tilde{y}/\partial z = \partial^2 \tilde{y}/\partial z^2 = 0$ at $z = 1$. We have now transformed the free-boundary-value problem to one on a fixed domain, a simplification that comes at the cost of a substantially more complicated differential equation, Eq. (B.1), that contains an advective term as well as γ, $\dot{\gamma}$, and $\ddot{\gamma}$. Our method is quasi-Eulerian in the sense that fixed values of the coordinate z correspond neither to fixed material points nor to fixed locations in space.

In order to obtain the weak form for a typical interior element $\Omega^e = (z_1^e, z_2^e) \subset (0, 1)$, we multiply Eq. (B.1) by the test function $w = w(z, t)$ and integrate the result over Ω^e. After applying integration by parts twice to the bending stiffness term, we obtain the following:

$$\begin{aligned}&\int_{\Omega^e} w \rho_0 \frac{\partial^2 \tilde{y}}{\partial t^2} \,\mathrm{d}z + \left[2 \left(\frac{\dot{\gamma}}{\gamma} \right)^2 - \ddot{\gamma} \right] \int_{\Omega^e} w \rho_0 z \frac{\partial \tilde{y}}{\partial z} \,\mathrm{d}z \\ &- \frac{2\dot{\gamma}}{\gamma} \int_{\Omega^e} w \rho_0 z \frac{\partial^2 \tilde{y}}{\partial z \partial t} \,\mathrm{d}z + \left(\frac{\dot{\gamma}}{\gamma} \right)^2 \int_{\Omega^e} w \rho_0 z \frac{\partial^2 \tilde{y}}{\partial z^2} \,\mathrm{d}z \\ &+ \frac{1}{\gamma^4} \int_{\Omega^e} \frac{\partial^2 w}{\partial z^2} EI \frac{\partial^2 \tilde{y}}{\partial z^2} \,\mathrm{d}z + \int_{\Omega^e} w \rho_0 g \,\mathrm{d}z \\ &+ \left[w \frac{\partial}{\partial z} \left(EI \frac{\partial^2 \tilde{y}}{\partial z^2} \right) - \frac{\partial w}{\partial z} EI \frac{\partial^2 \tilde{y}}{\partial z^2} \right]_{z_1^e}^{z_2^e} = 0 \,,\end{aligned} \tag{B.2}$$

which can be readily discretized in the spatial dimension. We define the vector of element-wise generalized displacements to be

$$[\mathbf{q}^e(t)] = \left[\tilde{y}(z_1^e, t) \,,\, \frac{\partial \tilde{y}}{\partial z}(z_1^e, t) \,,\, \tilde{y}(z_2^e, t) \,,\, \frac{\partial \tilde{y}}{\partial z}(z_2^e, t) \right]^T , \tag{B.3}$$

and the element test function vector $[\mathbf{w}^e(t)]$ analogously. Introducing the normalized coor-

dinate $s = (z - z_1^e)/h^e$, we use the following shape functions to interpolate $\tilde{y}$ and w:

$$N_1^e(s) = 1 - 3s^2 + 2s^3\,, \tag{B.4a}$$
$$N_2^e(s) = h^e s(1-s)^2\,, \tag{B.4b}$$
$$N_3^e(s) = s^2(3-2s)\,, \tag{B.4c}$$
$$N_4^e(s) = h^e s^2(s-1)\,. \tag{B.4d}$$

Writing the shape functions as the row vector $[\mathbf{N}^e(s)] = [N_1^e(s)\ N_2^e(s)\ N_3^e(s)\ N_4^e(s)]$, the interpolations are $\tilde{y} = [\mathbf{N}^e][\mathbf{q}^e]$ and $w = [\mathbf{N}^e][\mathbf{w}^e]$.

After assembly and imposition of the z-domain versions of the first four boundary conditions in Eq. (3.3), Eq. (B.2) gives rise to a global matrix problem of the form

$$[\mathbf{M}][\ddot{\mathbf{q}}] - \frac{2\dot{\gamma}}{\gamma}[\mathbf{D}_1][\dot{\mathbf{q}}] + \left\{ \left(2\left(\frac{\dot{\gamma}}{\gamma}\right)^2 - \frac{\ddot{\gamma}}{\gamma} \right)[\mathbf{D}_1] + \left(\frac{\dot{\gamma}}{\gamma}\right)^2 [\mathbf{D}_2] + \frac{1}{\gamma^4}[\mathbf{D}_3] \right\} [\mathbf{q}] = [\mathbf{F}(\gamma, \dot{\gamma}, \ddot{\gamma})]\,. \tag{B.5}$$

The corresponding element matrices, which are apparent from Eq. (B.2), are

$$[\mathbf{M}^e] = \int_{\Omega^e} [\mathbf{N}^e]^T \rho_0 [\mathbf{N}^e]\, \mathrm{d}z\,, \tag{B.6a}$$
$$[\mathbf{D}_1^e] = \int_{\Omega^e} [\mathbf{N}^e]^T \rho_0 z \left[\frac{\mathrm{d}\mathbf{N}^e}{\mathrm{d}z}\right] \mathrm{d}z\,, \tag{B.6b}$$
$$[\mathbf{D}_2^e] = \int_{\Omega^e} [\mathbf{N}^e]^T \rho_0 z \left[\frac{\mathrm{d}^2\mathbf{N}^e}{\mathrm{d}z^2}\right] \mathrm{d}z\,, \tag{B.6c}$$
$$[\mathbf{D}_3^e] = \int_{\Omega^e} \left[\frac{\mathrm{d}^2\mathbf{N}^e}{\mathrm{d}z^2}\right]^T EI \left[\frac{\mathrm{d}^2\mathbf{N}^e}{\mathrm{d}z^2}\right] \mathrm{d}z\,, \tag{B.6d}$$
$$[\mathbf{F}^e] = \int_{\Omega^e} -[\mathbf{N}^e]^T \rho_0 g\, \mathrm{d}z\,. \tag{B.6e}$$

We introduce the temporal discretization $t = t_k$ for $k = 1, 2, \ldots$ and define $\Delta t_n = t_{n+1} - t_n$. Given $[\mathbf{q}_n]$, $[\dot{\mathbf{q}}_n]$, $[\ddot{\mathbf{q}}_n]$, γ_n, $\dot{\gamma}_n$, and $\ddot{\gamma}_n$, we seek to use Eq. (B.5) to determine $[\mathbf{q}_{n+1}]$, $[\dot{\mathbf{q}}_{n+1}]$, $[\ddot{\mathbf{q}}_{n+1}]$, γ_{n+1}, $\dot{\gamma}_{n+1}$, and $\ddot{\gamma}_{n+1}$ by way of the Newmark method. Thus we assume

$$\mathbf{q}_{n+1} = \mathbf{q}_n + \dot{\mathbf{q}}_n \Delta t_n + \frac{\Delta t_n^2}{2}[(1-2\beta)\ddot{\mathbf{q}}_n + 2\beta\ddot{\mathbf{q}}_{n+1}]\,, \tag{B.7a}$$
$$\dot{\mathbf{q}}_{n+1} = \dot{\mathbf{q}}_n + [(1-\gamma)\ddot{\mathbf{q}}_n + \gamma\ddot{\mathbf{q}}_{n+1}]\Delta t_n\,. \tag{B.7b}$$

and similarly for γ. A nonlinear matrix problem for $[\mathbf{q}_{n+1}]$ and γ_{n+1} results upon inserting Eq. (B.7) into Eq. (B.5). To solve, we iterate $[\mathbf{q}_{n+1}]$ and γ_{n+1} until the z-domain counterpart of Eq. $(3.3)_5$ is satisfied. Then the velocities and accelerations at $t = t_{n+1}$ can be computed from Eq. (B.7).